UNIVERSITY OF MISSOURI-ROLLA

ROCK MECHANICS & EXPLOSIVES

RESEARCH CENTER

INVESTIGATION OF THE USE OF SHAPED EXPLOSIVE CHARGES FOR INCREASING THE PERMEABILITY OF COAL

Final Report for

Contract No. G0101590 (MIN-36)

Pittsburgh Mining Research Center
United States Bureau of Mines

December 1970

DISCLAIMER

The overall objective--to determine the use of the unique ability of shaped charges to directionalize energy to fracture and increase in situ permeabilities of coal--was not achieved. The results of this preliminary laboratory research indicate that the probability of development of a safe and practical system is very low. Therefore, although the contractor performed satisfactorily and completed programmed research, further work in this area has been discontinued.

INVESTIGATION OF THE USE OF SHAPED EXPLOSIVE CHARGES FOR INCREASING THE PERMEABILITY OF COAL

by Ronald R. Rollins, George B. Clark, and Calvin J. Konya

Professor of Mining Engineering
Professor of Mining Engineering
Research Assistant in Mining Engineering
University of Missouri-Rolla
Rolla, Missouri

ABSTRACT

The three areas of this investigation were: permeability changes in coal models before and after jets from shaped explosive charges were fired into confined blocks; jet penetration and fracture formation in coal, Plexiglas and dolomite; and jet penetration capabilities of charges loaded with permissible explosives. The average permeability along the bedding in natural coal was 0.348 millidarcys and across the bedding was 0.014 millidarcys for flow through the microfractures. Gas flow through the major points (Darcy flow) varied from about 1.5 to 4.0 darcys for the preshot condition, and from about 4 to 11 darcys for postshot values. Optimum penetration and permeability values were obtained for 60 deg, Cu lined, shaped charges using high explosives.

Permissible explosives gave minimal results in the small (0.5 in. diam) charges used in this study. Fracture formation was studied by use of highspeed photography and radiographs and indicated that jet penetration depth in brittle materials was proportional to the detonation velocity and inversely proportional to the natural log of the static tensile strength, Young's modulus, and the longitudinal wave velocity of the target. The permeability of coal can be increased for degasification purposes by the use of shaped charge jets.

CONTENTS

LIST OF TABLES

LIST OF FIGURES

I. INTRODUCTION

One of the oldest problems associated with the mining of coal is the emission of methane gas and the subsequent hazard of explosive concentrations accumulating in the mine workings.

Methods of degasification practiced in the United States are by means of surface and underground boreholes, water infusion, foam infusion, underground blocking methods, and modifications of these. Long boreholes with confined explosives to increase the fracturing have been tested but do not significantly increase the rate of gas liberation. Geologic features such as mud seams and partings may seal a portion of the seam, reducing flow or preventing gas migration across discontinuities. Thus, portions of the seam will retain their high methane content until mined (Ref. 1). The energy from confined explosives causes local crushing which may have a detrimental effect on gas flow. Ammosov and Eremim (Ref. 2) concluded that exogenetic shear fractures such as those which result from compression normal to the bedding could cause blockage of the channels and would decrease the permeability.

The research described herein deals with experimentation with chemical explosive energy to fracture the coal in advance of working faces (1) to enhance the outflow of methane gas, and (2) to increase the permeability for water infusion. In order to protect the roof rock of the coal mine and also to give control over the fracture patterns developed in the coal, experiments were designed to utilize

shaped charges to direct explosive energy to obtain the maximum possible effect in creating controlled fracture patterns.

There is no information in the literature on the response of coal to concentrated impact pressures such as those from shaped charge jets, which are of magnitudes as high as 2×10^6 psi, although considerable quantitative information is available on jet impact effects on several types of rock (Ref. 3).

While there are no data available on shaped charge effects on coal or material with characteristics similar to coal, many other properties have been investigated which affect its response to the stress waves generated by impact and the release and flow of methane.

Shaped charges produce fracturing and directionality with a small crushed zone. They are commercially available in a wide range of types and sizes and selected designs were used in this model study to determine the effect of induced fractures on the permeability of sample blocks of coal.

II. PERMEABILITY OF COAL

One of the underground methods explored for reduction of the causes of coal mine explosions of methane and coal dust has been to drill holes ahead of the working face to provide a means for the escape of the methane and for infusion of water into the coal to form a barrier to methane flow (Refs. 4-10). However, methane gas does not exist in pockets in the coal, but is adsorbed and is totally released only when the coal is fractured and equilibrium is reached at a low (atmospheric) pressure. Some gas bed pressures have been reported as high as 550 psi (Ref. 9).

Cervik (Ref. 8) reports that gas may occur in coal either as adsorbed gas whose flow through the pore spaces is governed by Fick's law, or as free gas in fracture systems with its flow governed by Darcy's law.

Gas transport through the micropore structure (Fick's law) is by means of diffusion (Ref. 4):

$$q = DA \frac{dC}{d\ell} \tag{1}$$

where

q = volume flow rate

D = diffusion coefficient

A = cross-sectional area

C = gas concentration in solid coal

ℓ = length

The driving force is the concentration gradient and this type of transport is described as "slow bleeding".

Flow through fractures is the only type which is rapid enough to be of importance in degasification in situ. Darcy's law is given by

$$q = \frac{kA}{\mu} \frac{dP}{d\ell} \tag{2}$$

where

q = rate of volume flow

k = permeability

μ = gas viscosity

A = cross-sectional area

P = pressure

ℓ = length

These two modes of gas flow are different but they are interdependent. The equilibrium quantity of gas contained in the micropore structure is directly proportional to the gas pressure in the fracture system according to the empirical relationship (Ref. 4):

$$C_o = bP^n \tag{3}$$

where

C_o = equilibrium quantity of adsorbed gas per unit weight of coal

P = pressure

b and n are constants

Coal is a porous material with a pore diameter on the order of a few angstroms. The pores are classified as dispersed or connected. Dispersed pores have little interconnection and flow from pore to pore is difficult if not impossible. Material having a small connected pore porosity has a greater permeability than material with dispersed pores of a higher porosity.

From equation (2) it is noted that the flow of gas is directly proportional to the area, the permeability and the pressure gradient. The latter is a characteristic of a particular location in a given coal bed and cannot be controlled. However, if the permeability and the flow area can be increased, the flow will increase as the product of these values.

The standard Darcy equation for gases (Ref. 11) may be written:

$$k = \frac{\mu q_{AV} \ell}{A(P_1 - P_2)} \tag{4}$$

where

q = rate of flow

μ = viscosity of flowing fluid

A = cross section of sample

ℓ = length of flow through sample

k = permeability constant

$P_2 - P_1$ = pressure difference across sample

The standard unit for k is the darcy. The units for the above equation are

$$\text{darcy} = \frac{(\text{cp})\ (\text{cm}^3/\text{sec})\ (\text{cm})}{(\text{cm})^2\ (\text{atmos.})} \tag{5}$$

where

cm = centimeters

cp = centipoise

sec = seconds

atmos. = atmospheres

The above equation is valid subject to the following limitations (Ref. 6):

1. The fluid is an inert homogeneous gas.
2. The flow is for rates applicable for flow.
3. The effect of gas slippage is taken into consideration.

Air is commonly used as the fluid for determination of permeability. The air permeability values, however, do not agree with those determined with gases such as hydrogen or carbon dioxide (Ref. 12) and none of the above agree with the values obtained by using water (Ref. 13). Klinkenberg (Ref. 14) proved that the discrepancies in gas permeability and liquid permeability are due to gas slippage, a well-known phenomenon related to gas flow in capillary tubes.

Fulton (Ref. 15) states that in the viscous flow of a fluid through a capillary, the velocity of a thin layer of fluid adjacent to the walls of the capillary is theoretically zero, but when the ratio of the radius of the capillary to the mean free path of the gas is such that intermolecular collisions decrease, then the molecular collisions with the walls increase in importance. The thin layer of zero velocity gas may lose its attachment to the capillary surface and will have a finite velocity. Gas slippage occurs when the diameter of the capillary openings approach that of the mean free path of the gas molecules. The mean free path is a function of molecular size and kinetic energy. The observed permeability to gas approaches a limiting value as the reciprocal mean pressure approaches infinity, i.e., at the value for liquid permeability. The Klinkenberg (Ref. 14) equation is:

$$k_1 = \frac{k_2}{1 + \frac{b}{P_m}} \tag{6}$$

where

k_1 = permeability of the medium to a single phase liquid at constant temperature

k_2 = permeability of the medium to a gas at constant temperature

P_m = mean pressure at which the gas is flowing

b = constant (Klinkenberg) for a given gas and a given medium

If the Klinkenberg extrapolation technique is not used the resulting gas permeabilities may be too high. As capillaries increase in size the percentage error in Darcy's equation decreases. For a permeability of 0.5 millidarcys errors may be in excess of 100 percent, while for permeabilities of 100 millidarcys the error is about 5 percent. For practical problems such as sampling a petroleum reservoir the permeability to gas (air) at low pressure is taken as the single-valued permeability of a nonreactive porous material to fluids (air, water) with the error well within the statistical and experimental error from other causes (Ref. 4). Steward (Refs. 16,17) states that the slippage effect in a heterogeneous porous limestone had no measurable effect on permeability measurements because the hairline fracture width was large compared to the molecular mean free path of the gas molecules.

Flow through fracture systems of the coal is the primary type of mass transport of methane in coal beds in the United States, and initial investigations have been made to evaluate some of the parameters involved (Refs. 18,19,20,21,22).

Diffusion studies of gases through coal have been conducted by a number of investigators (Refs. 4,9,18,24,25,26,27). Karn (Ref. 26) found the diffusion rate across the bedding to be one-third to one-half that along the bedding. Gas flow along the bedding was reported to be 1.20×10^{-10} cm^2 sec^{-1} atm^{-1} and 0.56×10^{-10} across the bedding. Sevenster (Ref. 23) reported flows of 0.28×10^{-10} cm^2 sec^{-1} atm^{-1} without specifying bedding orientation. The coal samples for both studies were from different locations which could account for the different values. These flow rates are low in comparison to those

observed in samples of larger dimensions, which supports the conclusion that diffusion is not the primary mode of gas transport through the coal seam. In situ investigations of methane flow rates have been performed (Refs. 23,28,29) but these do not define the permeability of the seam because neither the cross-sectional flow area nor the flow path length is known.

Evans and Skinner (Ref. 30) measured the permeability of some English coking coals to water at low pressure, but used an equation only one term of which involved Darcy's law. However, they found that continuity of fractures is necessary for the flow of gases. The flow rate of water was found to decrease exponentially with time.

Alpern (Ref. 31) points out that the distribution of gas in a coal seam is related to geologic conditions and mine workings. He states also that extensive microfissuring of the coal may transform it into mylonites and breccias, which are impermeable to gas flow when they are under pressure. A classification of fissure systems as related to tectonics is mentioned, but not described in detail. Information on intensive microfissuring is employed primarily to assist in identifying "privileged zones" for the outburst of gas.

There is a growing literature concerned with the adsorption of gases in coal, much of which is discussed in References 4-10. Considerable research has been performed in the USSR and reviewed by Alpern (Ref. 31). Bertard, et al. (Ref. 32), indicate that in the pore spaces and fissures in coal some gas molecules adhere to the walls (are adsorbed), and the remaining gas is free. Porosities of French coals are reported to be from 0.015 to 0.074 cm^3/gm, the latter for anthracite. Moisture content affects the gas content and a confining pressure increase from 0 to 300 bars results in a decrease of the permeability

of anthracite from 1 to 10^{-2} darcy, and from 10^{-2} to 10^{-5} darcy for less permeable coal. Desorption is accomplished by decrease in pressure by fracturing and crushing, the rate of desorption depending upon the particle size of the coal.

Ettinger, et al. (Ref. 33) (USSR) give information that indicates that the different petrographic constituents of coal (fusain, vitrain) have different sorption properties.

Structure of Coal. The macrostructure of coal beds consists of bedding, cleats, inclusions, fractures, faults, and other features. Most coal beds have stratified impurities such as shale, thin rock bands, or mud seams.

When coal is examined in thin sections under a microscope, it is found that it consists of macerals (analogous to minerals in rocks). European terminology includes those constituents whose origin is due to woody tissues, such as sporinite, cutinite, resinite, alginite and sclerotinite, and those not originating from woody tissues, micrinite. The equivalent U.S. nomenclature is given in Table I.

Strength of Coal. The unconfined (Ref. 34) and triaxial strength (Ref. 35) of cylindrical or rectangular specimens of coal have been measured. Compressive stress causes failure along cracks, and strength is usually greater normal to the bedding. Failure under confinement can be represented by Coulomb's equation for given types of coal. On the other hand, small particles of coal under compression fail either by degradation or plastic flow (Ref. 36). The type of failure also depends upon particle size and rank of coal.

However, the strength properties of coal most important in relation to fracture by shaped charges are its resistance to penetration and strength in tension and shear under in situ conditions.

TABLE I

Nomenclature of the European Macerals and the American Constituents

European nomenclature			U.S.A. nomenclature	
Maceral grouping	Macerals		Components	Constituents (component grouping)
Vitrinite	Telinite		Megascopic anthraxylon (>500μ) Attrital anthraxylon (500-15μ)	Anthraxylon
	Collinite		Sub-anthraxylon (15-3μ) Humic matter (<3 μ) Light brown matter	Translucent Attritus
Exinite	Resinite Cerinite		Red resins Yellow resins Amorphous	
	Sporinite Cutinite Suberinite		Spore coats Cuticles Suberin	
	Alginite		Algal bodies	
Inertinite	Massive micrinite Granular micrinite		Dark brown matter Amorphous opaque matter Granular opaque matter	Opaque Attritus
	Sclerotinite Semi-fusinite Fusinite		Fusinized fungal matter Dark semi-fusain Attrital fusain (<500 μ) Megascopic fusain (>500 μ)	Petrologic Fusain

III. SHAPED CHARGES

Shaped Charge Jet Formation and Penetration. The classical two-dimensional theory of jet formation utilizing Bernoulli's theorem (Refs.47,48)has been modified (Ref.49) to account for jet tip velocity and velocity gradient. This assumes that two incompressible jets impinge upon each other and that a fast and slow jet are formed. However, it is believed that a three-dimensional mathematical analysis will be more fruitful when carried through to completion and correlated with existing data (Ref.3).

The well-known first order theory of jet penetration is given by

$$P = \sqrt{\frac{\lambda \rho_j}{\rho_t}} \tag{7}$$

where

P = penetration

λ = correction factor for discontinuous jet

ρ_j = density of jet

ρ_t = density of target

The basic assumption employed in the derivation of (7) is that the pressure of the impinging jet exceeds the strength of the target and the penetration process is hydrodynamic in character, with incompressibility of jet and target also being assumed. Equation (7) with empirical correction factors for target strength has been employed with considerable success to explain effects of target strength, jet breakup, and standoff relationships. This equation indicates, however, that the depth of penetration is independent of jet velocity, and as derived does not account for the strength of target material.

Recent developments by personnel from BRL, Aberdeen Proving Ground (Refs. 37-40) have utilized additional parameters to define penetration-standoff relationships. The equations developed take into account the jet property of breakup time and the minimum penetration velocity of the target. These values can be determined experimentally and are related to as yet undefined properties of the jet and target materials.

The concept of this theory (Ref. 40) treats three cases. The first is for a continuous jet, the second for a jet partially continuous, and the third for a jet after complete breakup. Three equations which were derived for these conditions are

$$P_T = Z_o \left\{ \left[\frac{V_j^o}{(1+\gamma)\, U^{min}} \right] \right\}^{1/\gamma} - 1 \qquad (8)$$

$$P_T = \frac{(1+\gamma)(V_j^o t_1)^{1/(1+\gamma)} Z_o^{\gamma/(1+\gamma)}}{\gamma} - \frac{\sqrt{(1+\gamma) U^{min} t_1 (V_j^o t_1)^{1/(1+\gamma)} Z_o^{\gamma/(1+\gamma)}}}{\gamma} - Z_o \qquad (9)$$

and

$$P_T = \frac{V_j^o t_1 - \sqrt{U^{min} t_1 (V_j^o t_1 + \gamma Z_o)}}{\gamma} \qquad (10)$$

where

P_T = total penetration depth

Z_o = distance from virtual origin (assumed point of origin of jet)

V_j^o = velocity of jet tip

t_1 = time of jet breakup

U^{min} = minimum penetration velocity of target material

$\gamma = (\rho_t/\rho_j)^{\frac{1}{2}}$

ρ_t = target density

ρ_j = jet density

The basic assumptions made in the development of equations (8), (9), and (10) are that both the target and jet are incompressible, the jet originates at a distance Z_o from the target, jet breakup occurs simultaneously along the jet, and all jet particles above a minimum velocity (determined by the hardness of the target) contribute to penetration in proportion to their length.

For a given charge and target the penetration increases linearly with Z_o for a continuous jet (equation 8). For variation in charge and target parameters, penetration increases with jet tip velocity and with a decrease in U^{min}. The minimum penetration velocity is a measure of target resistance to penetration and can be determined experimentally. Jet tip velocity is a function of liner and explosive properties. Only short continuous jets are obtainable, however, and consequently, penetration cannot continue indefinitely with increase in Z_o.

Maximum penetration is obtained at the upper limit of application of equation (11) which defines the penetration for a virtually continuous jet.

The maximum penetration is given by

$$P_{max} = \frac{L}{\gamma} = \left(\frac{V_j^{\,o} - V_j^{\,*}}{\gamma} \right) t_1 \qquad (11)$$

where

$V_j^{\,*}$ is the jet cutoff velocity or the velocity of the last penetrating jet particle and is given by

$$V_j^{\,*} = \sqrt{U^{min} \left(V_j^{\,o} + \gamma \frac{Z_o}{t_1} \right)} \qquad (12)$$

Hence

$$P_{max} = \sqrt{\frac{\rho_j}{\rho_t}} \left[V_j^{\,o} - \sqrt{U^{min} \left(V_j^{\,o} + \gamma \frac{Z_o}{t_1} \right)} \right] \qquad (13)$$

for a given liner and target.

Maximum penetration is obtained for high jet tip velocity and optimum jet breakup time t_1. This equation gives one explanation of why high velocity explosives and high density cohesive jets produce the greatest penetration.

Impact, Penetration and Fracture. The stress wave pattern generated in a target impacted at high velocity is complex (Ref. 41). For the velocity range of shaped charge jets the impact pressure exceeds the yield strength of target material and the impact process is hydrodynamic in character. That is, the pressure exceeds the yield strength so that immediately around the stagnation point as the jet penetrates, both the jet and the target may approximate fluid behavior. The factors which appear to influence the amount of stress wave energy which is transmitted into the mass of the target are (1) the magnitude of the pressure (stress) at some radial distance from the axis of jet

beyond the distance where crushing and plastic flow phase into elastic behavior, (2) the duration of the pressure, and (3) the velocity of crack propagation in the material.

For single short aluminum projectiles impacting basalt targets Gault and Heitowit (Ref. 42) estimated that of the projectile kinetic energy the energy utilization was: waste heat - 23 to 35%; comminution - 10 to 24%; ejecta throwout - 45 to 53%; elastic wave energy - 1%. Because of the longer residence impact time of jets and their smaller diameter the energy transmission process probably results in a larger portion of energy going into the stress waves in the target.

The contemplated geometry of use of shaped charges in boreholes provides no means for creating reflected waves and, hence, fracture must be accomplished by the tangential (tensile) stresses generated by the outgoing radial dilatation (compressive) wave. However, the maximum velocity at which cracks can propagate in a brittle solid is about one-half the velocity of dilatation waves (Ref. 41). Consequently, arrested fractures are observed.

In addition to the fracturing caused by the jet, confined charges in a borehole generate a high gaseous pressure which follows into the hole created by the jet and causes fracturing in the surrounding material. The marked success of perforating charges employed for increasing inflow of crude petroleum into oil wells indicates the combined effects of penetration and after pressure. However, only the effects of unconfined shaped charges were investigated in the project described in this report.

Design of Shaped Charges. Although explosive charges may be formed in many shapes for given purposes, most investigations have been concerned with cylindrical shaped charges with conical cavity liners. A concise summary of design of shaped charges for military purposes by Klamer (Ref. 43) gives most of the important interrelationships between charge parameters and penetration of steel targets.

Cylindrical shaped (cavity lined) explosive charges are designed primarily for penetration of armor for military purposes, of blast furnace plugs by jet tappers, and of drill hole casing and rock for increasing inflow into oil wells. Linear (two-dimensional) charges are employed for cutting metal plate and for similar purposes.

Design factors (Refs. 43 and 44) deal with material properties of explosives, liner and casing, and geometric items such as charge and liner geometry, and standoff. While all of the factors are important, some are more critical than others. Charge design factors are length, size of booster, shape, if tapered, charge to cone diameter ratio, and cone alignment. Special geometries utilize wave shapers such as inert cones and other devices.

For non-tapered cylindrical charges the penetration into steel increases rapidly with charge length up to about 2 diameters and then increases slowly to about 5 diameters. Beehive-shaped charges are capable of producing a jet of greater penetrating power per unit weight of explosive than a straight cylindrical charge with a height greater than optimum. The best diameter of charge to diameter of cone ratio appears to be somewhat greater than 1.0, providing for a small width of explosive at the base of the cone. Greater widths may be detrimental. Cone misalignment greater than 1 deg and off center displacement as much as 1/64 of the charge diameter may seriously affect penetration.

Penetration performance is related to the detonation pressure of the explosive, which is in turn related to the square of the detonation velocity. Detonation velocity increases linearly with density. Hence, a high velocity, dense explosive produces the greater penetration, and of the commercial explosives 100 percent blasting gelatin is probably the most effective. Sensitivity and storage characteristics are important for both military and industrial purposes.

Cavity liners investigated for armor penetration have included cones, hemispheres, cylinders, trumpet shapes, and combinations. Hemispheres turn inside out, while cones collapse upon themselves leaving 70 to 80 percent of their mass in the slug. For most purposes cones are the most effective in penetration, and the percentage division of mass in slug and jet depends to a great extent upon the apex angle. Penetration and apex angle, liner thickness are all interrelated.

For various metals reported in the literature copper is among the most effective because of (1) its density, and (2) its ductility. According to the first order penetration law the depth of penetration should be proportional to the square root of the jet density. The face centered cubic metals are the most ductile and aluminum and copper are most effective for their particular density. One would expect, therefore, that gold would be even more effective. Annealing which improves ductility also improves penetration performance in steel targets.

The variation of penetration for steel liners is a function of standoff as well as apex angle. Somewhat similar families of curves would be expected for other metals, but not necessarily the same sequence of shapes as for steel targets. Optimum standoff varies with

apex angle and material properties. The optimum liner thickness varies with cone angle and density, and within a range of 0.025 to 0.040 diameters the penetration is relatively insensitive to changes in liner thickness.

Scaling. DiPersio (Ref. 45) et al., have found that penetration of shaped charge jets from aluminum and copper liners did not scale for charges smaller than 2 inches diameter, but does scale for larger charges. That is, the penetration of a jet from 3/4 in. diameter charges is less than one-half of that of scaled 1-1/2 in. charges. This may be due to relative manufacturing precision of small charges or lack of scaling of the detonation wave.

Charge Length. The effective head (height) of the explosive above the apex of the liner is constant for a given diameter.

Jet Characteristics. (Ref. 44). The number of jet particles from a charge of given design is independent of the charge size, but particle sizes vary with the diameter. Increase of the apex angle decreases the number of particles, increases their average size, decreases the jet tip velocity and increases the breakup time of the jet.

The values of the various parameters described above for penetration in steel were employed as guides for the design of charges for experimentation in rock, coal and other brittle materials tested in this project.

Reactive and Pressure Jets. The jet from an unlined cavity is composed of the gaseous products of the detonation of the explosive. The stagnation pressure of these gases is of the same order of magnitude as the detonation pressure, but is not effective in penetrating solid materials.

Oil well perforation experiments (Ref. 46) have shown that jet materials which will react with the target medium, create an exothermic reaction and higher lateral pressures around the hole. This type of reaction was found to be more effective for lower velocity jets and those from titanium liners were found to create considerable fracturing around holes in limestone, which was not present for conventional metals such as zinc, lead, copper, or steel. Lateral pressures in rock cylinders around the jet hole were increased by 50 percent.

In hard formations in oil production the increase in water injection rates and reduction in formation breakdown pressure were found to be marked. Also operators were able to recover oil in less time with a reduction of overall production cost.

IV. EXPERIMENTATION

The primary objectives of this study were to determine the penetration and fracturing of confined coal caused by shaped charge jets and the consequent effects on the permeability of the coal to flow of gas. The type of explosive and cavity liner material were expected to be the most important shaped charge parameters, and four liner metals and six types of explosives, three of which were permissibles, were employed. Two other brittle materials, dolomite and Plexiglas, were also subjected to jet penetration. Fracture patterns were observed and permeability measurements were made on larger coal blocks (12 in. cubes), both parallel and perpendicular to the bedding planes, and containing the naturally occurring joints, cleavage planes, etc. Smaller blocks (0.5 in. cubes) without visible cleavage planes or fractures were tested to determine the gas flow through the microfracture system or "true" permeability of the undisturbed coal.

Coal Samples. In order for a coal sample to be representative of in situ properties and behavior it should be unfractured by the cutting processes and subject to the same pressures in the laboratory. Experiments were designed to test coal blocks which had been cut with care, and confined in a steel box on four sides. No attempt was made, however, to duplicate in situ confining pressures in the first year of experimentation, because this initial phase of the project was planned largely to determine the feasibility of shaped charge usage before proceeding with in situ modeling.

The dimensions of the coal test blocks were determined by the following factors:

1. Penetration depth of jet
2. Ease of encapsulation
3. Geologic features in coalbed
4. Ease of obtaining undisturbed coal specimens

Preliminary penetration tests were conducted on two coal blocks confined in wet sand to offer some lateral restraint. Shaped charge liners of 0.5 in. and 0.625 in. diam with 60 deg apex angles made of yellow brass were placed in charges utilizing composition C-4 as the explosive. The 0.625 in. diam charge gave the greatest penetration, which was 4.75 in. or 7.6 cone diameters (CD).

The difficulties of encapsulation in a steel confining chamber increased with the volume of the sample. The coal blocks were coated with an epoxy resin and encapsulated in wax inside a steel chamber with removable end plates. Wax (paraffin) was found to be impermeable and to bond well to both the sealed coal and steel. Disassembly of the model was accomplished by heating the chamber until the model slid out under its own weight.

As many geologic features as possible, including joints, were included in the models in order that typical gas flow in natural fracture systems could be investigated. One set of coal blocks was obtained from a site in north central Missouri but the samples were unsatisfactory due to fractures caused by the mining method. The Illinois number 6 seam was then considered as a possible source of samples. The jointing pattern for this coal was on the order of 3 inches.

A 12 in. coal cube was found to satisfy the size requirements without being too large to handle. Coal samples were obtained from an underground mine which used conventional mining methods. This coal was found to be unsatisfactory because calcite filled joints were shattered by the use of Airdox in the mining method. Usable coal blocks were obtained from the Inland Steel mine near Sesser, Illinois. Samples were cut from a face in virgin coal which had been exposed for less than 24 hours, sealed in plastic bags and stored at 65 deg F until used.

A masonry saw with a 36 in. diameter blade was first employed to trim the models to the correct size for encapsulation. This method of cutting wet was abandoned because the water tended to wash out fine material from joints and bedding planes. It also reduced the tensile strength between some bedding planes causing the samples to fall apart.

To approximate in situ conditions as nearly as possible a dry cutting technique was employed. A Homelite XL-12 chain saw was used to cut large blocks but it did not have the capability to be used as a trim saw. A metal cutting Wellsaw, Model 8, with a bimetal blade was used to trim the coal blocks to size, cutting coal, pyrite, and shale bands with equal ease.

The cut coal samples were brushed clean and the four sides which would later be covered with wax were coated with E-2 Epoxy adhesive manufactured by the Sealoid Company. The sample was then sealed in the metal chamber (Fig. 1) with melted wax. No attempt was made to dry the sample and remove its natural moisture content. It was felt that heating a large sample above 100 deg C would change the coal sufficiently to induce more error in the permeability measurements

than those which would result from the moisture. The two faces which were to be tested for gas flow permeability were left as received from the sawing operation. The encased model and box weighed over 400 lbs. A small sample holder for permeability measurements was also constructed to accommodate samples less than 2 in. by 2 in. (Fig. 2).

Apparatus. The permeability measurement apparatus (Fig. 3) consisted of: a source of dry compressed air; two U tube Hg manometers; two U tube water manometers; flowmeters; large and small permeability chambers; a blast chamber; a barometer and thermometer. Connections could be made to different points on the permeability chamber and flow measurements obtained in both the forward and reverse directions.

A homogeneous core of sandstone was cut and used as a standard to calibrate the permeability apparatus. Permeability measurements were made as outlined in the Recommended Practice for Determining Permeability of Porous Media (Ref. 11). The oven dried sample had a permeability of 745 millidarcys (Fig. 4). Applying Klinkenberg correction the permeability was 725 millidarcys which was well within the inherent experimental error and therefore was omitted.

Two, 600 kv, 730-2660 series, flash X-ray units (Field Emission Corporation) were employed to take radiographs as the shaped charge jet penetrated the coal. From these radiographs shaped-charge-induced fractures were observed and jet penetration velocities were calculated.

A Cordin model framing camera with a maximum framing rate of 1.25×10^6 frames per second was used to record penetration phenomena of shaped charges in Plexiglas. Models simulating bedded and homogeneous deposits were photographed.

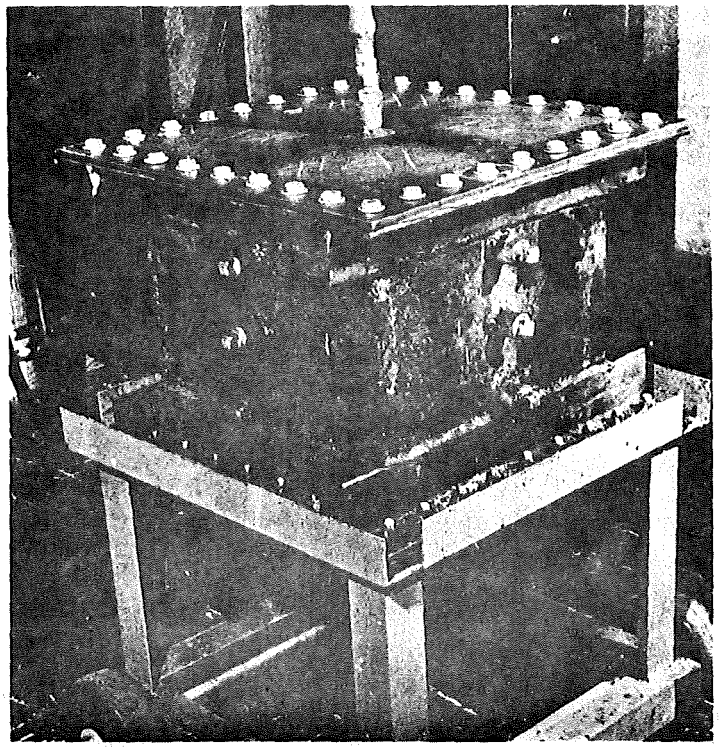

Fig. 1 LARGE PERMEABILITY CHAMBER

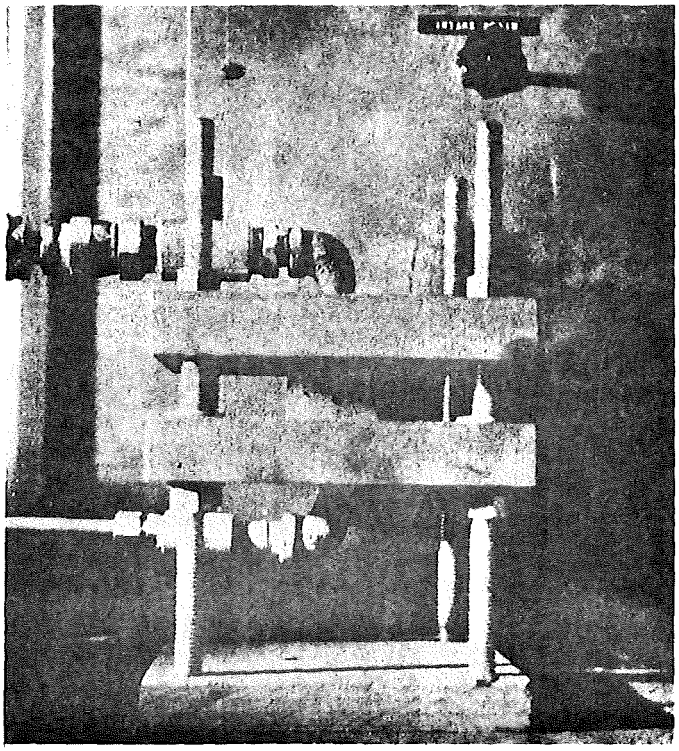

Fig. 2 SMALL PERMEABILITY CHAMBER

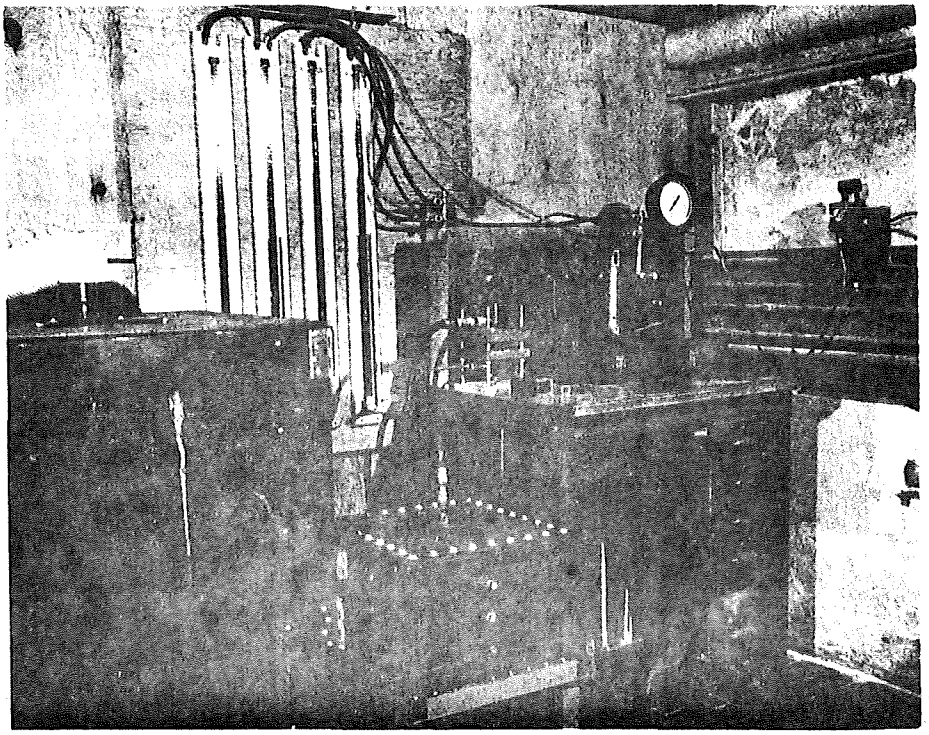

Fig. 3 PERMEABILITY MEASUREMENT APPARATUS

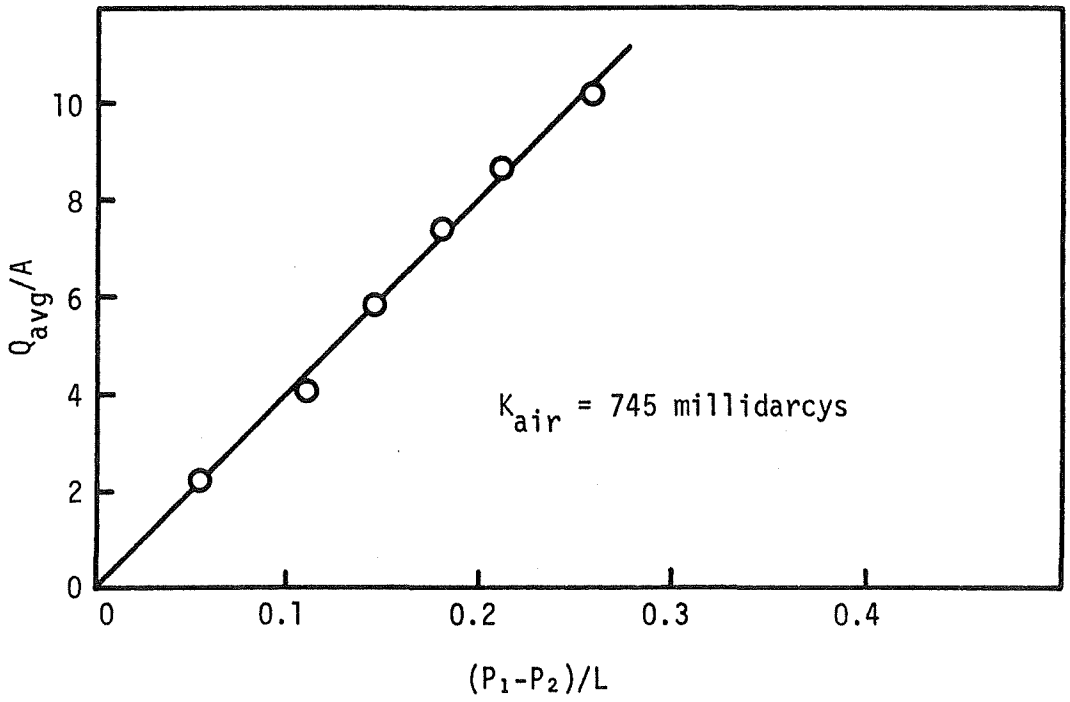

Fig. 4 PERMEABILITY OF SANDSTONE STANDARD

Shaped Charge Design. The shaped charge design factors for military purposes given by Klamer (Ref. 43) were employed for charges used in this project. The following parameters were considered in the design of the shaped charges for this investigation:

1. Liner material
2. Liner apex angle
3. Type and velocity of explosive
4. Charge dimensions
5. Standoff

After testing several metals, Zernow (Ref. 50) concluded that jets of face-centered cubic metals all stretch more or less taffy-like in flight, body-centered cubic metals show early fracture into large pieces and hexagonal metals fracture early into small pieces. Low melting point metals generally form a broad dispersed spray-like jet, a common behavior independent of their crystal structure. Metals such as copper, nickel, aluminum, and silver behave similarly and are all face-centered cubic in crystal structure. Iron is body-centered cubic in structure while metals such as magnesium, cobalt and titanium are hexagonal in structure. Titanium slowly changes its crystal structure from hexagonal to cubic when raised to temperatures above 880 deg C.

As indicated earlier experiments (Ref. 46) have shown that some jet materials may react with the target producing exothermic reactions which increase lateral pressure in the holes. Titanium jets fired into limestone created fractures extending beyond the hole, which were not present for other metal jets. Liner materials used for this study included brass, copper, aluminum, and titanium.

The optimum cone apex angle was shown by Brimmer (Ref. 44) to be near 60 deg. Borehole degasification techniques involving 3 in. diameter boreholes would limit the height of the charge. Cone diameter could be increased only by increasing cone angle. Liners utilizing 60 deg, 80 deg, and 100 deg cone angles were used in this investigation.

Explosives with velocities in the neighborhood of 8,000 meters per second are normally used in shaped charges to maximize the detonation pressure and jet penetration depth. This study included explosives having velocities between 1,800 and 8,100 meters per second. Both high explosives and coal mine permissibles were used (Table II).

Long, cylindrical, explosive charges of three to four charge diameters produce maximum penetration, while beehive shaped charges of shorter dimensions give greater penetration per unit weight of explosive (Ref. 51). Penetration of shaped charge jets from aluminum and copper does not scale for charges less than 2 in. in diameter (Ref. 45). Therefore, the penetration of a 1.0 in. diameter charge is less than one-half the penetration of a 2.0 in. diameter charge.

Model size restrictions dictated that charges with cone diameters of 0.5 in. would be necessary. Hand-loaded cylindrical charges were employed together with selected commercially available charges purchased from the Jet Research Center (JRC) (Table III). The JRC charges were machine-loaded and the explosive was pressed to 100,000 psi. Although the length-to-diameter ratio of these charges was approximately 1.0, their penetration capabilities were similar to hand-loaded cylindrical charges having length-to-diameter ratios between two and three. A uniform loading density due to pressing at high pressures could account for this.

Table II. Explosive Properties

Explosive	Type	Density (g/cm^3)	Unconfined Velocity (m/sec)
Composition C-4	H.E.	1.50	8040
Cyclonite (RDX)	H.E.	1.65	8180
DuPont 40 Special Gelatin	H.E.	1.60	3048
Atlas Coalite 5Y	permissible	0.83	1828
Atlas Coalite 5U	permissible	1.07	2590
Atlas Gelcoalite Z	permissible	1.33	4267

Table III. JRC Charge Data

Liner Material	Liner Angle (deg)	Liner Thickness (in.)	Charge Diameter (in.)	Explosive Weight (g)
Cu	100	0.021	0.5	1.1
Cu	60	0.019	0.5	1.2
Aℓ	100	0.050	0.5	1.1
Aℓ	80	0.420	0.5	1.1
Ti	100	0.021	0.5	1.1

V. EXPERIMENTAL RESULTS

Fracturing and Penetration. Penetration of shaped charge jets and resultant fracture formation were studied in three brittle materials and three ductile materials. Because of the heterogeneity and bedding planes of coal, numerous shots are necessary to define the effects of shaped charges of different liner materials and varying liner angles. For these reasons experiments were performed in Plexiglas, where visual observations could be made, and dolomite, which was readily available, as well as in coal. Jet penetration data were also obtained for steel, titanium, and lead to compare with experimental data from the literature for steel and to confirm the penetration depth versus tensile strength relationship that was observed.

Plexiglas. Models of Plexiglas were photographed (Fig. 5) during the jet penetration process, and fracture and jet velocities were calculated (Table IV). The jets from 60 deg copper liners exhibited a greater initial penetration velocity than those from 100 deg copper liners (Fig. 6), while the change in jet velocity as related to penetration distance was greater for jets from the 100 deg copper liners. The majority of the fractures caused by impact and stagnation pressure of the jet were complete in less than 100 μsec.

Aluminum liners with 100 deg apex angles were photographed utilizing standoffs of one and two cone diameters (Fig. 7) and charges fired at a 2 CD standoff produced jets with both the highest initial penetration velocity and the greatest total penetration.

Jets from 80 deg aluminum liners with varying standoff showed trends similar to those observed in 100 deg aluminum liners except

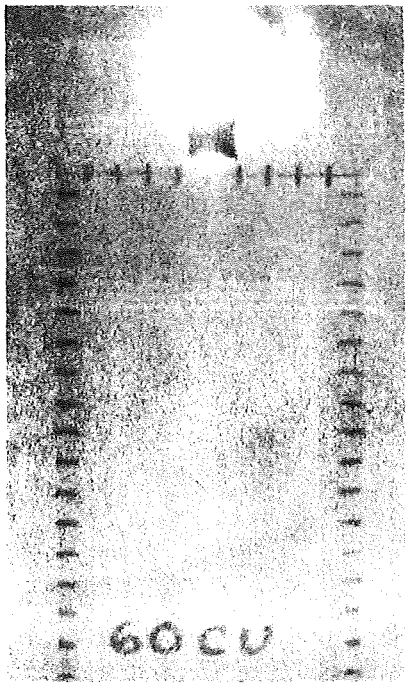

3 μsec

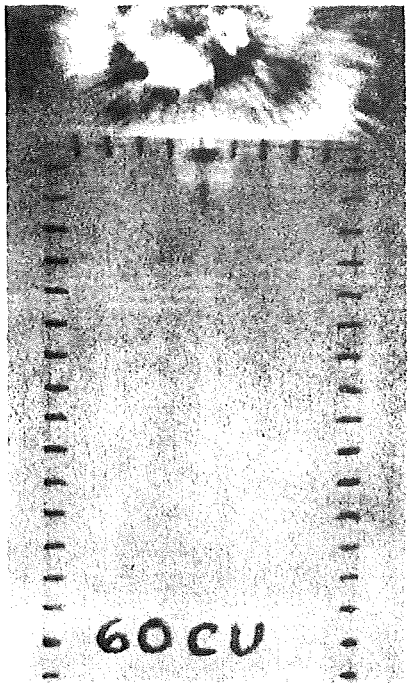

12 μsec

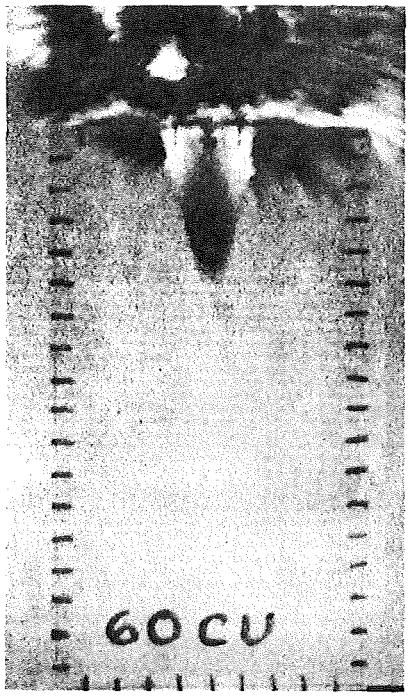

21 μsec

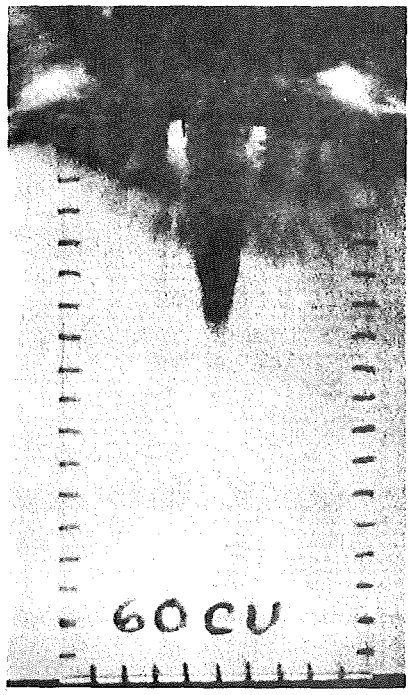

30 μsec

Fig. 5 PENETRATION OF 60° COPPER JRC IN PLEXIGLAS

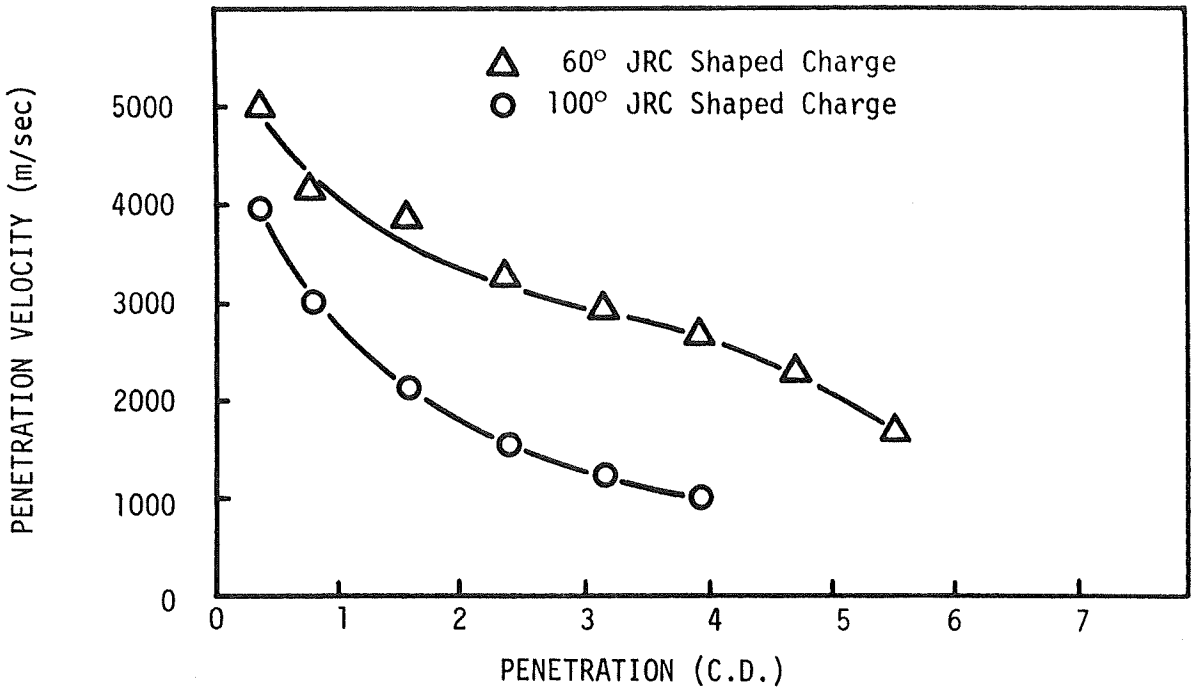

Fig. 6 PENETRATION VELOCITY FOR 60° AND 100° COPPER JRC IN PLEXIGLAS

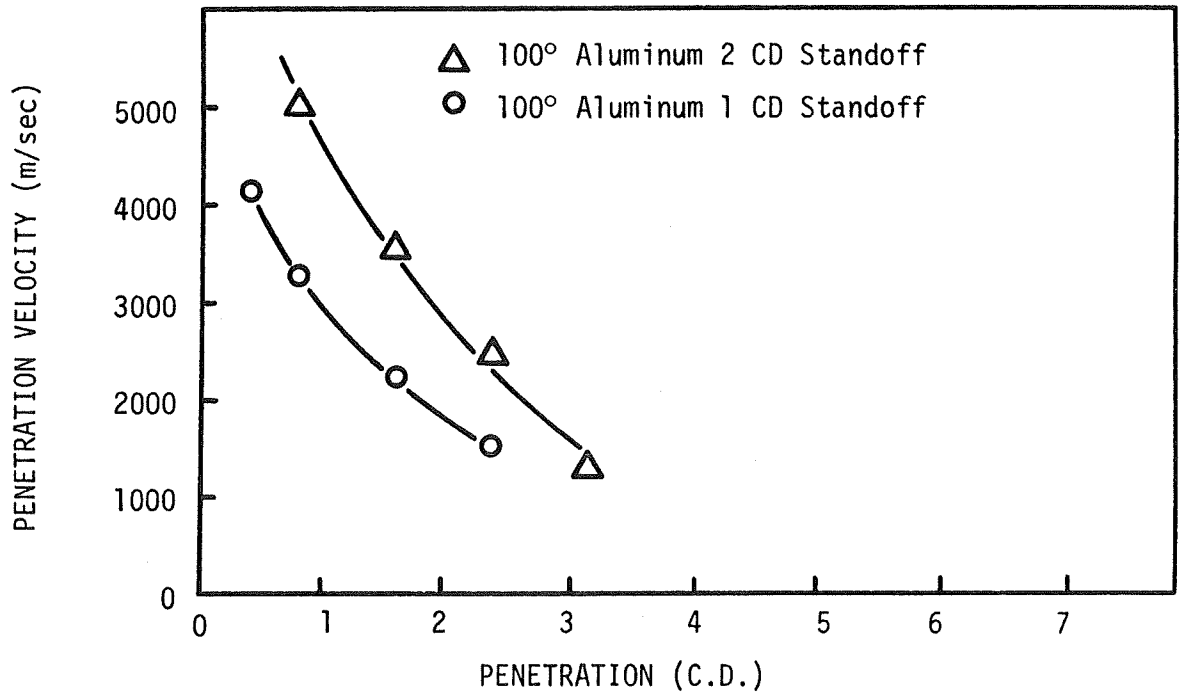

Fig. 7 PENETRATION VELOCITY FOR 100° ALUMINUM JRC IN PLEXIGLAS

TABLE IV

JET PENETRATION IN PLEXIGLAS

Shot Number	Liner Material	Liner Angle (deg)	Liner Diameter (in.)	Standoff (CD)	Penetration (in.)	Penetration (CD)
1	Cu	100	0.5	1.25	2.06	4.12
5	Cu	100	0.5	1.25	2.67	5.35
14	Cu	100	0.5	1.25	2.36	4.72
15	Cu	100	0.5	1.25	2.44	4.88
16	Cu	100	0.5	1.25	2.50	5.00
18	Cu	100	0.5	1.25	2.44	4.88
21	Cu	100	0.5	1.25	2.63	5.26
22	Cu	100	0.5	1.25	2.38	4.76
23	Cu	100	0.5	1.25	2.00	4.00
24	Cu	100	0.5	1.25	2.25	4.50
25	Cu	100	0.5	1.25	2.875	5.75
2	Cu	60	0.5	1.25	3.00	6.00
3	Cu	60	0.5	1.25	2.31	4.62
4	Cu	60	0.5	1.25	2.95	5.9
6	Cu	60	0.5	1.25	3.04	6.08
19	Cu*	60	0.5	1.25	0.38	0.76
20	Cu	60	0.5	1.25	3.00	6.0
11	Al	100	0.5	1.25	1.3	2.6
7	Al	100	0.5	2.25	1.81	3.62
10	Al	80	0.5	1.25	1.51	3.02
9	Al	80	0.5	2.25	2.15	4.30
8	Ti	100	0.5	1.25	1.26	2.52
29	Al	60	0.625	2.00	3.32	5.31

*5Y Explosive used instead of RDX

that the initial penetration velocity was greater for the liner using a 2 CD standoff (Fig. 8). Penetration velocities of jets from the 100 deg and 80 deg aluminum liners at one CD standoff were identical.

A comparison of the effect of liner material on penetration velocity (Fig. 9) of jets from 100 deg liners of the same geometry and the same standoff shows that titanium had the highest initial penetration with lower values for aluminum and copper. Titanium and aluminum jets also evidenced the greatest decrease of velocity with penetration distance. The copper liner gave the deepest penetration of the three.

Plexiglas models constructed of 0.75 in. thick plates clamped together were used to simulate bedded models. Jets from shaped charges with 100 deg copper liners shot perpendicular to the bedding demonstrated a rapid decrease in velocity in relation to penetration distance. The fracture formation relative to the position along the jet length was no longer conical in form but approached a cylindrical limit with fracturing due to tensile reflections at the interfaces as an important breakage mechanism (Fig. 10).

For comparison purposes a bedded Plexiglas model was drilled to a depth of two inches and loaded with 10 grain per foot mild detonating fuse (MDF) explosive charge. In this model the conical form of fracture was also modified by tensile reflections at the interface and was again cylindrical in outline (Fig. 11).

Holes created by shaped charges fired parallel to the bedding exhibited penetration and fracture comparable to those in homogeneous models. However, fractures induced by the jet did not cross the bedding planes but were channeled between them (Fig. 12). A similar model was drilled parallel to the bedding, loaded with 10 grain per foot MDF, and shot. The fractures likewise did not cross the bedding planes (Fig. 13).

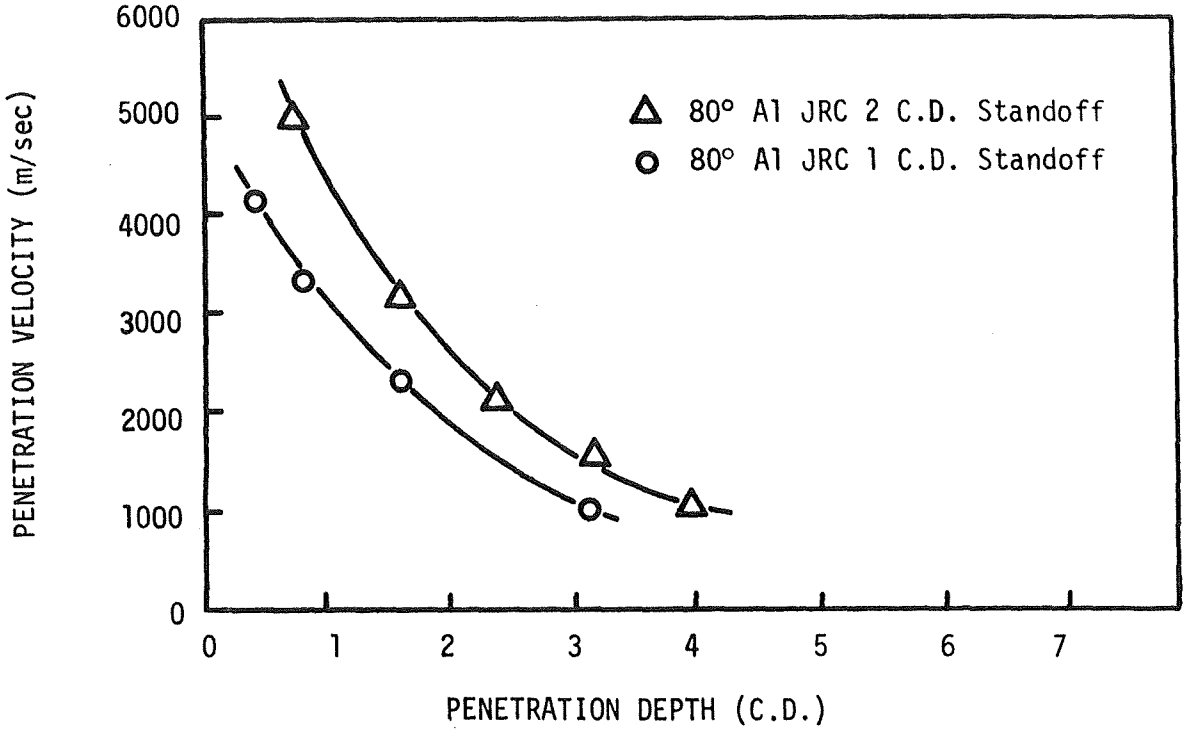

Fig. 8 PENETRATION VELOCITY FOR 80° ALUMINUM JRC IN PLEXIGLAS

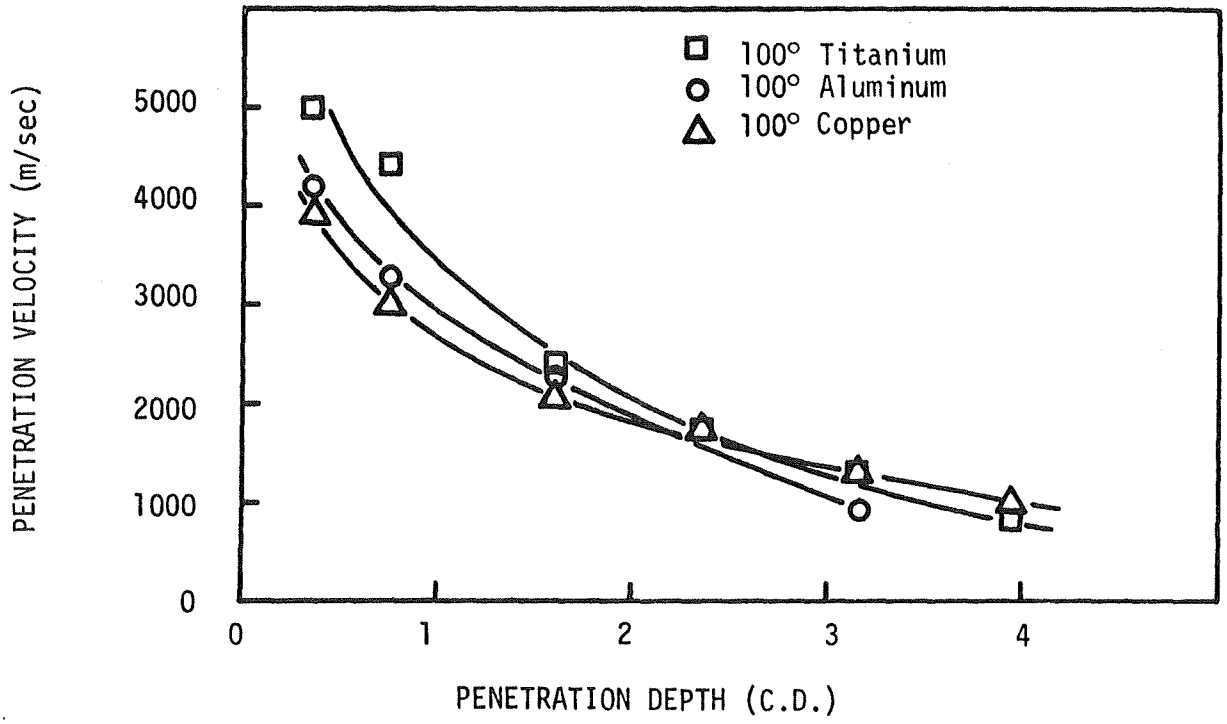

Fig. 9 PENETRATION VELOCITY FOR 100° JRC IN PLEXIGLAS

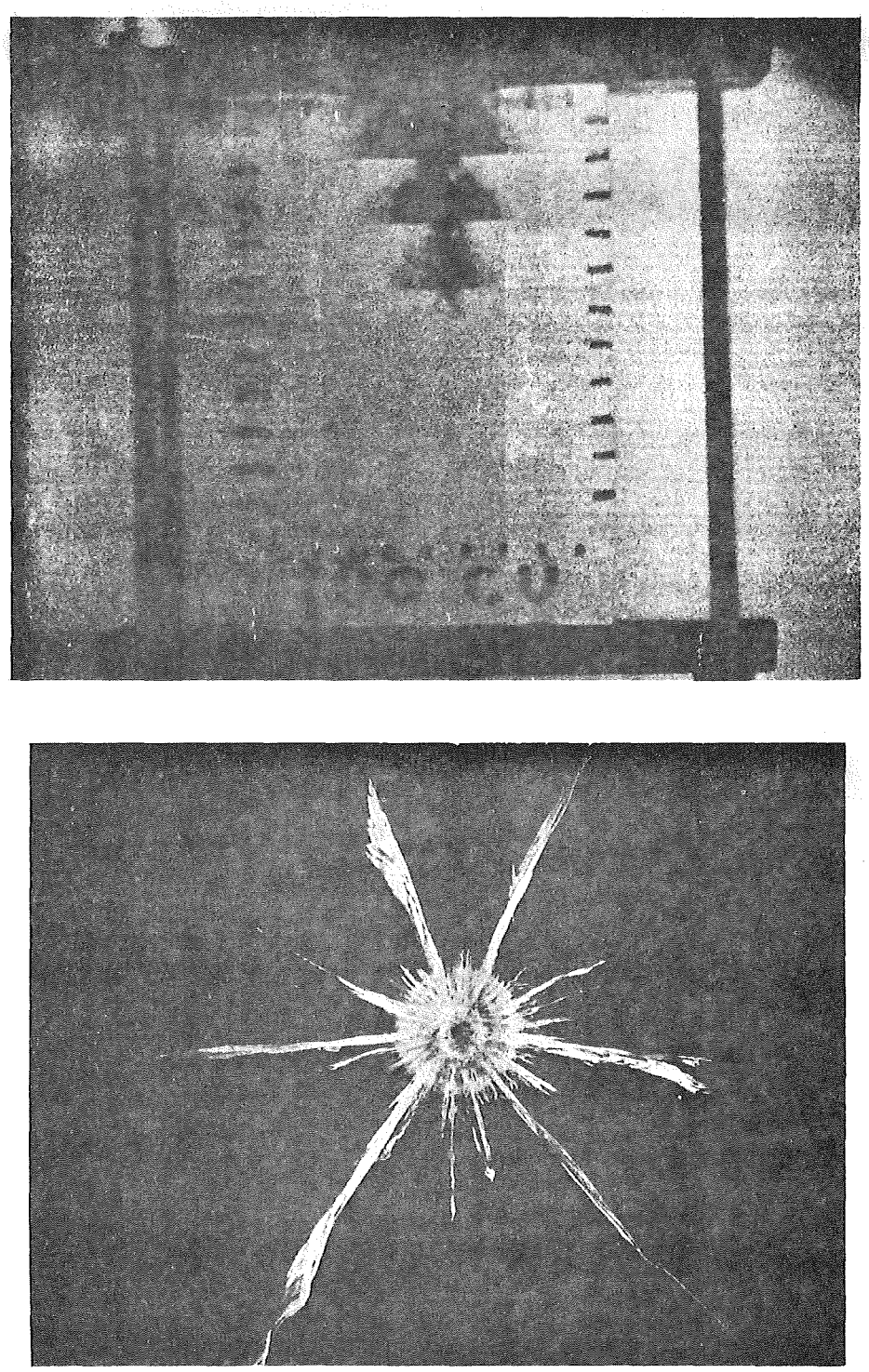

Plan View of Second Layer

Fig. 10 JET PENETRATION ACROSS PLEXIGLAS PLATES (100° COPPER JRC)

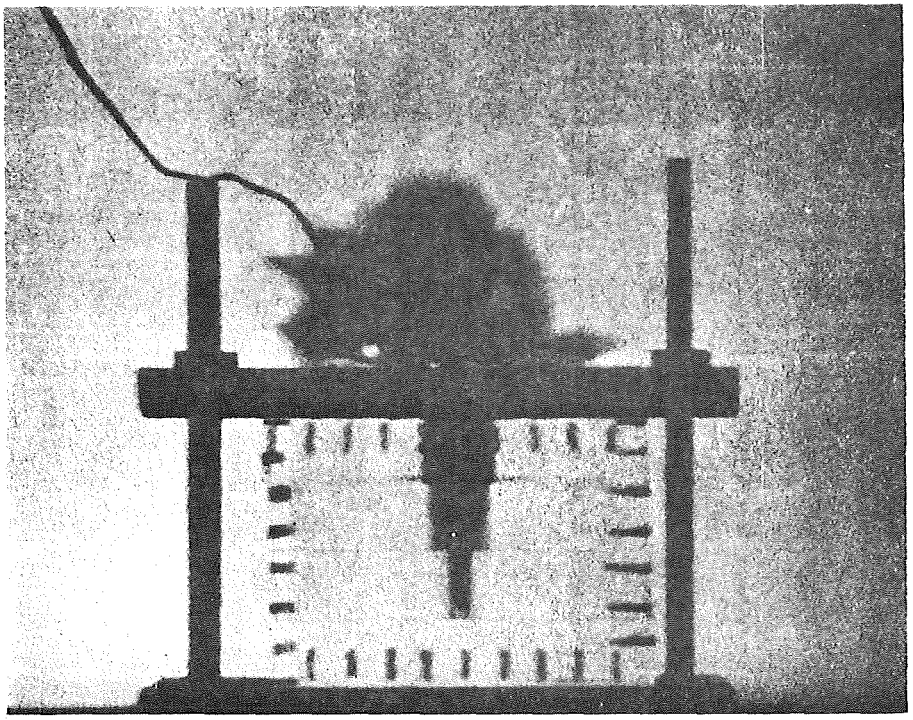

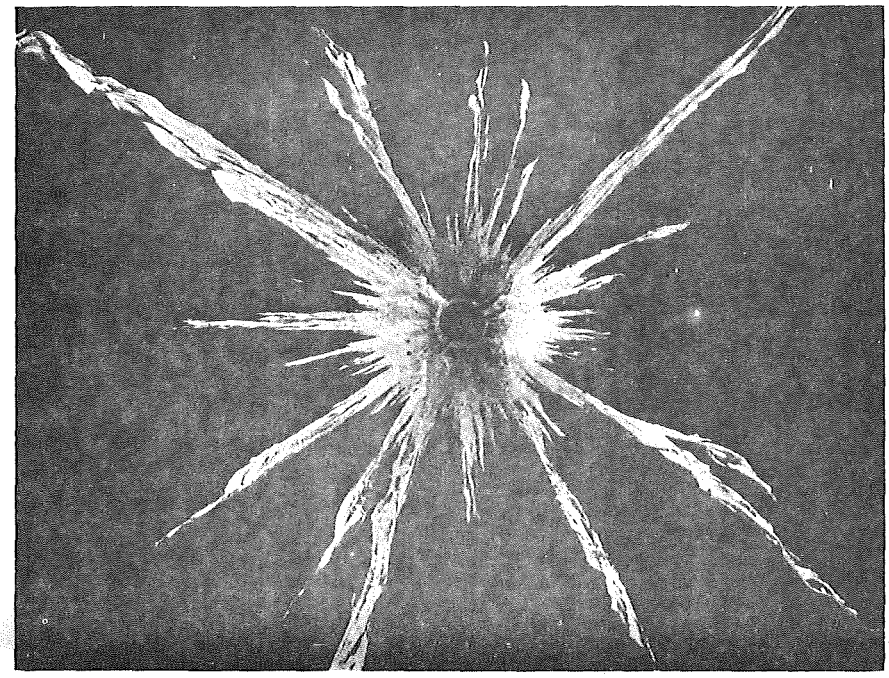

Plan View of Second Layer

Fig. 11 10 GRAIN MDF ACROSS PLEXIGLAS PLATES

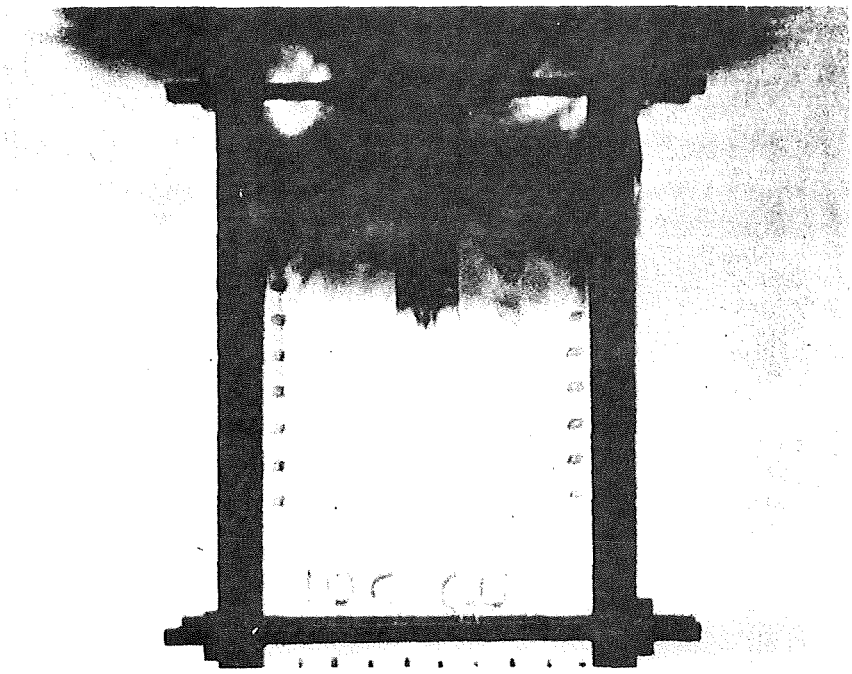

Fig. 12 JET PENETRATION PARALLEL TO PLEXIGLAS PLATES (100° COPPER JRC)

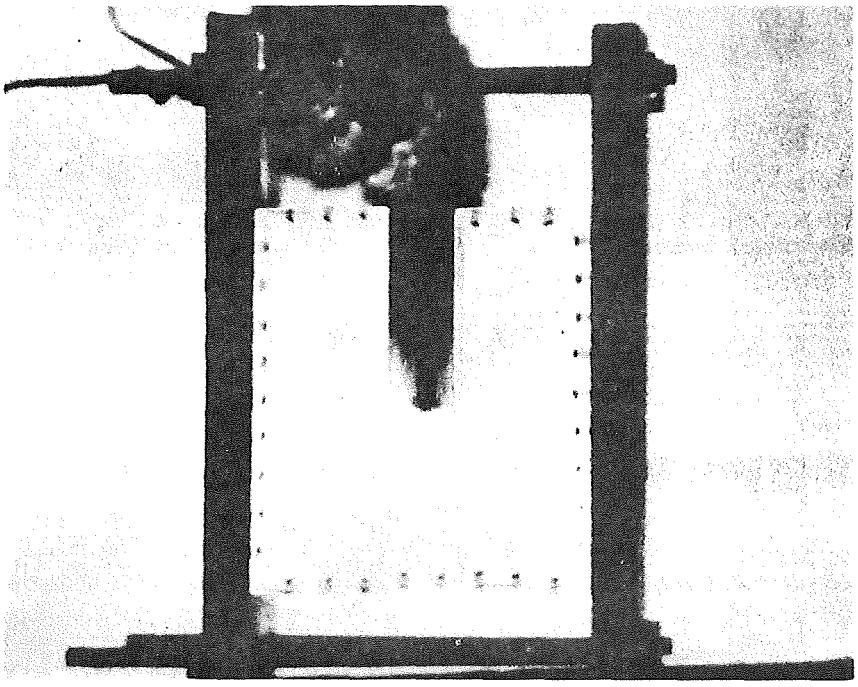

Fig. 13 10 GRAINS MDF PARALLEL TO PLEXIGLAS PLATES

A 100 deg copper lined charge was also fired into a model at a 45 deg angle with the bedding (Fig. 14), with a standoff of 2.5 CD. The initial penetration velocity was lower because of the increase in standoff, but the rate of change of velocity with penetration depth was also less (Fig. 15). This indicates that in accordance with theory there is an optimum standoff that maximizes continuous jet formation before it strikes the target.

A comparison was made of penetration and associated phenomena caused by charges with 100 deg copper liners fired at one CD standoff into homogeneous and bedded material. Penetration velocities for the initial two charge diameters were approximately the same for two jets fired into homogeneous samples and for one shot parallel to the bedding (Fig. 16), while the velocity of the jet penetrating perpendicular to the bedding decreased more rapidly possibly due to energy losses at the interfaces. A 100 deg JRC fired at one CD standoff along the plane of the interface between two tightly clamped Plexiglas blocks resulted in fractures immediately around the hole but no large fractures were formed in either block (Fig. 17). The maximum jet penetration velocity in Plexiglas was approximately 1040 meters per second.

Dolomite. Charges of 1.875 in. diameter were hand loaded with composition C-4 and Gelcoalite Z, a permissible explosive, for tests in dolomite utilizing brass and aluminum (Table V) liners with apex angles of 30 deg and 80 deg with liner thicknesses scaled to the dimensions of the 0.5 in. diameter JRC charges (Table VI). Standoff for brass liners was one CD while that for aluminum was 3 CD. Charges of composition C-4 utilizing 80 deg brass liners gave the best average penetration of 6.84 CD, and 80 deg brass liners also functioned best for

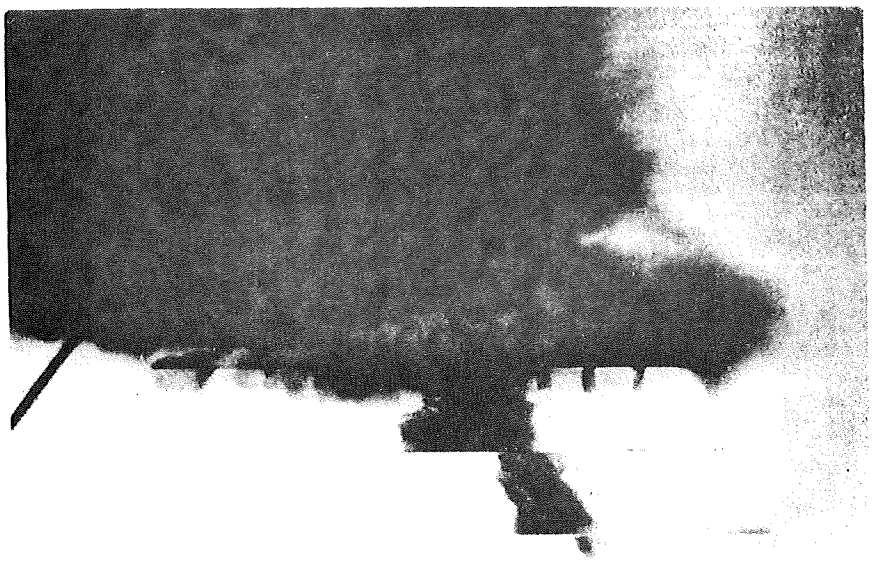

Fig. 14 JET PENETRATION FOR 100° COPPER JRC AT 45° TO PLEXIGLAS PLATES

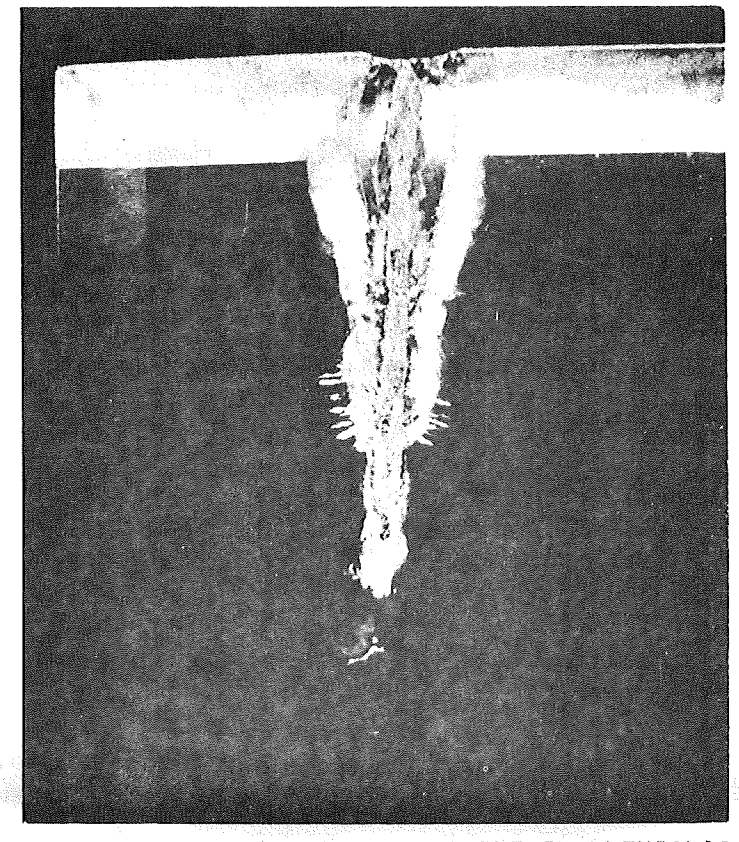

Fig. 17 JET PENETRATION PROFILE IN PLEXIGLAS

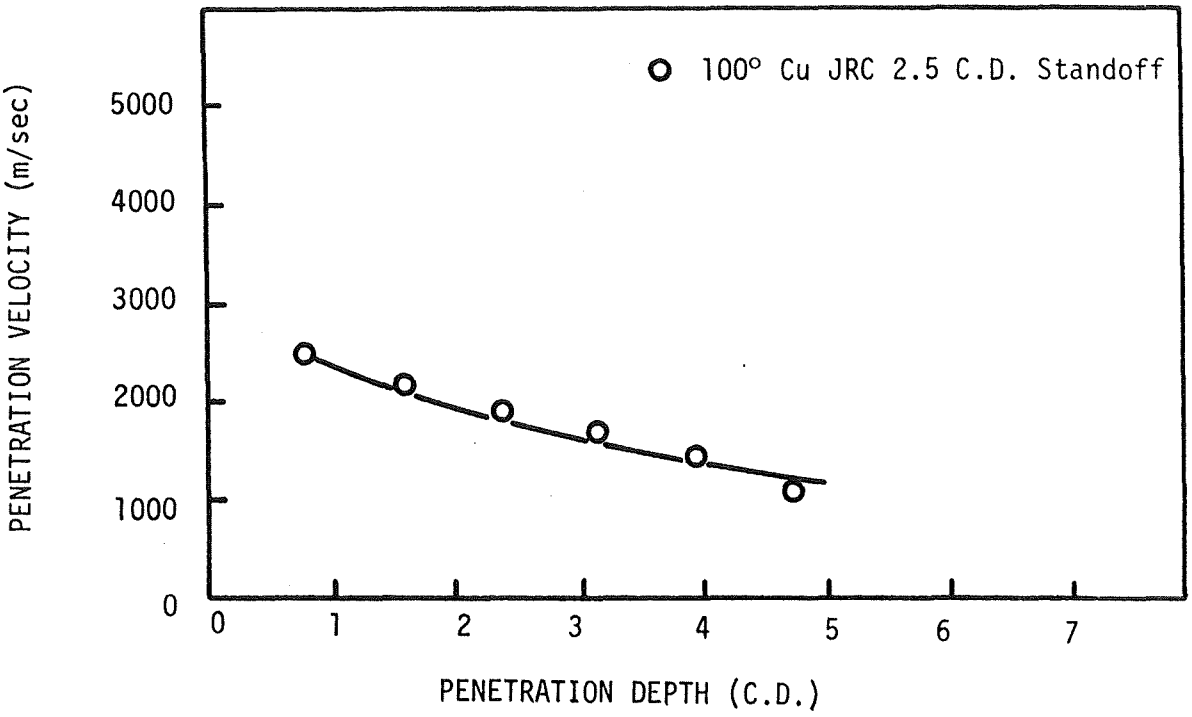

Fig. 15 PENETRATION VELOCITY AT 45° TO PLEXIGLAS PLATES

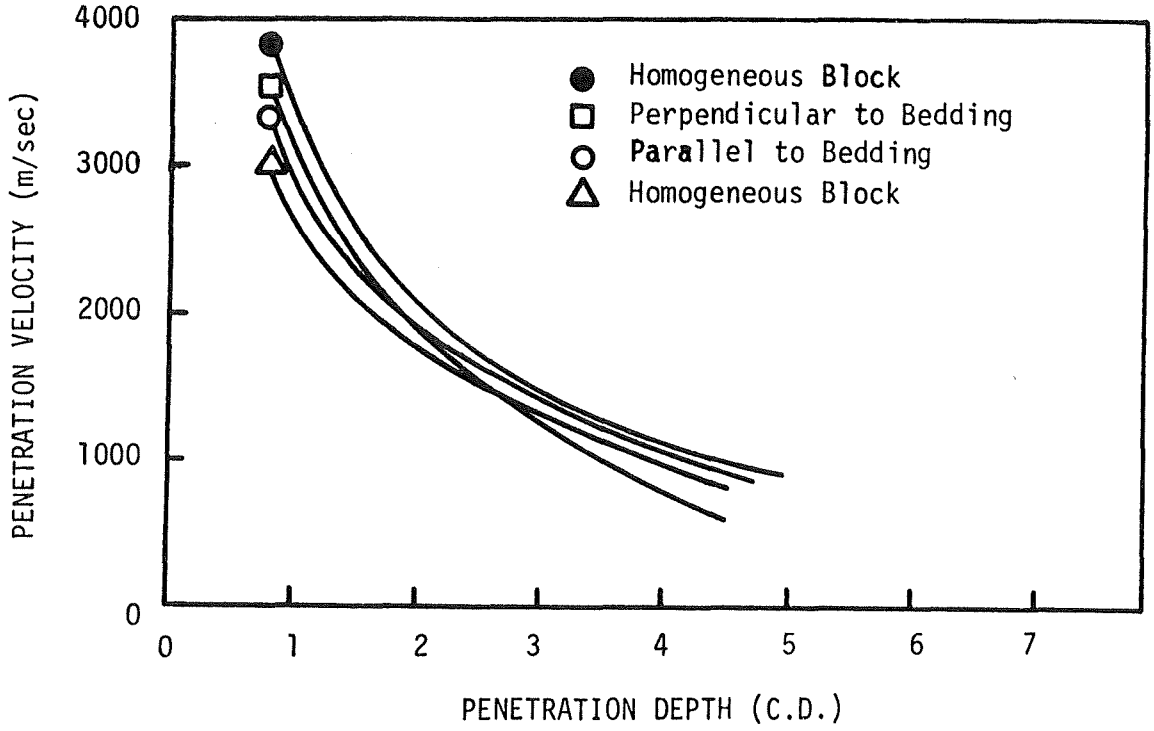

Fig. 16 PENETRATION VELOCITIES FOR 100° Cu JRC IN PLEXIGLAS

TABLE V

JET PENETRATION IN DOLOMITE FOR 1.875 IN. DIAMETER CHARGES

Liner Material	Liner Angle (deg)	Liner Thickness (in.)	Explosive	Standoff (CD)	Penetration (in.)	Penetration (CD)
Al	80	.150	Gelcoalite Z	3	3.25	1.73
Al	80	.150	Gelcoalite Z	3	2.13	2.13
Al	80	.150	Gelcoalite Z	3	3.50	1.87
Al	30	.150	Gelcoalite Z	3	2.00	1.06
Al	30	.150	Gelcoalite Z	3	2.19	1.16
Al	30	.150	Gelcoalite Z	3	2.00	1.06
Al	80	.150	C4	3	8.13	4.33
Al	80	.150	C4	3	10.13	5.4
Al	80	.150	C4	3	11.00	5.86
Al	80	.150	C4	3	10.50	5.6
Al	80	.150	C4	3	9.00	4.8
Al	80	.150	C4	3	8.25	4.4
Al	30	.150	C4	3	9.00	4.8
Brass	80	.075	C4	1	15.00	8.0
Brass	80	.075	C4	1	12.00	6.4
Brass	80	.075	C4	1	11.50	6.13
Brass	80	.075	Gelcoalite Z	1	5.00	2.67
Brass	80	.075	Gelcoalite Z	1	4.00	2.13
Brass	80	.075	Gelcoalite Z	1	4.13	2.20
80° angle cavity (no liner)			C4	1	1.0	

TABLE VI

JET PENETRATION IN GRANITE, DOLOMITE AND COAL

Liner Material	Liner Angle (deg)	Liner Diameter (in.)	Thickness (in.)	Explosive	Standoff (CD)	Penetration (in.)	Penetration (CD)	Rock Type	Bedding Orientation
Cu	55	0.813	0.030	RDX	2.2	2.125	2.61	Granite	
Cu	100	1.30	0.040	RDX	2.3	4.00	3.07	Granite	
Cu	55	0.813	0.030	RDX	2.2	3.25	3.99	Dolomite	
Cu	100	1.30	0.040	RDX	2.3	5.50	4.2	Dolomite	
Al	80	0.5	0.040	RDX	3.0	1.75	3.5	Dolomite	
Al	80	0.5	0.040	RDX	3.0	1.50	3.0	Dolomite	
Al	80	0.5	0.040	RDX	3.0	1.875	3.75	Dolomite	
Brass	60	0.625	0.040	C4	0.8	4.25	6.8	Coal	parallel
Brass	60	0.625	0.040	C4	0.8	4.75	7.6	Coal	parallel
Cu	55	0.813	0.030	RDX	2.2	8.00	9.84	Coal	parallel
Cu	55	0.813	0.030	RDX	0.6	6.25	7.68	Coal	parallel

charges loaded with Gelcoalite Z, producing a penetration of 2.3 CD.

Crater formation at the surface of the dolomite is related almost directly to standoff. A charge (80 deg liner, C-4 explosive) fired at zero standoff created a crater 5 in. in diameter and 1 in. deep (Fig. 18). As the standoff was increased, the penetration also increased and the cratering or spallation decreased (Fig. 19).

Three 0.5 in. JRC charges with 80 deg aluminum liners also were fired into dolomite, resulting in an average penetration of 3.42 CD. The calculated scaled penetration for the 1.875 in. diameter liners with scaled dimensions was 3.42 CD but the measured value was 5.06 CD for an abnormal scaling factor of 1.48 between these two charge diameters.

Steel, Titanium, and Lead. A series of tests was conducted in steel, titanium, and lead to determine the jet penetration characteristics in non-brittle materials which exhibit distinctive hydrodynamic behavior when subjected to the concentrated pressure of a shaped charge jet (Table VII). Additional tests in steel using shaped charge jets having copper, aluminum, and titanium liners were also made (Table VIII).

The cavity cross-section in titanium and steel was similar to that observed in coal, dolomite and Plexiglas, being cylindrical in form and tapered slightly toward the bottom. The cross-section in lead, however, was of conical shape with radial dimensions 4 to 5 times greater than observed in the other materials tested.

Explosive Detonation Velocity. The studies which were conducted in dolomite suggest that jet penetration for geometrically similar charges at a given standoff is a function of the detonation velocity squared (Fig. 20). Data obtained from charges with 0.5 in. diameter, 60 deg and 100 deg copper liners, fired into coal, also follow the same trend (Figs. 21 and 22).

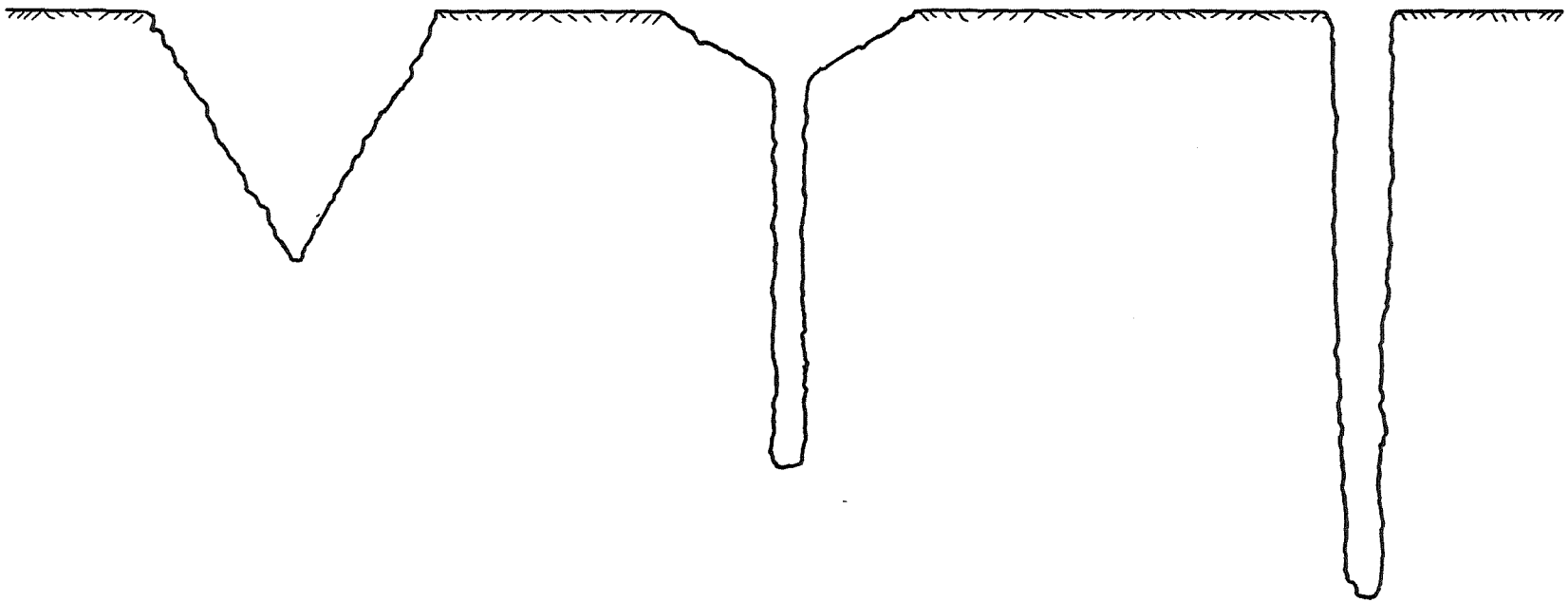

Surface Crater

Surface Crater and Hole
Formed by Jet

Hole Formed by Jet
with no Surface Crater

Fig. 18 CRATER PROFILES IN DOLOMITE

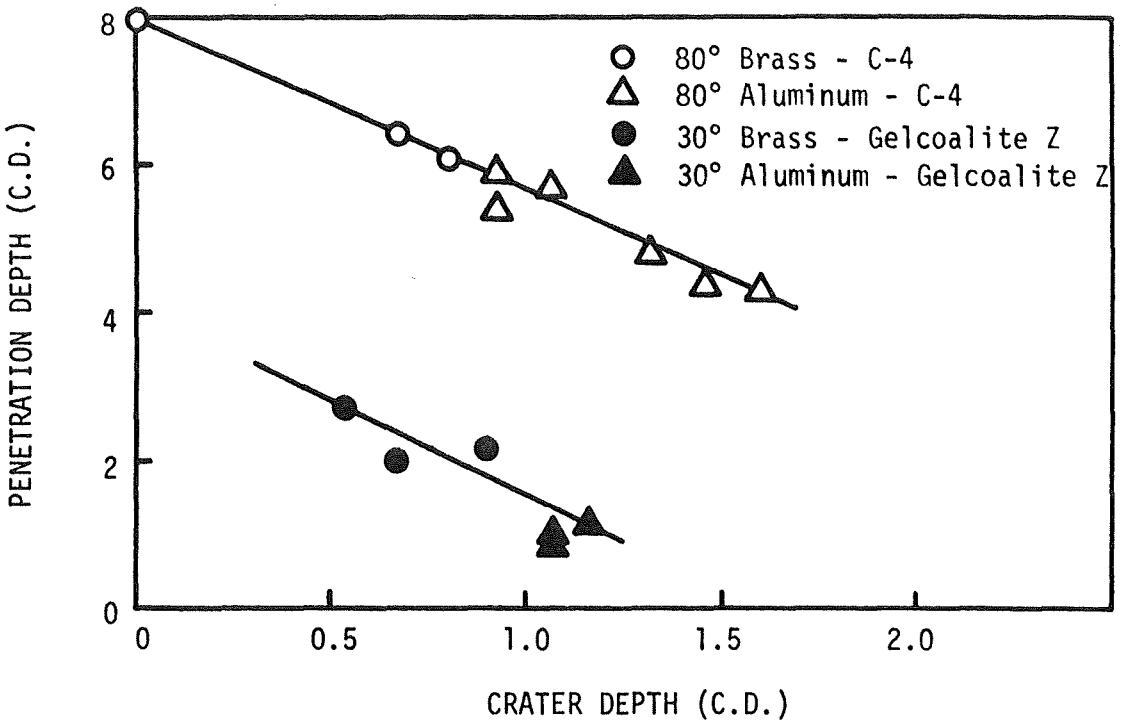

Fig. 19 PENETRATION DEPTH VS. CRATER DEPTH IN DOLOMITE

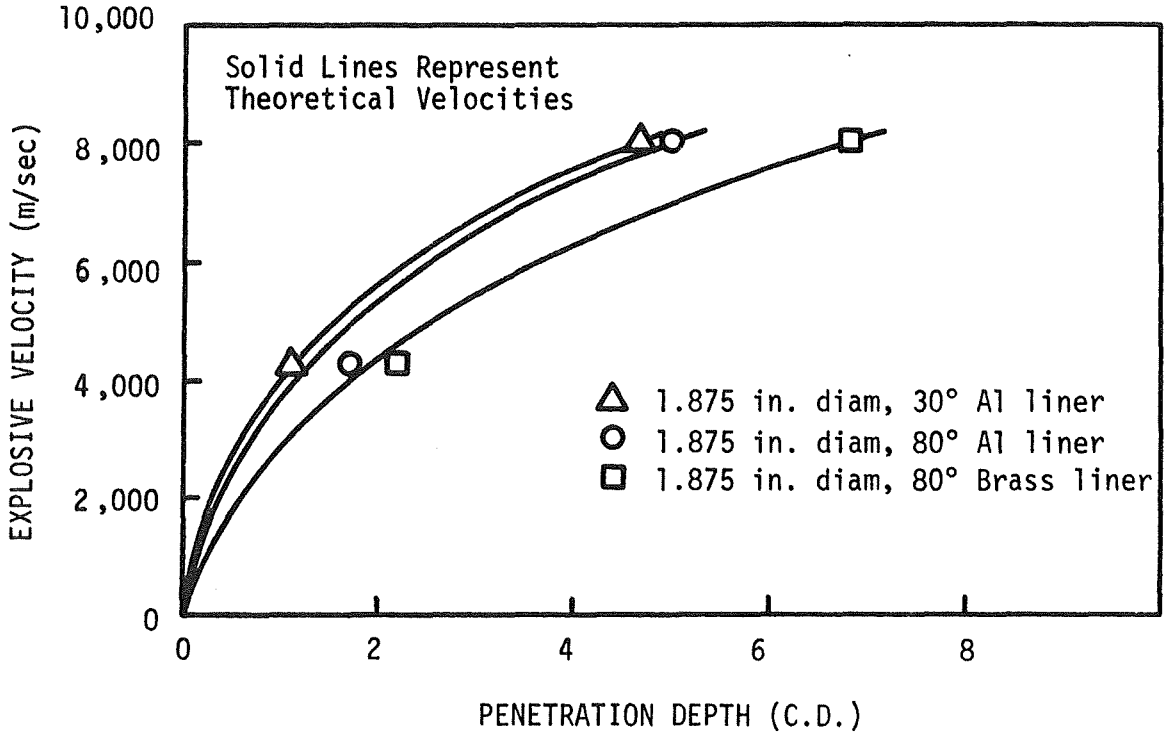

Fig. 20 EXPLOSIVE VELOCITY VS. PENETRATION DEPTH IN DOLOMITE

TABLE VII

PENETRATION DATA FOR METALLIC TARGETS

Liner Material	Liner Angle (deg)	Target Material	Penetration (cm)	(CD)	Diameter at Entry (cm)
Cu	100	Steel	1.54	1.21	0.62
Cu	60	Steel	3.50	2.75	0.50
Cu	60	Steel	2.15	1.69	0.50
Cu	60	Steel	3.81	3.00	-
Cu	60	Ti	3.50	2.75	0.43
Cu	60	Ti	3.56	2.80	0.36
Cu	100	Ti	2.03	1.60	0.36
Cu	60	Pb	6.60	5.20	2.09
Cu	60	Pb	6.42	5.06	2.10

TABLE VIII

PENETRATION TESTS IN STEEL FOR JRC CHARGES

Liner Material	Liner Angle (deg)	Standoff (CD)	Hole Diameter (in.)	Penetration (in.)	(CD)
Cu	100	1.0	0.19	0.65	1.30
Cu	60	1.0	0.22	1.42	2.84
Al	100	1.0	0.31	0.30	0.60
Al	80	1.0	0.27	0.41	0.82
Ti	100	1.0	0.31	0.26	0.52

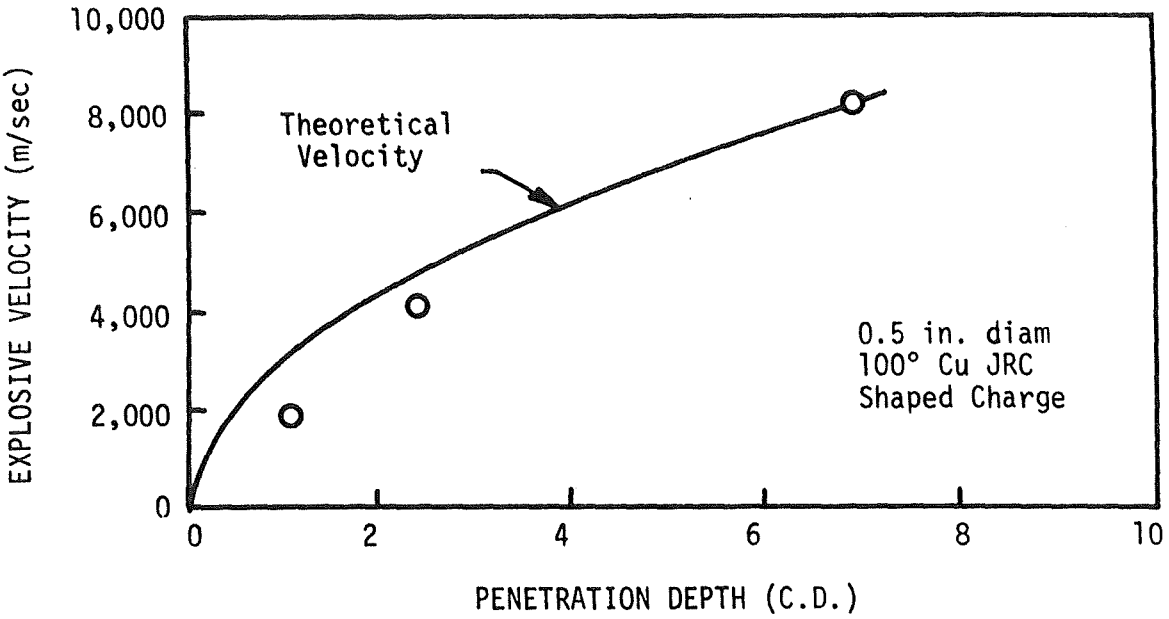

Fig. 21 EXPLOSIVE VELOCITY VS. PENETRATION DEPTH FOR 100° Cu LINER (Perpendicular to Coal Bedding)

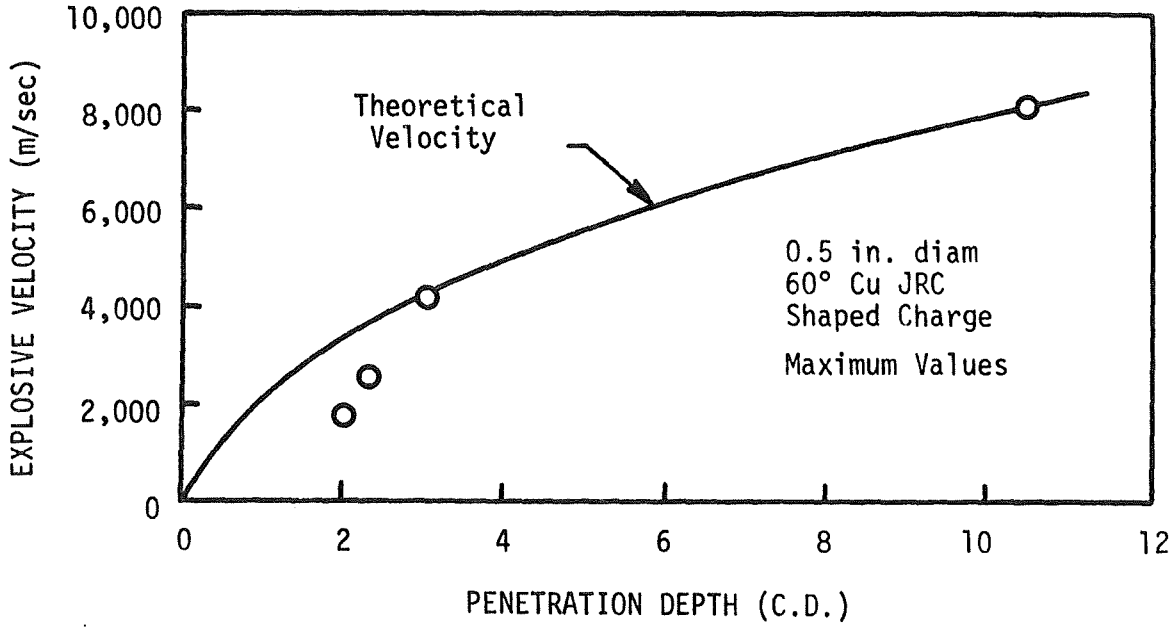

Fig. 22 EXPLOSIVE VELOCITY VS. PENETRATION DEPTH FOR 60° Cu LINER (Perpendicular to Coal Bedding)

Jet Tip Velocity. The pin oscillograph technique was employed to determine the velocity in air of the jet from a 60 deg copper JRC charge (Fig. 23). The velocity decreased to approximately 5000 meters/second after traveling about 10 cm from the charge, and maintained this velocity for the next 12 cm.

Permeability Studies of Coal. Initial permeability measurements were made on a cut block of coal to determine the magnitude of the gas flow rates through the coal and to test the equipment. Dimensions of this block were 10.75 by 10.75 by 12 in. and the sample was sealed into the permeability chamber with the top and bottom surfaces left open to permit gas flow. The specimen was oriented to test the flow of gas along the bedding planes. The rate of flow out of the face was 315 cm^3/sec with a pressure gradient of two atmospheres. The chamber was designed so that gas flow rates for the sealed faces could also be measured (Fig. 1). Three openings on each vertical side of the chamber, sealed by plugs, were provided and holes were drilled through the wax into the coal providing a variety of locations to experimentally measure the gas flow rates for various paths in the coal block. Holes were drilled through the top two openings on opposite sides, 0.5 inch in diameter and 0.375 inches deep, gas was introduced into the top of the vessel, and flow rates along and across the bedding were measured at the four side openings. The gas flow rates measured at the top opening and the center opening, on one side, parallel to the bedding planes, were 145 and 82 cm^3/sec, respectively. Flow rates measured perpendicular to the bedding were 30 and 115 cm^3/sec, respectively. A pressure gradient of two atmospheres was maintained for each test. This variation of flow rates in the same bedding orientation indicates that

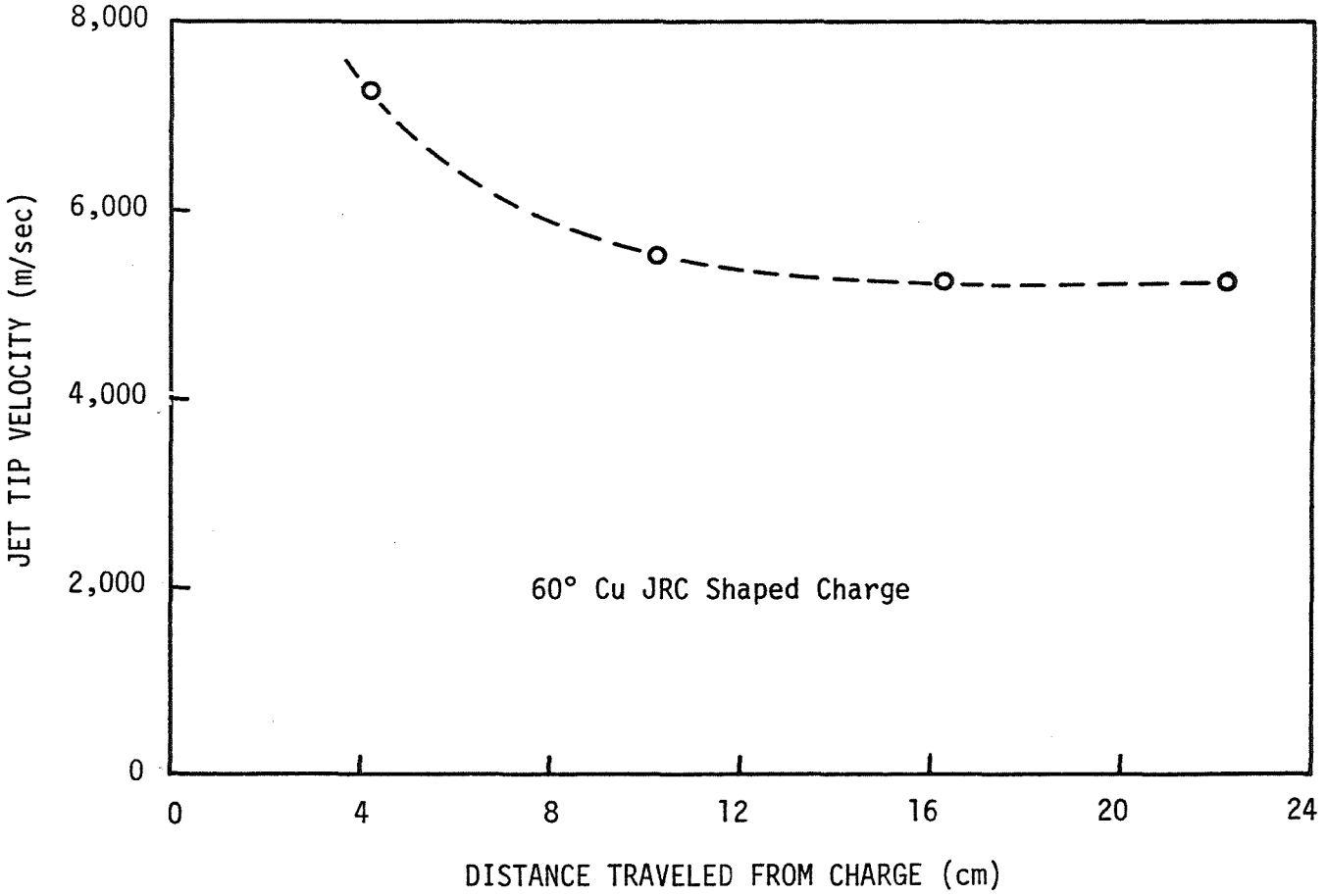

Fig. 23 JET TIP VELOCITY VS. DISTANCE TRAVELED FROM CHARGE

geologic features influence flow rates more than the micropore structure of the coal.

For standard tests homogeneous 1.25 in. cubes of sandstone were encased on four sides in "Quickmount," a quick setting epoxy resin. The epoxy bonded well to the rock and provided the necessary confinement on four sides of the sample which served as a standard to calibrate the permeability apparatus. Standard cubes were tested under three conditions, permeability graphs were drawn, and corrections made for the Klinkenberg effect (Appendix A). The experimental conditions were: 1) a specimen was moistened and placed in a 100 percent relative humidity environment for one week at 75 deg F, 2) a specimen was oven-dried for three days at 219 deg F, and 3) a specimen was oven-dried for three weeks at about 60 percent relative humidity and 75 deg F, tests being conducted for each.

The permeability sample for the two-phase (air-moisture) system is curved rather than a straight line (Fig. 24). The slopes of the room temperature and oven-dried permeabilities are essentially the same. Based on these results and the small error introduced by omitting the Klinkenberg correction (Fig. 25) the coal block permeabilities were measured under ambient conditions on the as received coal blocks.

Natural fractures in the coal seam are of two basic types, those formed during the coalification process and those formed by outside tectonic forces acting on the coal bed. Tectonic forces are responsible for the major and minor cleavage planes (cleats) in the coal. In order to determine the percentage of gas flowing through the major joints and cleats, and that through the microfractures, the permeabilities of 33 small coal blocks were measured. The samples were approximately

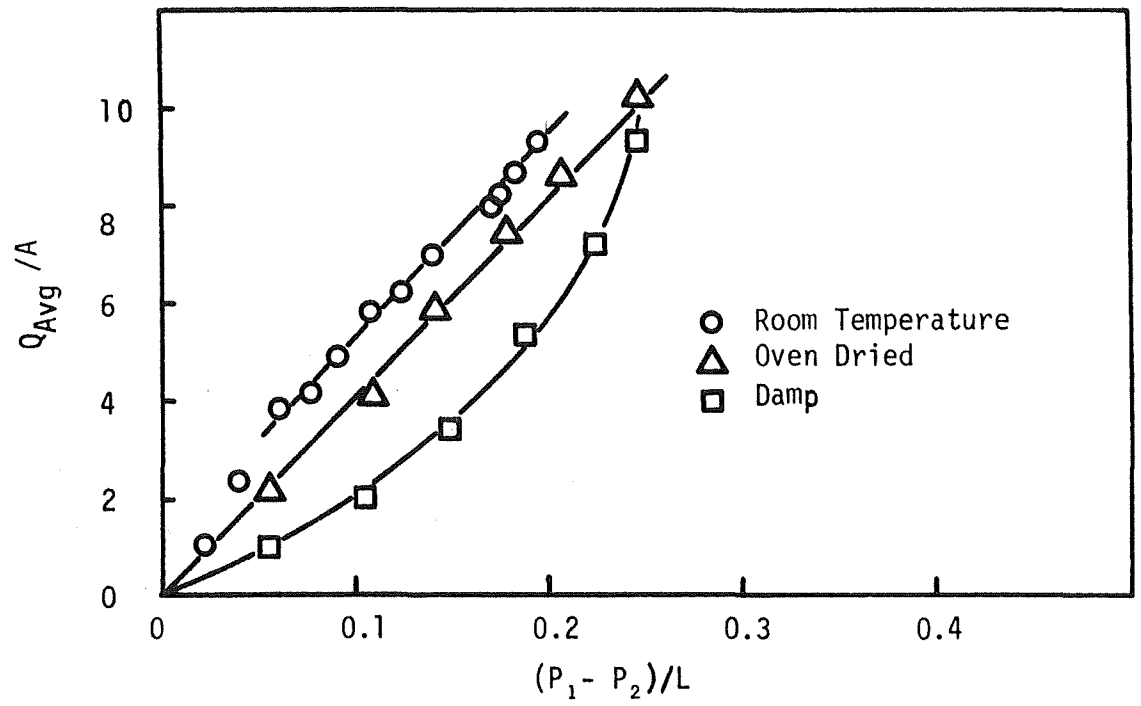

Fig. 24 PERMEABILITY OF SANDSTONE STANDARD

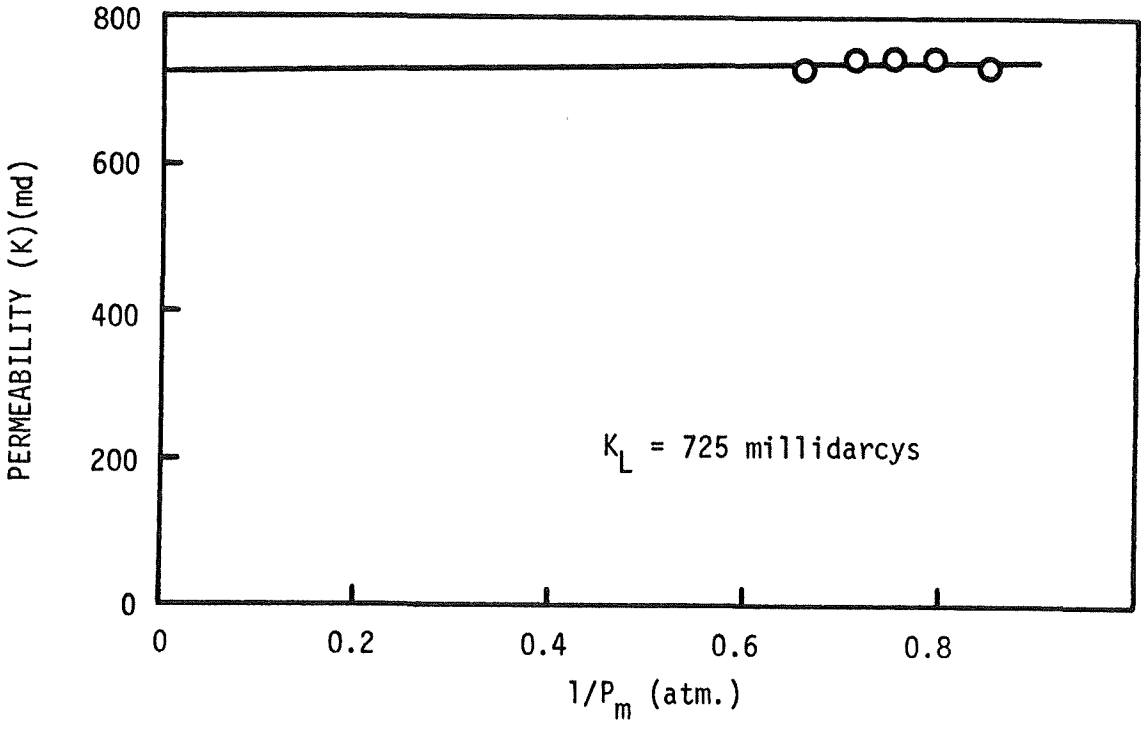

Fig. 25 KLINKENBERG CORRECTION FOR SANDSTONE

one-half inch cubes, cast in Quickmount, with the exposed faces machined parallel on a surface grinder. Twenty-five samples were cast in each bedding orientation in order to determine the effect of the bedding on flow through the microfracture system. Samples were selected such that only those without visible cleavage planes were tested for permeability, 17 being rejected. The average permeability across the bedding was 0.014 millidarcys (Table IX) while that along the bedding was 0.348 millidarcys (Table X), which confirms the findings of other investigators that the flow of gas through the microfracture systems and along the bedding planes is the dominant mode of gas migration, rather than across the strata. Microscopic examination of the coal surfaces verified that the number of fractures oriented parallel to the bedding planes was much greater than in the perpendicular direction. The gas flow rate was measured in both the forward and reverse directions on samples parallel to the bedding, which in some cases gave a different permeability value, indicating preferred directions of flow.

Preshot and postshot permeability measurements were made on 42 large coal blocks with both orientations (Tables XI and XII). Typical blocks are shown (Figs. 26 and 27) mounted in the permeability chamber. Gas flow through a coal seam is not only dependent on joint density but also on joint permeability. The pressure from deep penetrating shaped charges, such as the 60 deg copper JRC, caused joints to open and gas flow increased along these paths (Figs. 26 and 27). A section of one of the large blocks, showing the jet penetration path (Fig. 28), shows that there is a crushed zone around the hole and fractures induced beyond the periphery of the crushed zone.

TABLE IX

PERMEABILITY OF COAL SAMPLES PERPENDICULAR TO THE BEDDING PLANES

Sample Number	Area (cm^2)	Length (cm)	Permeability (millidarcys)
C-2	2.25	1.4	0.0018
C-3	2.56	1.3	0.0000
C-6	1.44	1.0	0.475
C-8	1.82	1.0	0.0000
C-10	1.82	1.2	0.0000
C-11	1.56	0.9	0.0000
C-14	1.80	1.1	0.0000
C-15	1.43	1.0	0.0000
C-16	1.69	1.3	0.1097
C-17	1.32	1.2	0.0000
C-18	1.68	0.9	0.0000
C-19	1.82	1.3	0.0549
C-20	1.82	1.1	0.0000
C-22	1.56	1.0	0.0000
C-23	1.68	1.2	0.0000

Note: Air permeability values with no Klinkenberg correction

TABLE X

PERMEABILITY OF COAL SAMPLES PARALLEL TO THE BEDDING PLANES

Sample Number	Area (cm^2)	Length (cm)	Permeability Normal (millidarcys)	Permeability Reverse (millidarcys)
C-25	1.821	1.11	0.8230	0.8230
C-28	2.041	1.11	0.2744	0.3109
C-29	1.815	1.11	0.0000	0.0000
C-30	1.815	1.11	0.0000	0.1280
C-31	1.928	1.11	0.5669	0.6219
C-32	2.13	1.14	0.5487	0.5487
C-33	1.94	1.14	0.6035	1.0059
C-34	1.77	1.14	0.0000	0.0000
C-35	1.77	1.14	0.0000	0.0000
C-36	1.77	1.14	0.0000	0.0000
C-37	1.77	1.14	0.2377	0.2377
C-38	1.61	1.14	0.0915	0.1829
C-39	1.95	1.14	0.4938	0.6767
C-40	1.77	1.14	0.5121	0.6584
C-41	1.95	1.14	0.4938	0.4938
C-45	1.88	1.14	0.3475	0.4572
C-46	1.93	1.14	0.2377	0.5304
C-47	1.61	1.14	0.3292	0.3292

Note: Air permeability values with no Klinkenberg correction

TABLE XI

PERMEABILITY OF COAL BLOCKS 1 THROUGH 25

Block Number	Area (cm^2)	Length (cm)	Bedding Orientation	Permeability Preshot Normal (darcys)	Permeability Preshot Reverse (darcys)	Permeability Postshot Normal (darcys)	Permeability Postshot Reverse (darcys)	Liner Angle (deg)	Liner Material	Penetration (CD)	Standoff (CD)
1	--	--	along	--	--	--	--	100	Cu	--	1.25
2	--	--	across	--	--	--	--	100	Cu	8.0	1.25
3	--	--	along	--	--	--	--	100	Cu	8.0	1.25
4	--	--	across	--	--	--	--	100	Cu	7.0	1.25
5	--	--	across	--	--	--	--	100	Cu	8.0	1.25
6	--	--	along	--	--	--	--	60	Cu	12.0	1.25
7	--	--	across	--	--	--	--	100	Cu	6.0	1.25
8	413	14.0	across	1.170	1.170	2.850	2.850	60	Cu	11.0	1.25
9	613	21.6	across	1.280	0.585	9.570	9.570	60	Cu	9.0	1.25
10			along					100	Ti	1.5	1.25
11	439	22.9	along	0.384	1.335	4.700	4.700	60	Cu	12.0	1.25
12	323	15.2	across	2.469	6.986	4.974	5.340	60	Cu	8.5	1.25
13	448	23.5	along	4.792	8.176	7.627	9.346	60	Cu	9.0	1.25
14	387	26.7	along	5.230	7.243	4.180	3.548	100	Al	9.25	2.25
15	448	25.4	along	5.907	9.620	4.060	3.658	100	Al	7.5	2.25
16	310	25.4	across	8.176	7.407	11.614	11.614	100	Al	7.5	2.25
17	548	17.8	across	2.944	2.944	5.725	3.109	80	Al	7.0	2.25
18	232	24.8	along	1.829	2.743	5.715	5.715	80	Al	8.5	2.25
19	329	19.1	across	4.902	4.902	7.316	6.584	80	Al	7.25	2.25
20	339	24.1	across	14.028	14.028	17.869	10.261	100	Cu	7.25	1.25
21	413	24.8	across	3.841	3.841	6.529	8.743	100	Cu	6.5	1.25
22	316	24.8	across	1.353	2.286	10.059	10.059	100	Cu	5.5	1.25
23	328	18.4	across	5.926	7.188	19.442	10.059	100	Cu	7.5	1.24
24	436	25.4	across	6.010	5.395	8.486	10.370	100	Cu	6.25	1.25
25	169	19.7	along	3.493	3.493	12.254	12.254	100	Cu	6.5	1.25

TABLE XII

PERMEABILITY OF COAL BLOCKS 26 THROUGH 42

Block Number	Area (cm^2)	Length (cm)	Bedding Orientation	Permeability Preshot Normal (darcys)	Permeability Preshot Reverse (darcys)	Permeability Postshot Normal (darcys)	Permeability Postshot Reverse (darcys)	Liner Angle (deg)	Liner Material	Penetration (CD)	Standoff (CD)
26	429	18.42	across	1.682	1.682	1.770	1.770	100	Cu	7.2	1.25
27	542	19.05	across	3.109	3.109	3.402	3.402	100	Al	6.8	2.25
28	413	17.78	across	4.572	4.572	3.365	3.365	100	Al	4.0	2.25
29	581	14.73	across	4.188	4.188	2.725	2.725	80	Al	9.0	2.25
30	377	25.40	along	7.609	7.609	7.609	7.609	100	Cu	9.6	1.25
31	377	18.42	along	8.633	8.633	8.633	8.633	100	Cu	8.2	1.25
32	232	18.73	along	7.225	7.225	9.145	9.145	100	Al	6.6	2.25
33	234	24.13	along	12.855	19.259	21.691	21.691	80	Al	6.6	2.25
34	348	25.40	along	13.990	13.990	13.990	13.990	80	Al	8.0	2.25
35	362	19.05	along	10.041	10.041	8.231	8.231	60	Cu	7.0	0.25
36	362	19.05	along	4.295	4.295	6.182	6.182	60	Cu	9.8	0.25
37	515	19.56	along	1.769	1.769	4.340	2.613	60	Cu	11.2	0.25
38	298	20.07	along	5.167	5.167	8.633	8.633	80	Al	4.0	0.25
39	311	19.56	along	9.236	9.236	6.559	6.559	80	Al	2.8	0.25
40	364	19.68	along	5.219	5.219	3.886	3.886	80	Al	3.0	0.25
42*	872	29.21	across	2.360	2.360	1.541	1.541	20	Brass	2.4	0.00

*Brass liner 1.0 in. diameter.

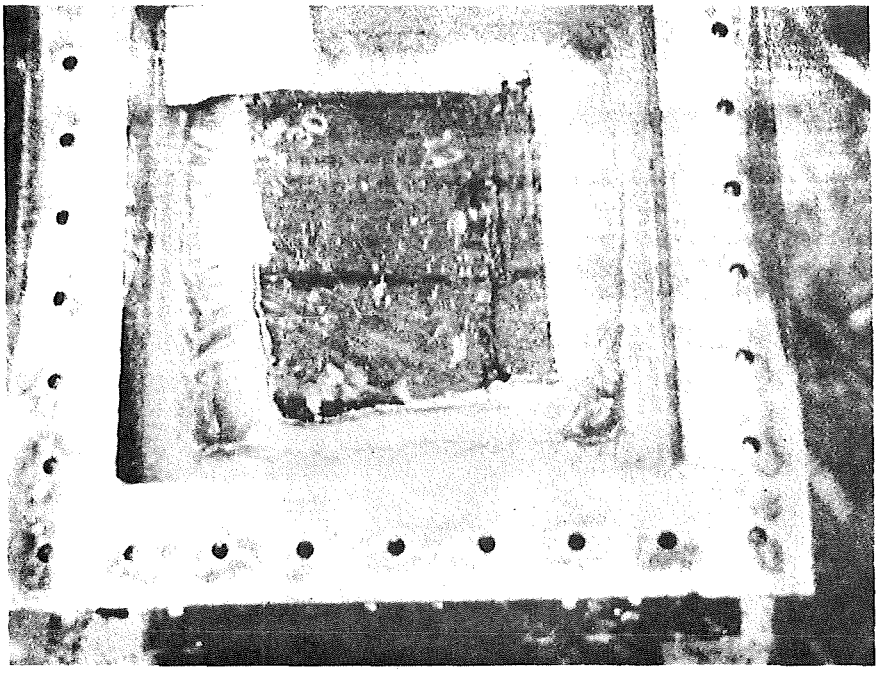

Preshot

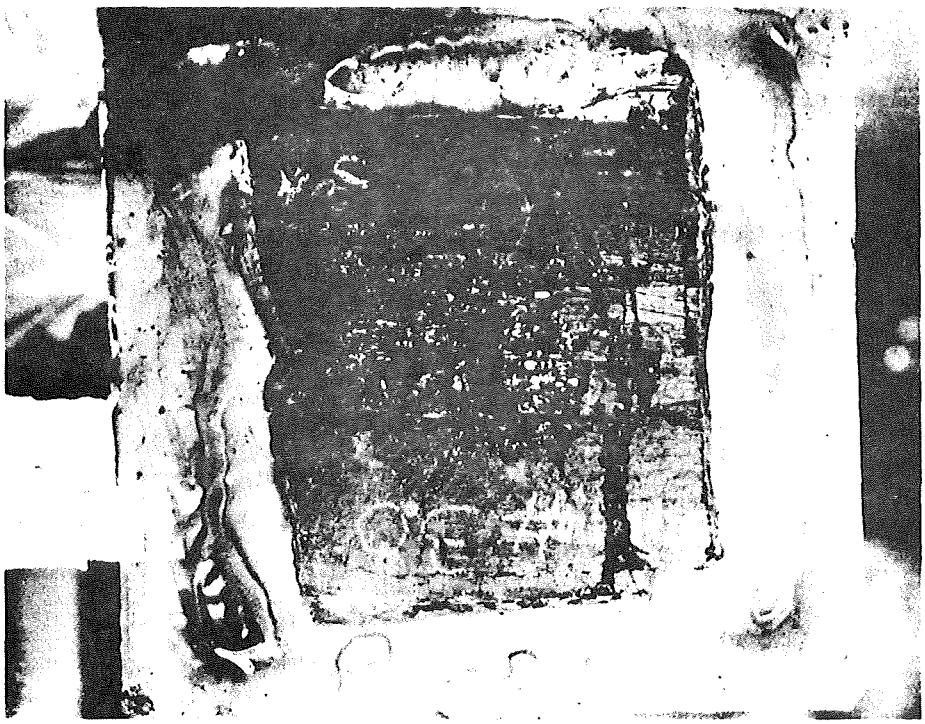

Postshot

Fig. 26 FRACTURE FORMATION IN COAL DUE TO SHAPED CHARGE JET FORMATION (Parallel to Bedding)

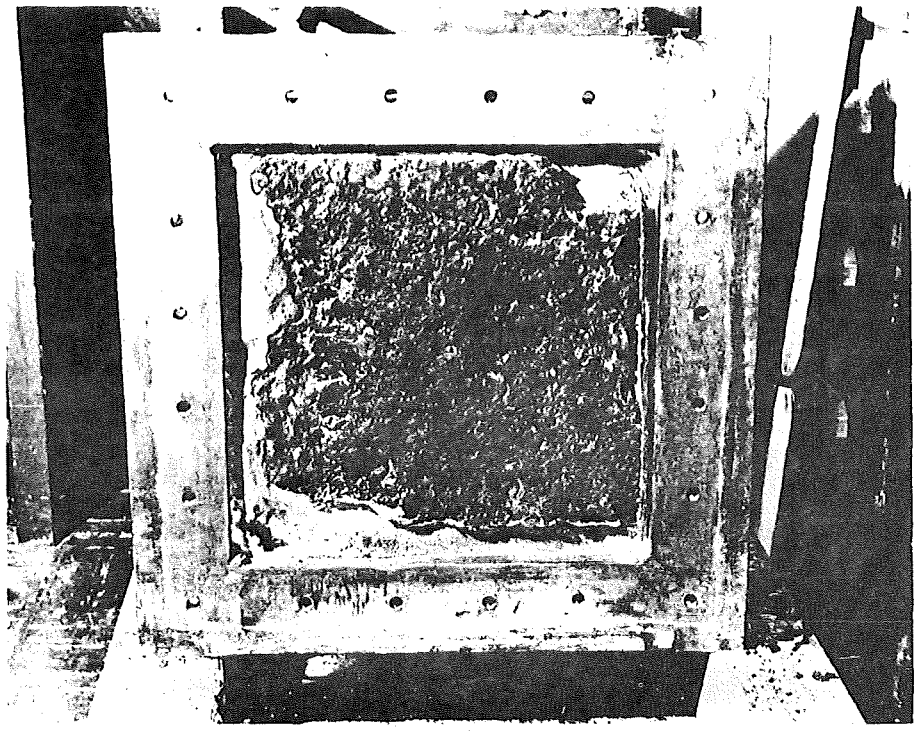

Preshot

Postshot

Fig. 27 FRACTURE FORMATION IN COAL DUE TO SHAPED CHARGE JET PENETRATION (Perpendicular to Bedding)

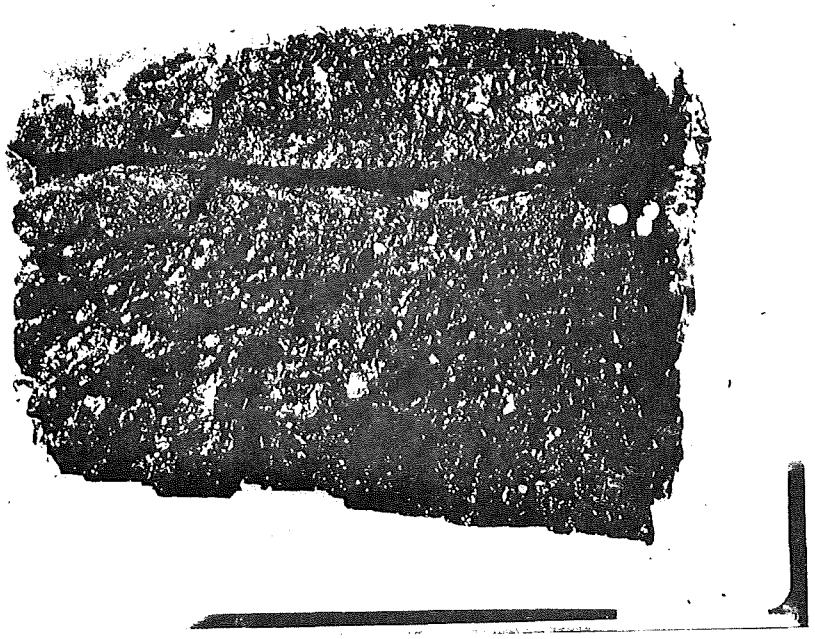

Fig. 28 HOLE PROFILE IN COAL DUE TO SHAPED CHARGE JET PENETRATION

Permeability tests on samples 5 through 25 (Table XI) indicated a preferred direction of flow. This effect was not observed in samples 26 through 42, which were obtained from a different face in the mine. The preshot values varied widely, which would be expected since permeability is not only dependent on the fracture density but also on the continuity of these fractures.

Measured gas flow rates for small solid coal blocks (Table XIII) and for some of the large blocks (Table XIV) are given as a function of the pressure gradient and the bedding orientation. Typical preshot and postshot plots for some large blocks (Figs. 29 to 33) showed an increase in permeability. For one of the small unfractured blocks, samples C-12, flow is much smaller, and increases linearly with increase in pressure gradient (Fig. 34).

Two preliminary shots were made into large coal blocks to determine the approximate extent of penetration and crushing around the hole created by jets from 0.625 in. brass cones. The explosive employed was composition C-4 with a 0.75 in. charge diameter, 3.6 CD (2.25 in.) length, and standoff of 2 CD (1.25 in.). The coal blocks were embedded in tamped sand to furnish a moderate confinement.

Relatively limited fracturing was obtained when a blast shield of 0.5 in. steel plate was employed with a 0.5 in. hole to allow only the passage of the jet (Fig. 35). The penetration was 6.8 cone diameters (4.25 in.) with a conical crushed zone 2.0 in. depth and 3.0 in. in diameter. A second block was subjected to the same size charge without a blast shield (Fig. 36). The crushed zone was much larger in this case and the block was parted along some of the bedding planes. Existing fractures were opened up, new fracture systems produced, some sections of the coal were displaced against the confinement of the damp

TABLE XIII

FLOW RATES IN SMALL SPECIMENS (cm^3/sec)

Flow Rates at the Indicated ΔP(cm^3/sec)

Sample No.	Area (cm^2)	Length (cm)	5 psi	10 psi	15 psi	20 psi	25 psi	30 psi	Orientation to Bedding
A-1-B	15.6	4.2	25	50	81.66	106.66	145.83	185	⊥
A-1-B	15.6	4.2	25	51.66	84.50	117.50	151.66	185	⊥
A-1-B	15.6	4.2	25	51.66	81.66	113.33	144.16	195	⊥
A-1-B*	15.6	4.2	17.50	35.83	60	84.16	108.3	135	⊥
B-1-B	10.08	3.15	0.68	1.36	2.50	4.00	5.25	6.75	∥
B-1-B	10.08	3.15	0.68	1.66	2.91	4.00	5.75	6.75	∥
B-1-B	10.08	3.15	0.68	1.58	2.91	4.00	5.61	7.41	∥
B-1-B*	10.08	3.15	0.83	1.86	3.33	5.08	6.91	8.66	∥
B-2-B	8.91	3.0	0.45	1.45	2.41	3.45	4.16	5.25	⊥
B-2-B	8.91	3.0	0.43	1.66	2.61	3.58	4.61	5.25	⊥
B-2-B*	8.91	3.0	0.45	1.86	2.90	3.86	4.91	6.05	⊥
B-3-B	8.99	3.1	0	0	0.01	0.04	0.06	0.09	⊥
B-3-B	8.99	3.1	0	0	0.01	0.04	0.06	0.09	⊥
B-3-B*	8.99	3.1							⊥
B-4-B	9.97	2.9	0	0	0.01	0.02	0.05	0.07	⊥
B-4-B	9.97	2.9	0	0	0.01	0.03	0.05	0.08	⊥
B-4-B	9.97	2.0	0	0	0.01	0.04	0.05	0.08	⊥
B-4-B*	9.97	2.9	0	0	0.02	0.04	0.07	0.09	⊥

*These measurements were made with a reversed gas flow

TABLE XIII

Flow Rates in Small Specimens (cm^3/sec) - continued

Sample No.	Area (cm^2)	Length (cm)	5 psi	10 psi	15 psi	20 psi	25 psi	30 psi	Orientation to Bedding
C-1-B	2.32	1.35	21.66	38.33	54.16	68.33	80.83	95.00	⊥
C-1-B	2.32	1.35	21.66	38.33	52.50	68.33	80.83	95.00	⊥
C-1-B	2.32	1.35	21.66	38.33	52.50	68.33	80.33	94.16	⊥
C-1-B*	2.32	1.35	17.50	32.50	45.00	59.16	71.66	80.83	⊥
C-2-A	2.40	1.25	0	0	0	0	0	.02	⊥
C-3-A	2.48	1.30	0	0	0	0	0	0	⊥
C-4-B	5.17	1.3	0.11	0.36	0.80	1.20	1.33	2.00	⊥
C-4-B	5.17	1.3		0.36	0.80		1.58	2.00	⊥
C-4-B	5.17	1.3		0.50	0.80		1.40	1.78	⊥
C-4-B*	5.17	1.3		0.42	0.80	1.12			⊥

*Measurements with reversed gas flow

Samples C-2-A and C-3-A at higher pressures

Sample No.	30 psi	40 psi	50 psi	60 psi	70 psi	80 psi	90 psi	100 psi
C-2-A	0.02	0.05	0.12	0.35				
C-2-A	0.05	0.10	0.21	0.54				
C-2-A	0.05	0.09	0.20	0.54				
C-2-A*	0.05	0.10	0.24	0.55				
C-3-A**	0	0	0	0	0	0	0	0
C-3-A**	0	0	0	0	0	0	0	0

*These measurements were made with a reversed gas flow
**Pressure Held at 100 psi for 25 min.

TABLE XIV

FLOW RATES IN LARGE BLOCKS

Input Press. psi	Block 2 Flow cc/sec	Block 3 Flow cc/sec	Block 4 Flow cc/sec
Before Shot			
2.5	176.6	188.3	178.37
5	240.0	240.0	255.0
6	266.6		
7	283.3		
7.5		301.6	310.0
8	310.0		
9	321.6		
10	340.0	343.3	348.3
12.5		378.3	381.6
15			
After Shot			
2.5	193.3	190.0	150.0
5	246.6	240.0	221.66
6	266.6		
7	290.0		
7.5		280.0	278.33
8	301.6		
9	18.3		
10	335.0	310.0	318.33
12.5		340.0	351.66
15		356.6	375.00
17.5		368.3	
20.0		391.6	

Block Number 2 and 4 were tested perpendicular to the bedding planes while Block Number 3 was tested parallel to the bedding planes.

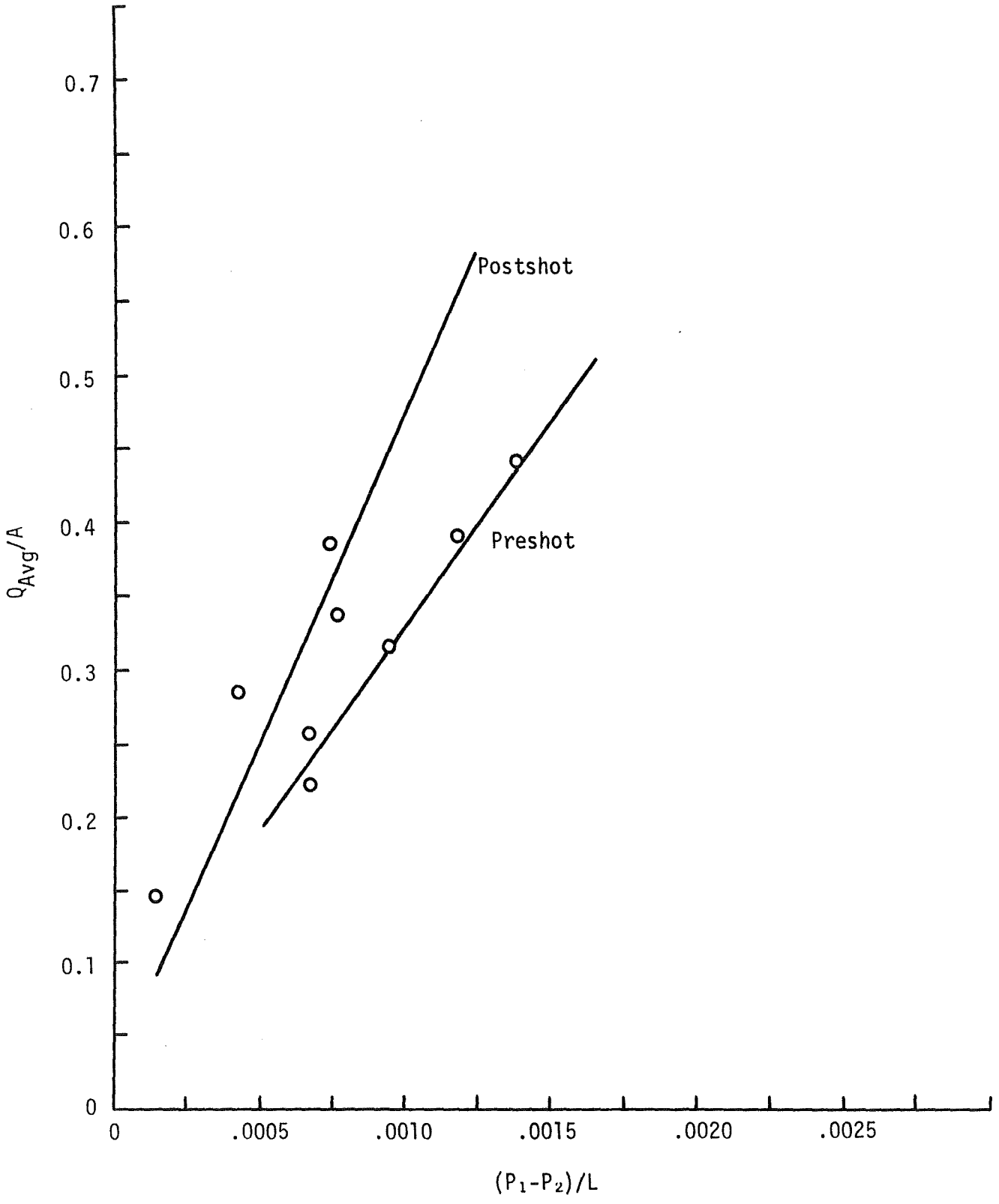

Fig. 29 Q_{Avg}/A vs. $(P_1-P_2)/L$ - BLOCK NO. 6

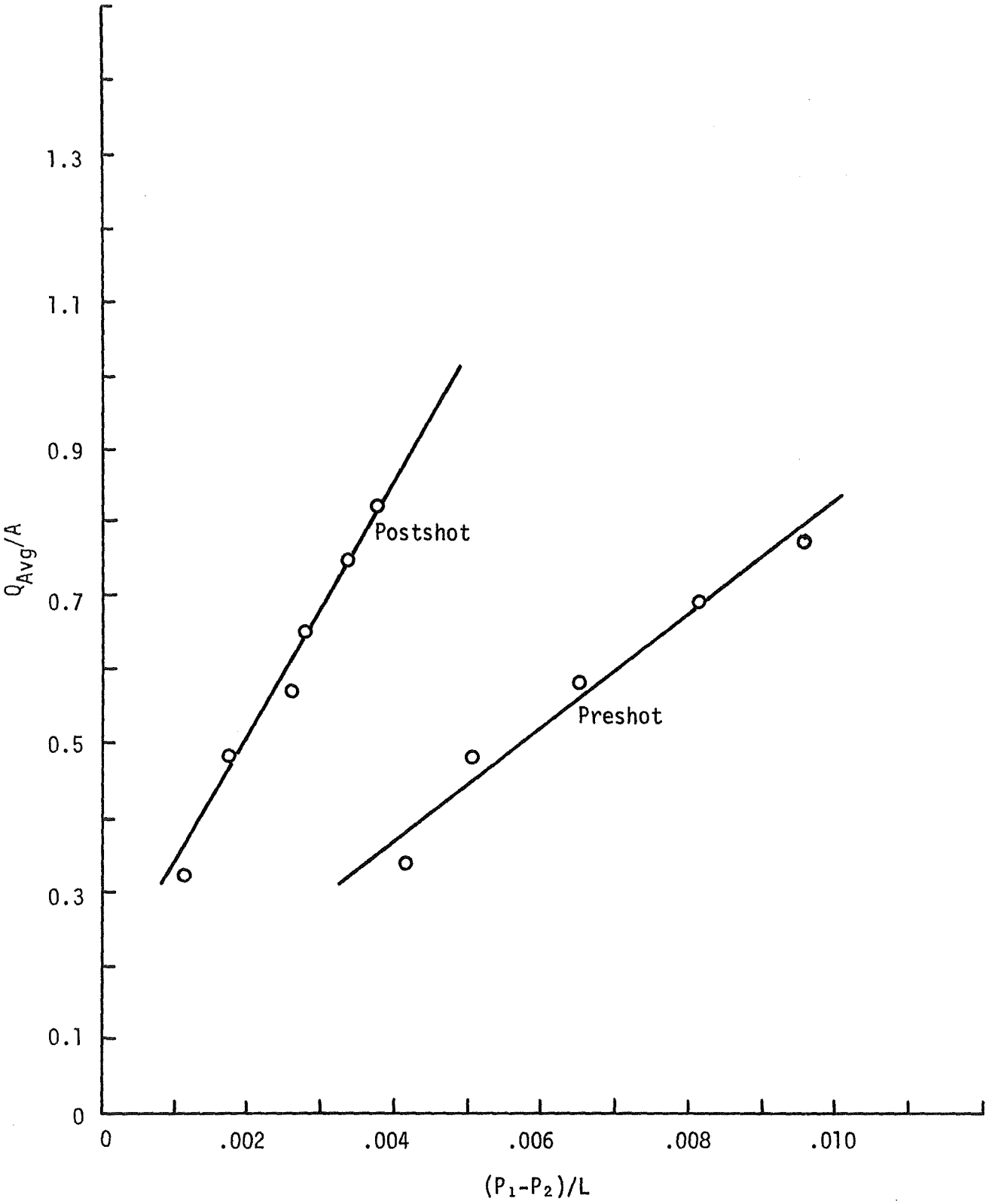

Fig. 30 Q_{Avg}/A vs. $(P_1-P_2)/L$ - BLOCK NO. 8

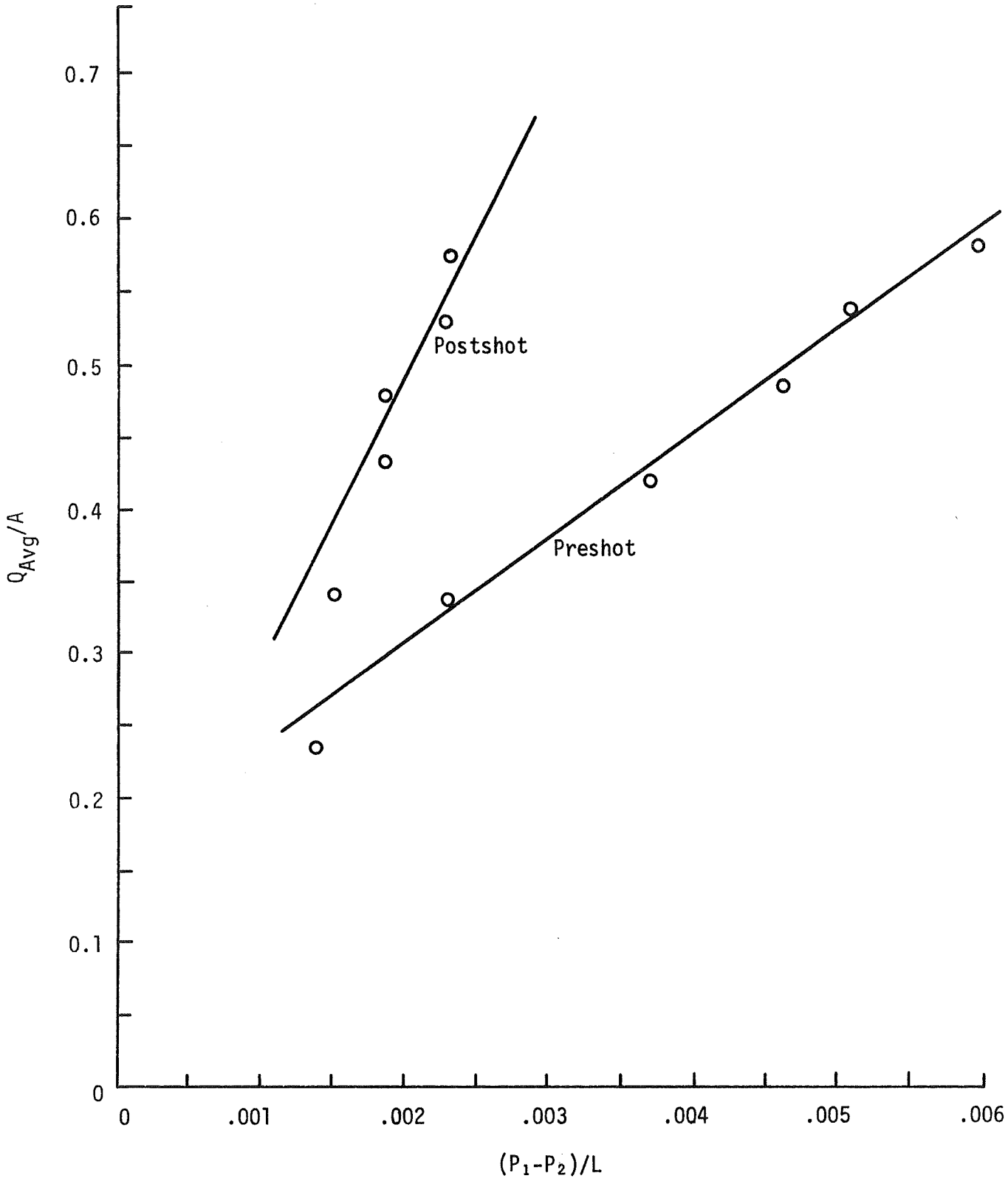

Fig. 31 Q_{Avg}/A vs. $(P_1-P_2)/L$ - BLOCK NO. 9

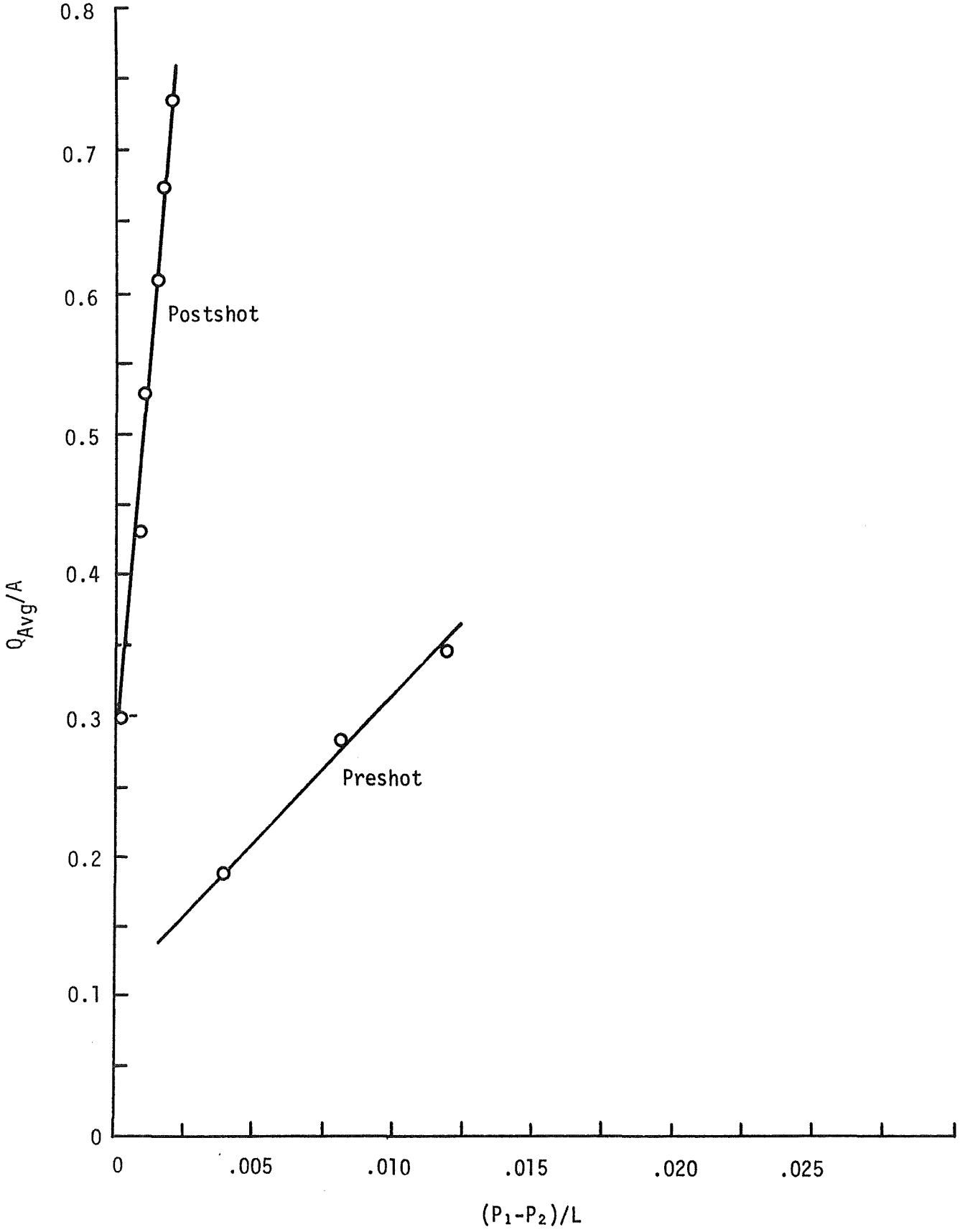

Fig. 32 Q_{Avg}/A vs. $(P_1-P_2)/L$ - BLOCK NO. 11

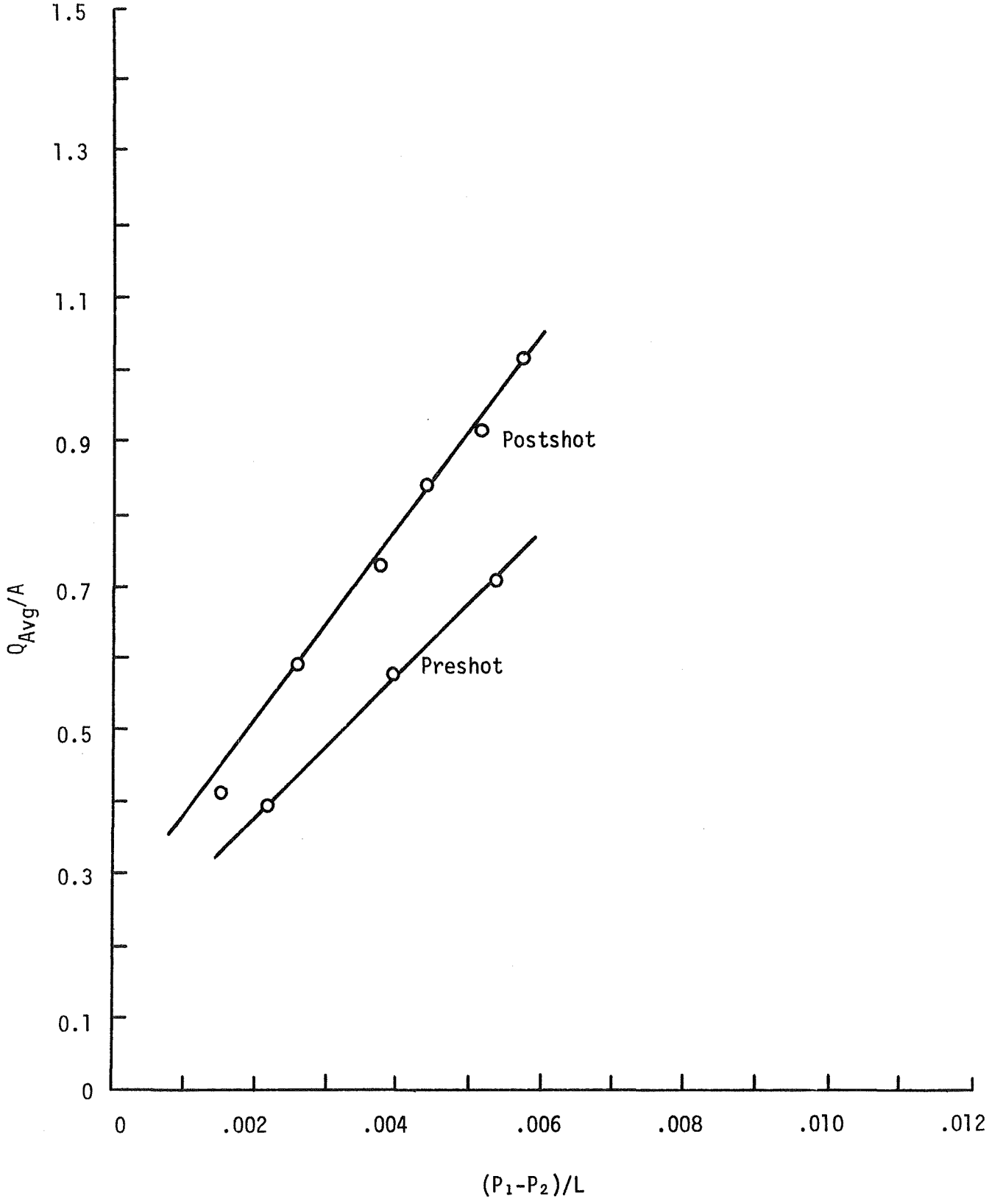

Fig. 33 Q_{Avg}/A vs. $(P_1-P_2)/L$ - BLOCK NO. 12

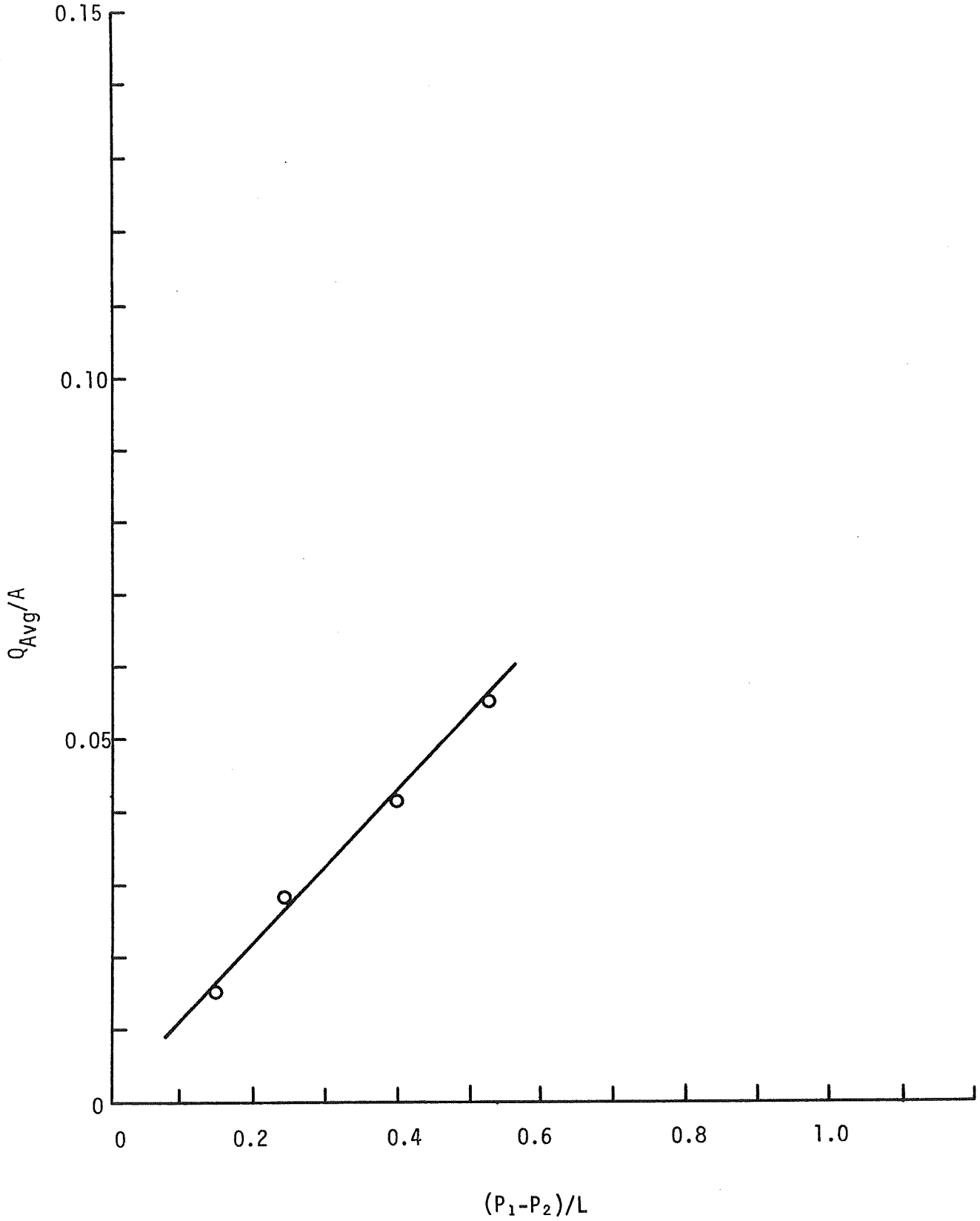

Fig. 34 Q_{Avg}/A vs. $(P_1-P_2)/L$ - SAMPLE C-12

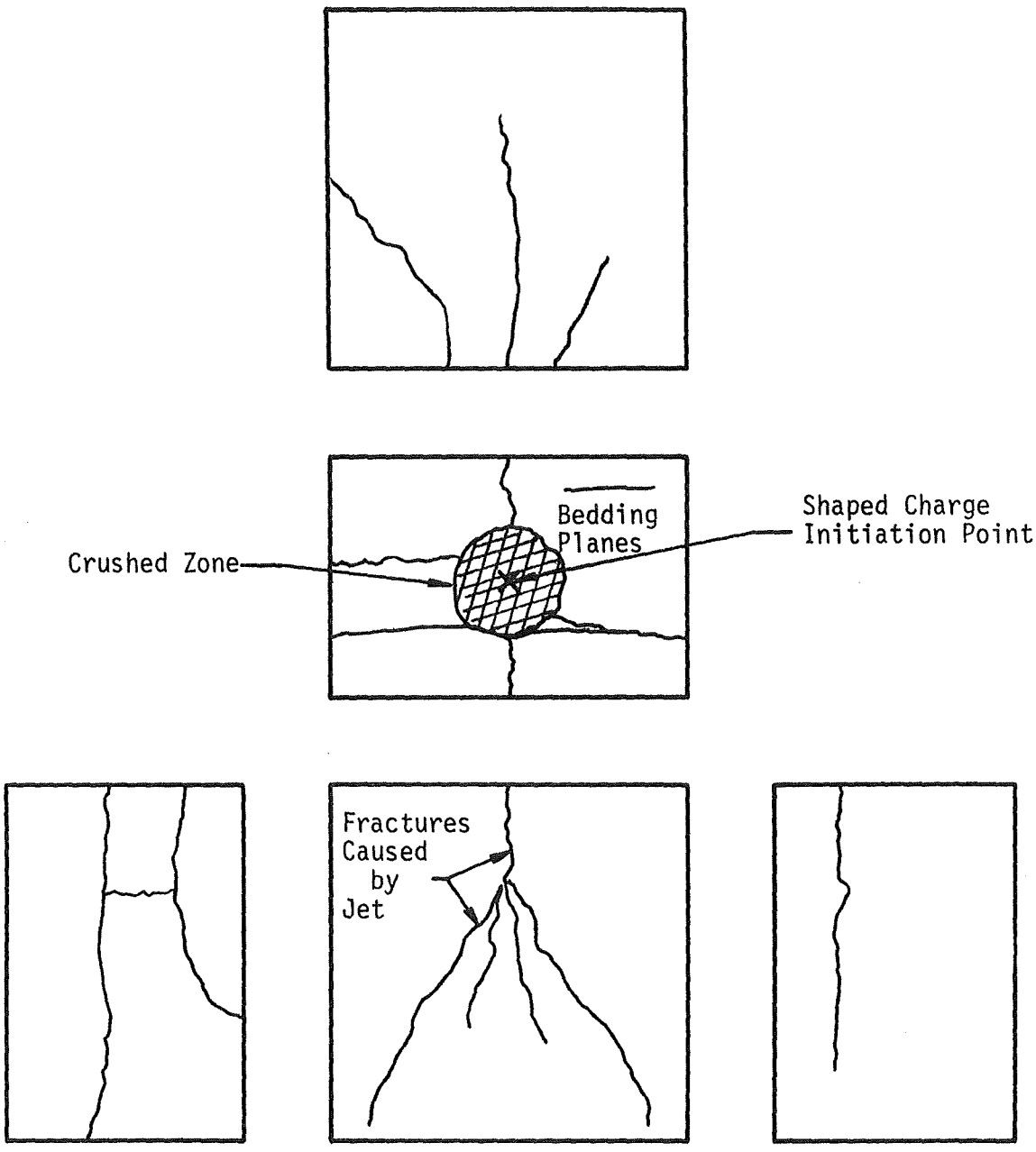

Fig. 35 FRACTURES AND CRUSHED ZONE IN COAL FROM SHAPED CHARGE JET USING A BLAST SHIELD (Scale 1" = 6")

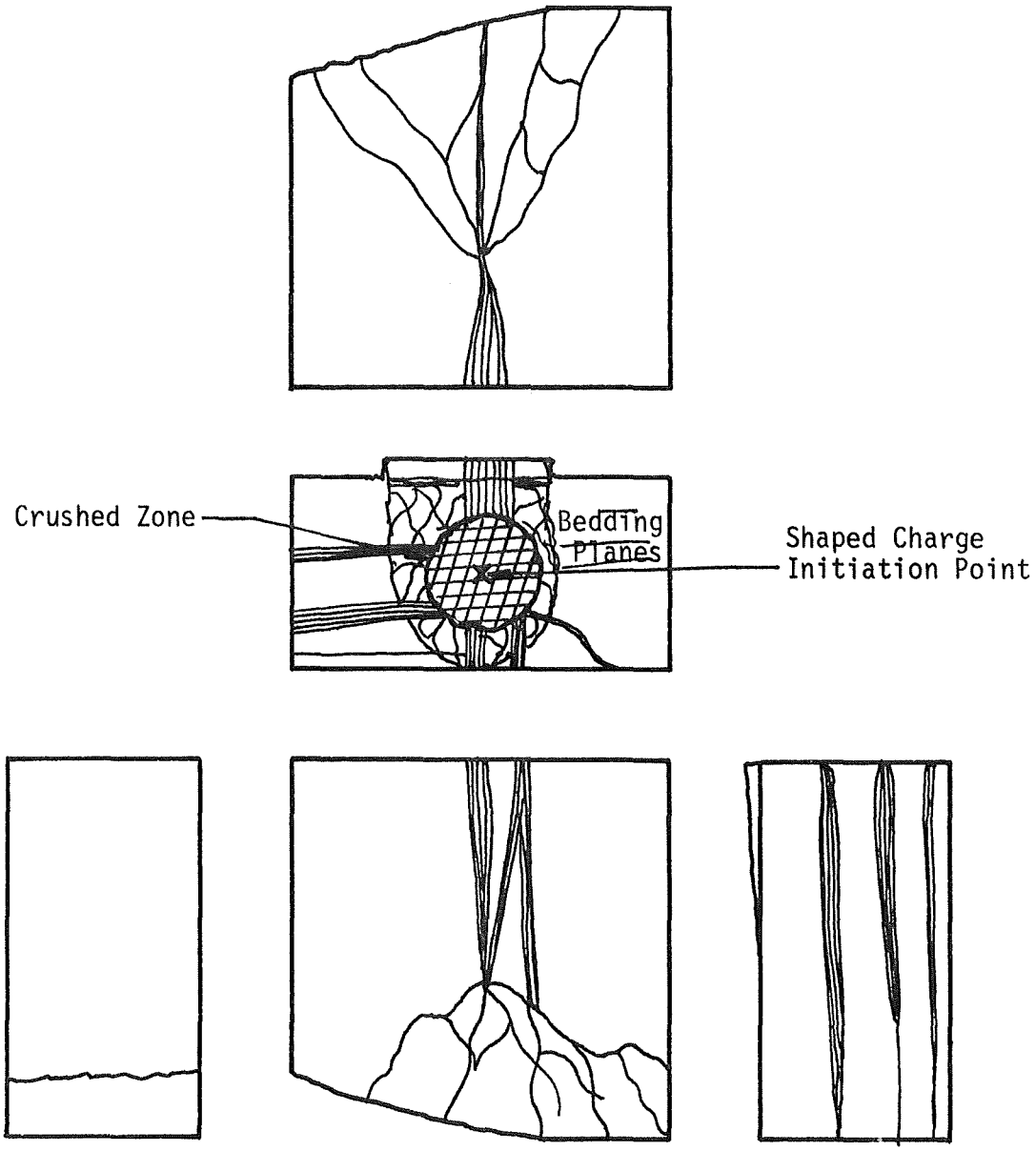

Fig. 36 FRACTURES AND CRUSHED ZONE IN COAL FROM SHAPED CHARGE JET WITHOUT A BLAST SHIELD (Scale 1" = 6")

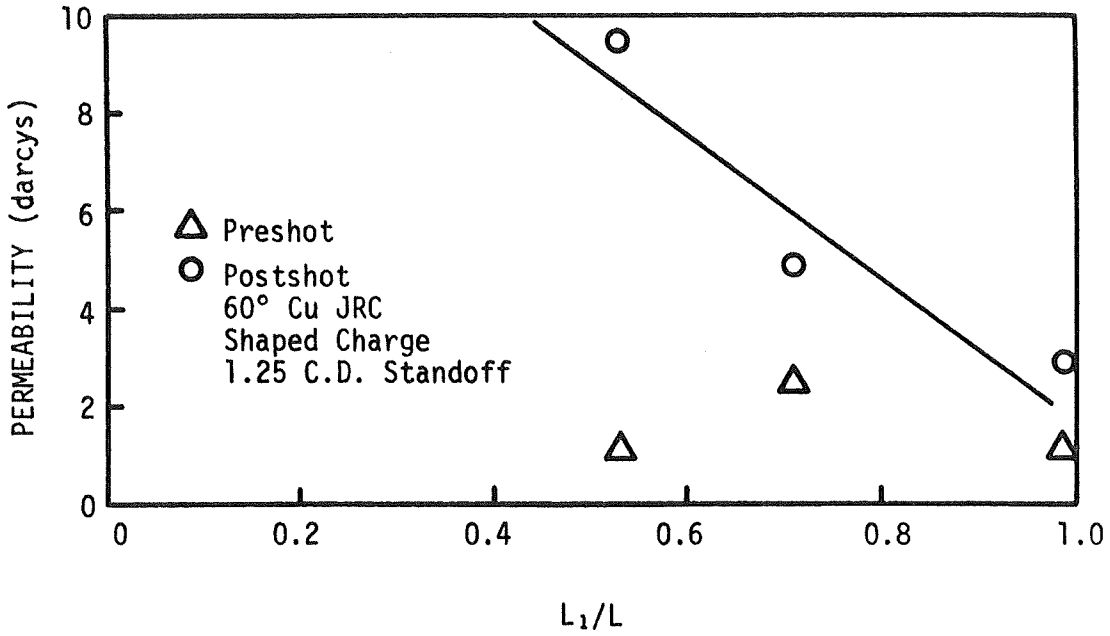

Fig. 37 PERMEABILITY vs. L_1/L IN COAL (perpendicular to bedding)

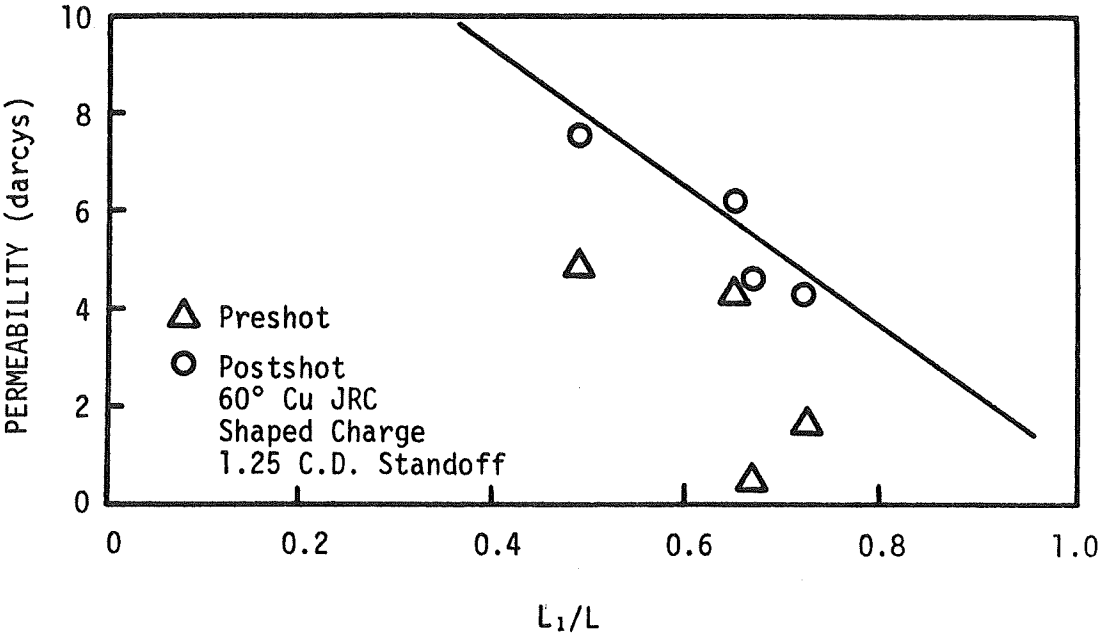

Fig. 38 PERMEABILITY vs. L_1/L IN COAL (parallel to bedding)

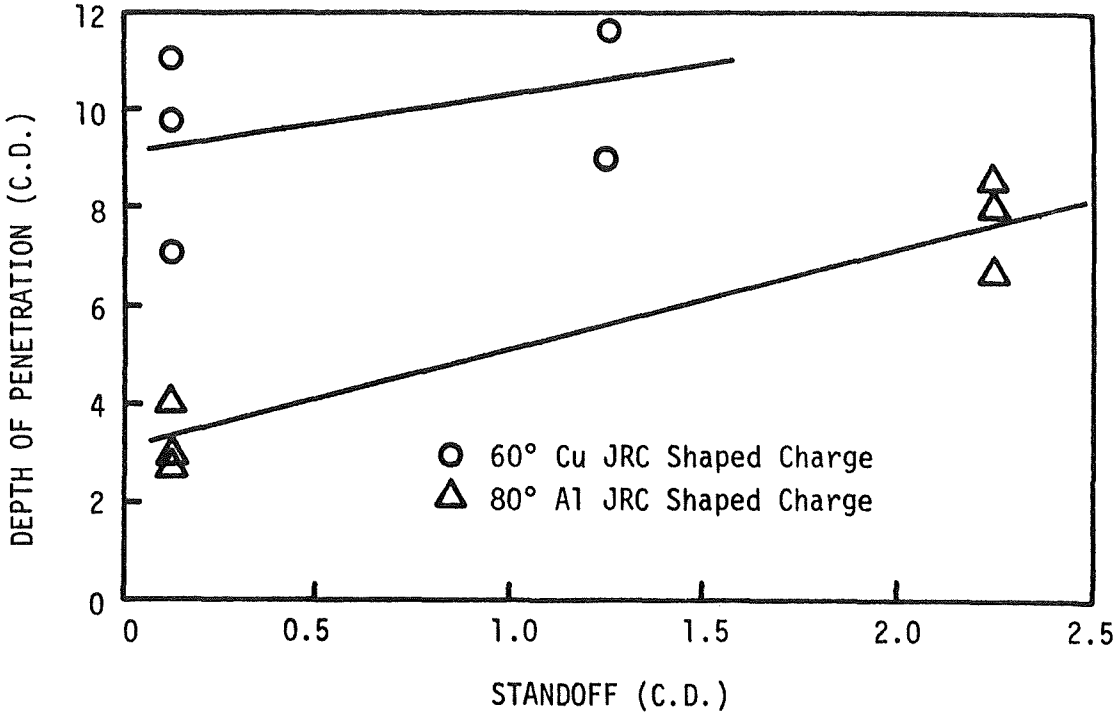

Fig. 39 DEPTH OF PENETRATION vs. STANDOFF IN COAL

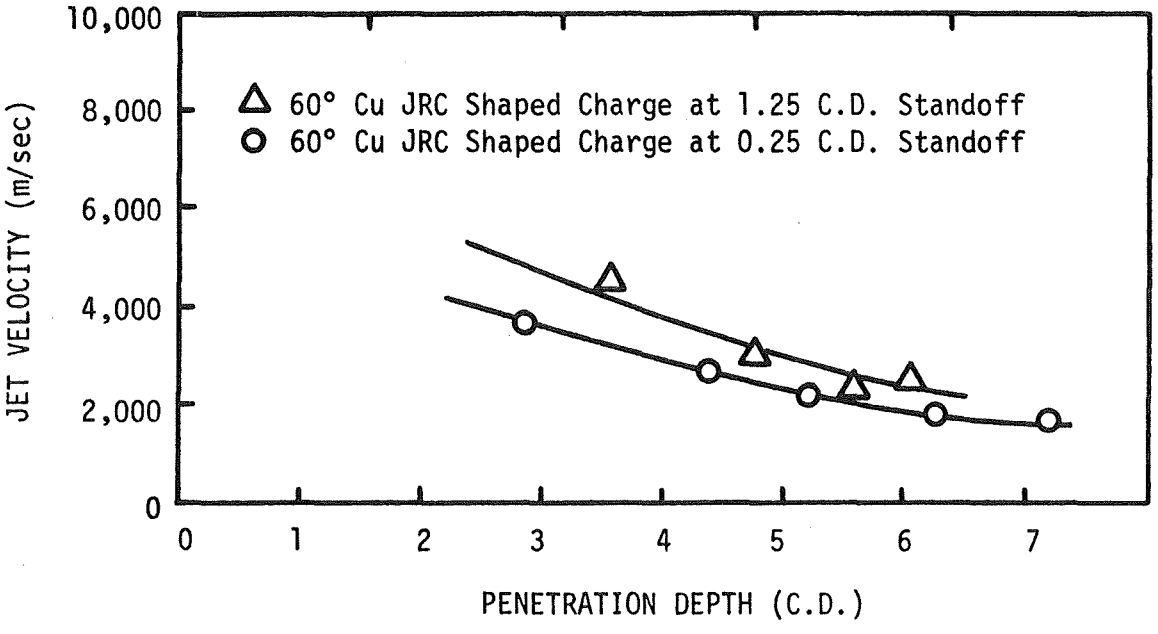

Fig. 40 JET VELOCITY vs. PENETRATION DEPTH IN COAL

observed 40 microseconds after initiation of the charge. The slug velocity was calculated to be 500 meters per second.

Both the depth of penetration and penetration velocity can be adjusted by varying the liner angle, the standoff, the type of explosive, and the loading density of the explosive. Shaped charges with permissible explosives (Table XV) were used to determine the effect of detonation velocity on jet penetration in coal perpendicular to the bedding (Figs. 21 and 22) for 60 deg and 100 deg copper liners. Charges loaded with Atlas 5Y, having a velocity of 1828 meters per second, formed weak, incomplete jets. Jet penetration from 60 deg copper liners was greater than that for all other liners tested (Table XVI), and slugs were recovered from all liner materials. The 60 deg copper liners collapsed toward the cone axis while the aluminum liners behaved more like projectiles (Fig. 41). Titanium liners (100 deg) turned inside out, and the central portion of the liner was destroyed. The collapse process of the 100 deg copper liner differed from that of the titanium in that a frozen jet was formed, indicating partial liner collapse.

Charges were also prepared with the other two permissible explosives: Atlas 5U, velocity 2590 meters per second, and Atlas Gelcoalite Z, velocity 4267 meters per second. These gave similar results to those obtained with Atlas 5Y, except the penetration was greater (Tables XVII and XVIII). The copper liners formed coherent jets, and deformed liners of other metals impacted into the coal acting as projectiles. DuPont 40 percent special gelatin was loaded in charges with 60 deg copper and 80 deg aluminum liners. The velocity of this explosive is comparable to that of Gelcoalite Z, but no jet formation was observed (Table XIX).

TABLE XV

EXPLOSIVE PROPERTIES

Explosive	Type	Density (gm/cc)	Velocity Unconfined (meters/sec)
Composition C-4	H.E.	1.50	8040
Cyclonite (RDX)	H.E.	1.65	8180
DuPont 40 Spec. Gel.	H.E.	1.60	3048
Atlas Coalite 5Y	permissible	0.83	1828
Atlas Coalite 5U	permissible	1.07	2590
Atlas Gelcoalite Z	permissible	1.33	4267

TABLE XVI

PENETRATION - ATLAS 5Y

Shot Number	Liner Material	Liner Angle (deg)	Liner Diameter (in.)	Standoff (CD)	Penetration (in.)	(CD)
5Y-1	Cu	100	.500	1.25	.625	1.25
5Y-2	Cu	100	.500	1.25	.563	1.12
5Y-3	Cu	100	.500	1.25	.563	1.12
5Y-4	Cu	100	.500	3.00	.625	1.25
5Y-5	Cu	100	.500	1.25	.625	1.25
5Y-6	Cu	60	.500	1.25	1.125	2.25
5Y-7	Cu	60	.500	1.25	.625	1.25
5Y-8	Cu	60	.500	1.25	1.190	2.38
5Y-9	Cu	60	.500	1.25	1.063	2.13
5Y-10	Al	100	.500	1.25	.375	.75
5Y-11	Al	100	.500	1.25	.375	.75
5Y-12	Al	100	.500	3.00	.563	1.12
5Y-13	Al	80	.500	3.00	.750	1.50
5Y-14	Al	80	.500	1.25	1.250	2.50
5Y-15	Al	80	.500	1.25	.875	1.75
5Y-16	Al	80	.500	1.25	.500	1.00
5Y-17	Ti	100	.500	1.25	.750	1.50

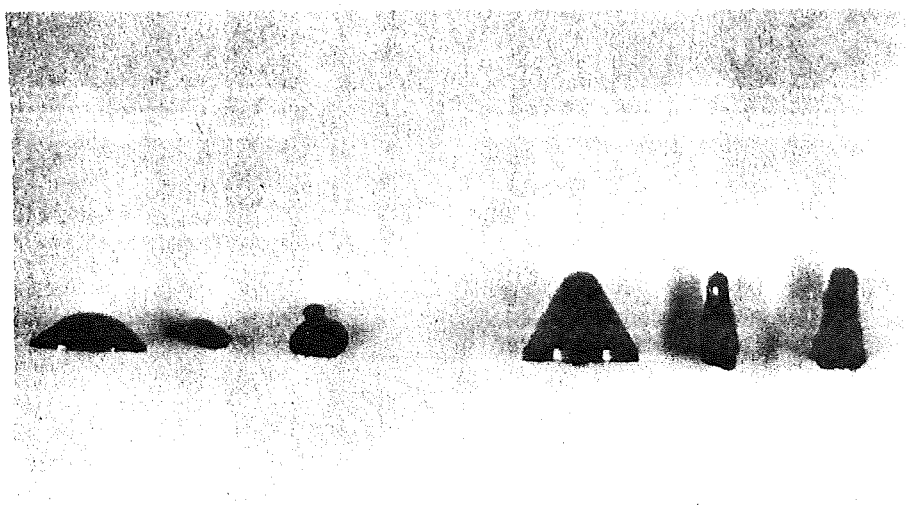

From Left: 100° Copper Liner, Slug using RDX, Slug using Coalite 5Y;
60° Copper Liner, Slug using RDX, Slug using Coalite 5Y

From Left: 100° Aluminum Liner, Slug using Coalite 5Y;
80° Aluminum Liner, Slug using Coalite 5Y;
100° Titanium Liner, Slug (inside out liner)
using Coalite 5Y

Fig. 41 SHAPED CHARGE LINERS AND SLUGS FOR TWO EXPLOSIVES

TABLE XVII

PENETRATION - ATLAS 5U

Shot Number	Liner Material	Liner Angle (deg)	Liner Diameter (in.)	Standoff (CD)	Penetration (in.)	(CD)
5U-1	Cu	60	.500	1.25	1.625	3.25
5U-2	Cu	60	.500	1.25	.875	1.75
5U-3	Cu	60	.500	1.25	1.000	2.00
5U-4	Al	80	.500	1.25	.675	1.35
5U-5	Al	80	.500	1.25	.875	1.75
5U-6	Al	80	.500	1.25	.675	1.35

TABLE XVIII

PENETRATION - ATLAS GELCOALITE Z

Shot Number	Liner Material	Liner Angle (deg)	Liner Diameter (in.)	Standoff (CD)	Penetration (in.)	(CD)
Z-1	Cu	100	.500	1.00	1.500	3.00
Z-2	Cu	100	.500	1.00	1.125	2.25
Z-3	Cu	100	.500	1.00	1.000	2.00
Z-4	Cu	60	.500	1.00	1.625	3.25
Z-5	Cu	60	.500	1.00	1.500	3.00
Z-6	Cu	60	.500	1.00	1.500	3.00
Z-7	Al	80	.500	1.00	0.688	1.37
Z-8	Al	80	.500	1.00	0.688	1.37
Z-9	Al	80	.500	3.00	0.875	1.75
Z-10	Al	100	.500	1.00	1.000	2.00
Z-11	Al	100	.500	1.00	1.000	2.00
Z-12	Al	100	.500	3.00	1.000	2.00

TABLE XIX

PENETRATION - DUPONT 40% SPECIAL GELATIN

Shot Number	Liner Material	Liner Angle (deg)	Liner Diameter (in.)	Standoff (CD)	Penetration (in.)	Penetration (CD)
SG-1	Cu	60	.500	1.25	.625	1.25
SG-2	Cu	60	.500	1.25	.500	1.00
SG-3	Al	80	.500	1.25	.500	1.00
SG-4	Al	80	.500	1.25	.250	.50
SG-5	unlined	80	.500	1.25	.750	1.50

Results of incomplete jet formation were observed in all charges using permissible dynamites and 60 deg copper liners. The inhomogeneity of the explosive caused many of the liners to collapse nonuniformly. The grain size of some of the explosives was large compared to the cone dimensions (0.5 in. diameter) resulting in nonuniform loading densities which affected the detonation velocity and liner collapse. The charges with 1.875 in. diameter brass liners loaded with Gelcoalite Z fired into dolomite formed coherent jets, probably because the effect of the relative grain size was not as pronounced. That is, smaller grain size permits a more uniform loading density and a higher detonation velocity, which in turn increase penetration depth.

Jet penetration from JRC charges in dolomite and Plexiglas produced holes with linear sides and uniform taper. The hole profiles in coal showed differences in diameter which were related to the type of material between the particular bedding planes. The hole axis did not always follow a straight line but some wavering was observed (Fig. 42). This indicates that liner imperfections and jet

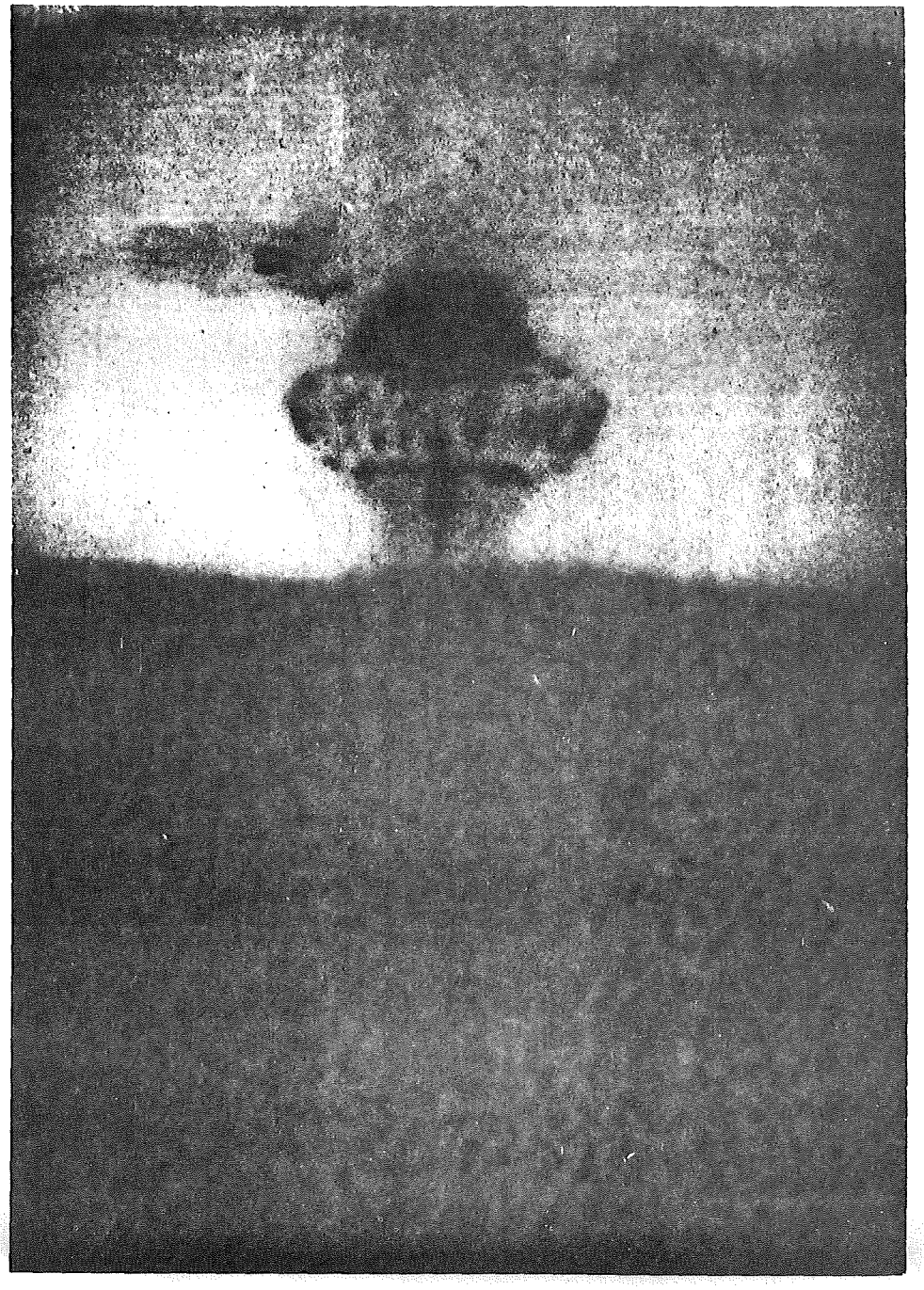

Fig. 42 RADIOGRAPH OF 60° Cu JRC JET IN COAL

formation influence the target response in terms of the size and direction of the final hole produced after the pressure and stress are relieved.

Penetration and fracture data obtained from the large samples used for the permeability study (Tables XI and XII) showed that jets from copper liners with 60 deg apex angles penetrated to almost 11 CD while all other liners tested penetrated between 7 and 8 CD, except for the 80 deg aluminum liner utilizing a standoff of only 0.25 CD. The jet from this liner penetrated only 3.26 CD, forming a crater, and no characteristic hole was observed (Table XX). Jet penetration effectiveness was less for 60 deg copper liners when the standoff was reduced to 0.25 CD (Fig. 39).

Results from experimentation with Plexiglas indicated that penetration velocity was slower when the jet crossed bedding planes in laminated models than that observed in homogeneous samples. That is, the average penetration in coal decreased by 8 percent when charges were fired perpendicular to the plates. The average penetration obtained from charges loaded with low velocity, permissible explosives was approximately 1/5 that obtained from high explosives. Results of tests conducted in dolomite (Ref. 52) suggest that the jet penetration depth for geometrically similar charges at a given standoff is a function of the explosive velocity squared. Early shaped charge studies with ideal explosives showed that the depth of penetration or the hole volume of shaped charge jets fired into steel targets varied directly as the detonation pressure, given by (Ref. 51):

$$P_2 \simeq 0.00987\ \rho_1 V^2/4 \qquad (15)$$

where

P_2 = Detonation pressure (atms.)

ρ_1 = Loading density of the unreacted explosive (g/cm^3)

V = Detonation velocity (m/sec)

That is, if the density is assumed to be constant, the depth of penetration is a function of the detonation pressure, and consequently the detonation velocity squared, as represented by the theoretical velocity curves in Figures 21 and 22, or

$$\text{Penetration Depth} \propto CV^2 \qquad (16)$$

where

V = Detonation velocity (m/sec)

C = A constant, dependent on the properties of the liner and target material

TABLE XX

AVERAGE PENETRATION IN COAL BY JRC CHARGES

Liner Material	Liner Angle (deg)	Standoff (CD)	Penetration Parallel (CD)	Penetration Perpendicular (CD)
Cu	100	1.25	8.16	6.92
Cu	60	1.25	11.00	10.55
Al	100	2.25	7.78	7.15
Al	80	2.25	7.70	7.75
Cu	60	0.25	9.33	--
Al	80	0.25	3.36	--

The conventional (elastic, plastic and strength) physical properties of the coal may be employed to add to an understanding of penetration and fracture mechanisms in coal due to shaped charge jets. Materials which deform plastically under an impact load do so because shear stresses exceed the yield strength, while fractures are produced in brittle materials when tensile stresses exceed the ultimate tensile strength. Bedding planes in coal can be considered as density discontinuities but not as free faces or boundaries. Therefore, stress waves are not totally reflected but are refracted into the next layer with tensile fracture possible at each boundary. A complex stress wave system results from reflected and refracted waves, and vertical discontinuities (joints) have similar effects to bedding.

Fracturing in coal near the jet penetration point has been observed to be intense and is usually bounded vertically by the joints with major fracturing confined between sets of jointing planes. The coal breaks into large and small pieces, usually parallelipipeds whose boundaries follow the natural cleavage planes. Some fractures are observed to cross joints and interconnect them. Fractures originating at the base of the jet penetration also travel across the bedding planes deep into the coal. Kolsky (Ref. 41) states that fracturing should be greater near the base of the jet penetration because the impulse is traveling near the fracture velocity of the material. Therefore, the stress waves do not outdistance the fractures and fracture tips are moving in a stressed area, which causes longer fractures to form. This was confirmed in the brittle materials tested as demonstrated by calcite deposits in vertical joints which were shattered at a distance from the charge by stress waves.

DiPersio has stated that hardness rather than density is a controlling factor in penetration in steel and aluminum plates (Ref. 53). Other investigators have also used correction factors based on hardness or strength of materials to modify the first order equations. Material strength properties under high confining pressures would seem to be the governing factor in jet penetration in brittle materials which fracture rather than flow plastically when they are subjected to high impulse pressures.

Jet hole profiles are characterized by a crushed and compacted zone immediately around the jet path. A well defined fracture zone exists beyond the crushed zone, followed by a zone of radial fractures. When shaped charge jets were fired into coal samples, with a steel blast shield to protect the sample, large quantities of coal dust were observed on the surface of the coal near the point of jet impact. The material from the surface crater in the coal was comprised of small coal particles, the dust being ejecta from the jet penetration.

Penetration was observed to be related to static tensile strength in three materials tested (Fig. 43):

$$P_d \propto \frac{1}{\ln \sigma_t} \tag{17}$$

where

P_d = Penetration

σ_t = Static tensile strength

Jet penetration is also a function of the explosive velocity, that is, jet penetration in brittle materials can be represented by:

$$P_d \propto \frac{V^2}{\ln \sigma_t} \tag{18}$$

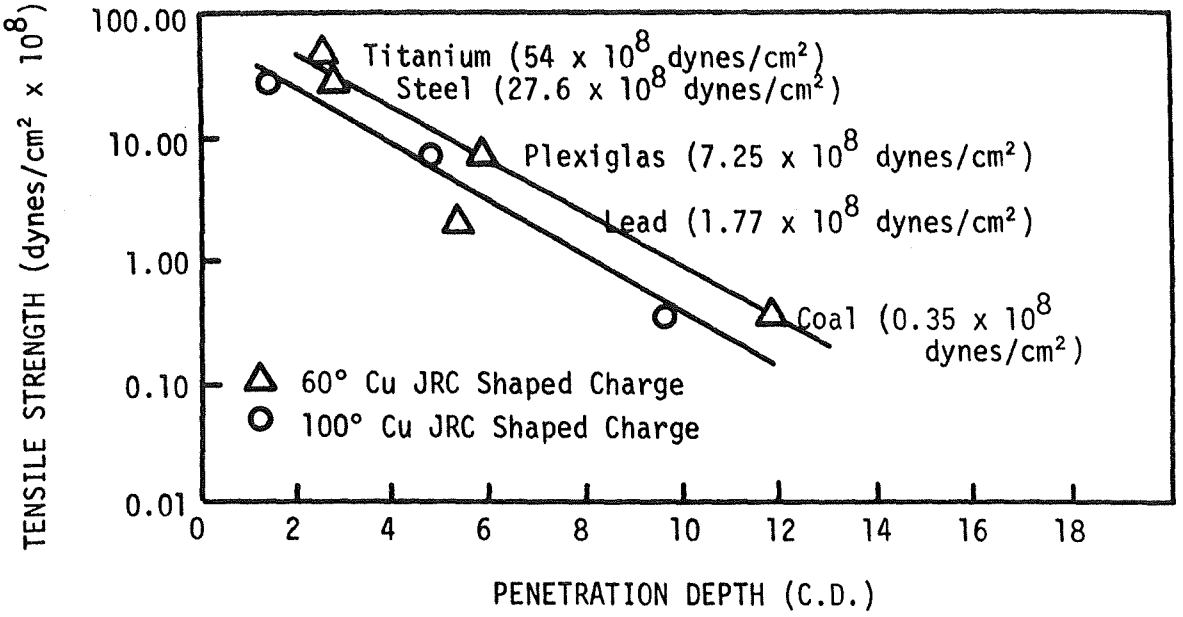

Fig. 43 TENSILE STRENGTH vs. PENETRATION DEPTH FOR TITANIUM, STEEL, PLEXIGLAS, LEAD, AND COAL

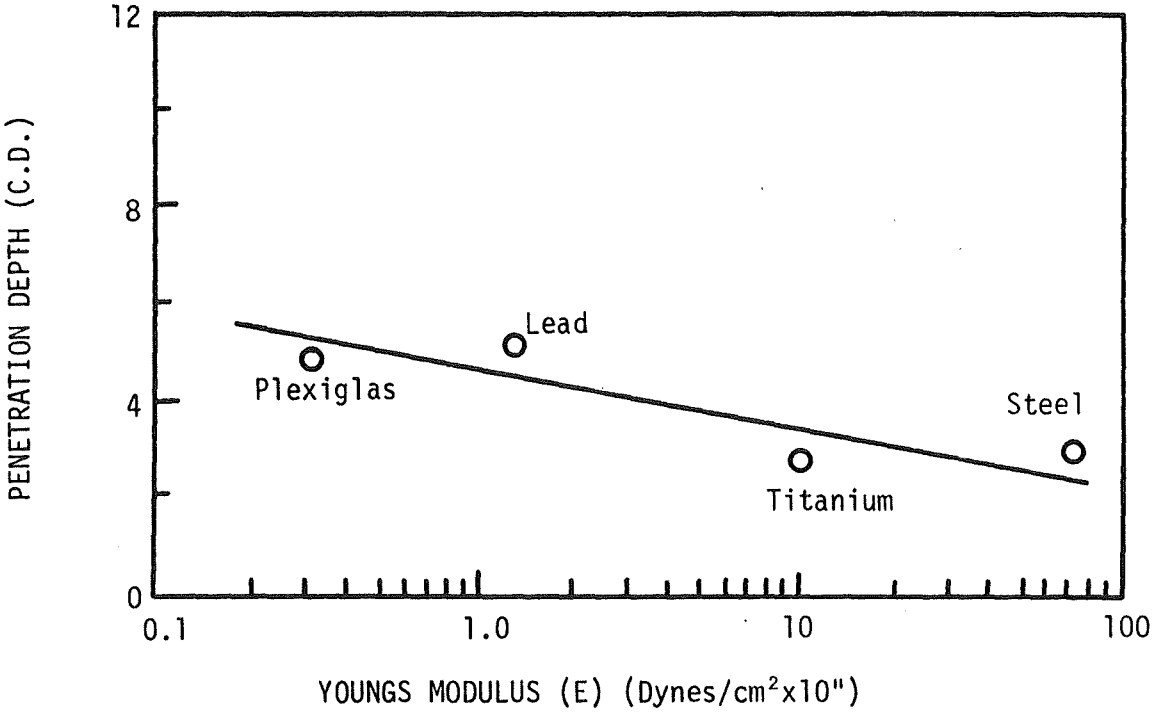

Fig. 44 PENETRATION DEPTH vs. YOUNGS MODULUS

where

P = Penetration

σ_t = Static tensile strength

V = Detonation velocity of the explosive

Approximate values for Young's modulus were obtained from the literature for four of the five target materials (Appendix B). Young's modulus for coal could not be determined because of the heterogeneity of the material. Results from the four target materials, excluding coal, indicate that jet penetration increases as Young's modulus decreases (Fig. 44).

$$P_d \propto \frac{1}{\ln E} \tag{19}$$

where

P_d = Penetration depth

Jet penetration in the target material is accompanied by a rapidly deteriorating shock wave which moves ahead of the jet tip. The natural log of the wave propagation velocity through the target material is inversely related to the depth of penetration for target materials tested (Fig. 45).

$$P_d \propto \frac{1}{\ln V_p} \tag{20}$$

Since material properties other than density are related to jet penetration the impact cannot be totally hydrodynamic, and plastic processes and physical properties other than density have an effect on the penetration process (Fig. 46).

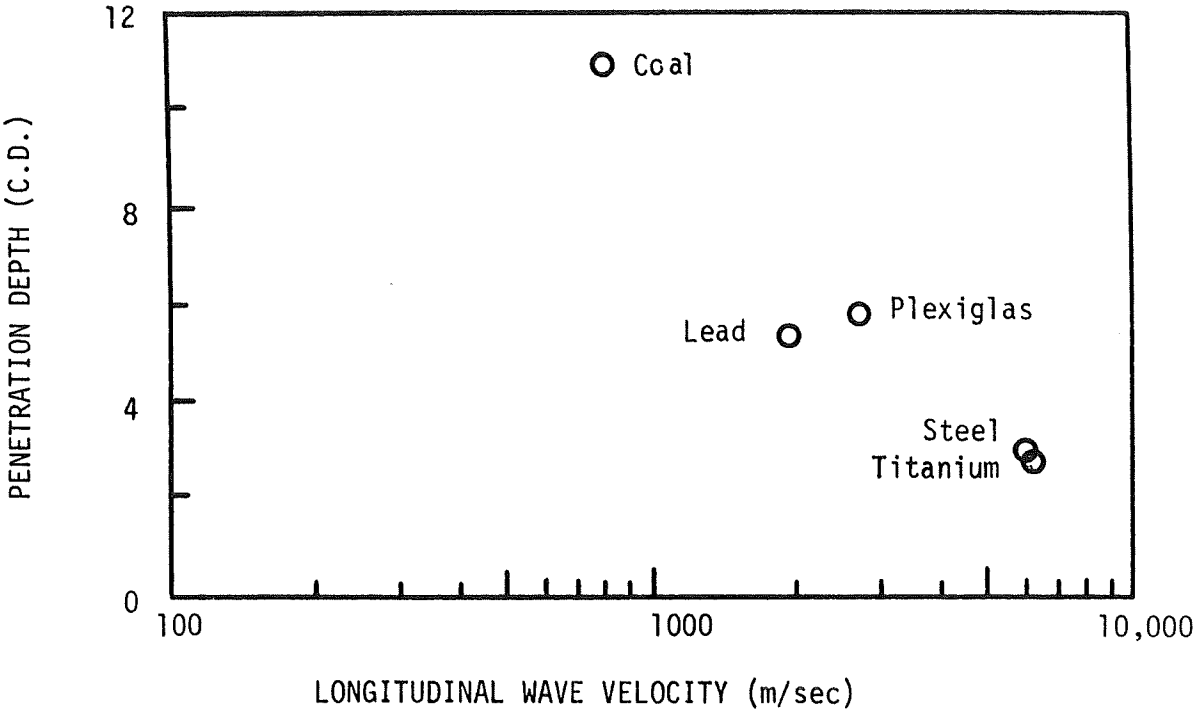

Fig. 45 PENETRATION DEPTH vs. LONGITUDINAL WAVE VELOCITY

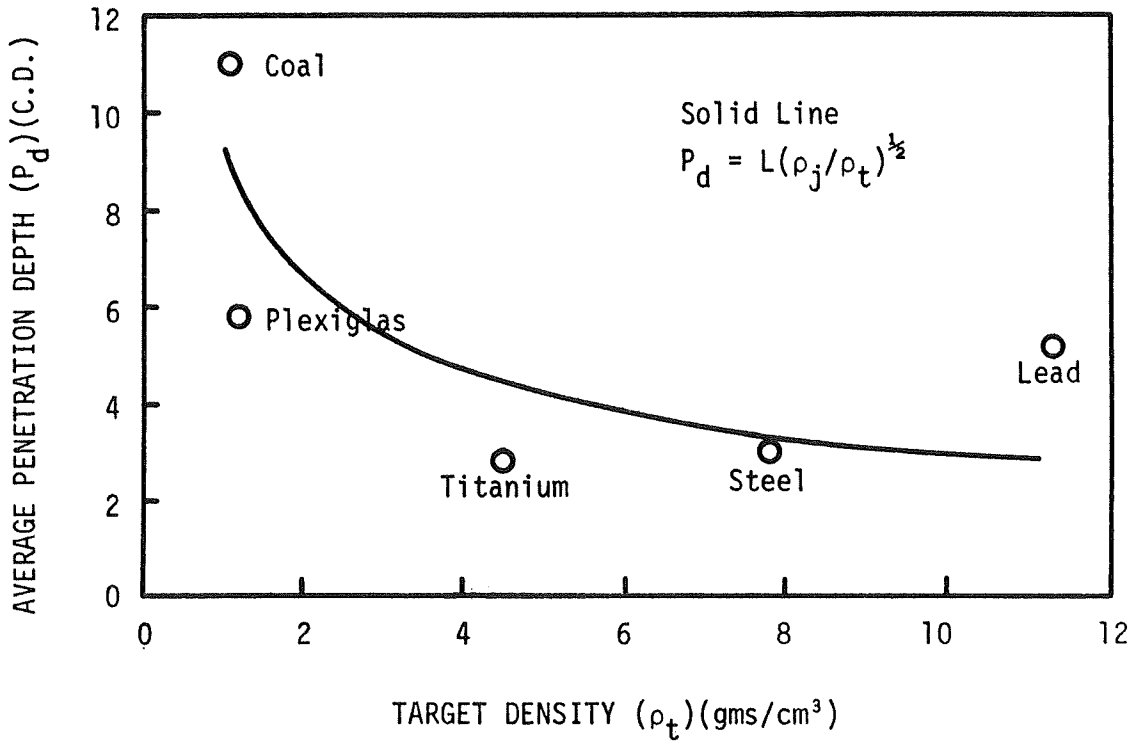

Fig. 46 AVERAGE PENETRATION DEPTH vs. TARGET DENSITY FOR 60° Cu JRC SHAPED CHARGES

VI. SUMMARY AND CONCLUSIONS

To furnish quantitative information on hole formation models of Plexiglas were photographed during the jet penetration process, and fracture and jet velocities were calculated. Jets from 0.5 in. diameter, Jet Research Corporation (JRC), shaped charges penetrated from 0.38 in. to 3.04 in., depending on the explosive and liner angle utilized. Shots made into 0.75 in. thick plates clamped together to simulate bedded models showed that existing partings have a marked effect on fracture propagation. Similar penetration and fracture phenomena were observed in both Plexiglas models and coal blocks.

Dolomite was used as a control target material for penetration tests utilizing charges of 1.875 in. in diameter since coal blocks of the necessary large size were not available. The depth of jet penetration in both dolomite and coal was proportional to the detonation velocity of the explosive used. The depth of the surface crater formed by shaped charge impact was inversely proportional to the jet penetration depth. The deepest penetration obtained was 15 in. for a jet from an 80 deg brass cone and Composition C-4.

Gas flow through the microfracture system in coal is dependent on bedding orientation and is greater parallel to the bedding. The average natural permeability along the bedding was 0.348 millidarcys and across the bedding it was 0.014 md. Gas flow through larger coal blocks, about 1 cubic foot, containing cleats, joints, etc. was dependent on the extent and interconnection of the fractures. The permeability of the joints is greater than that of the microfractures and they account for the majority of the gas flow through the coal seam.

Permeability values of the large preshot blocks was about 1.5 to 5 darcys. Postshot values were approximately 4 to 10 darcys. Shaped charges fired perpendicular to the bedding planes increased the permeability more than those fired parallel to the bedding, permeability being decreased in some cases because of fracture closure.

Jet penetration depths, however, decreased as the jet crossed bedding planes. A jet penetration of 11 C.D. (5.5 in.) resulted from the use of 60 deg Cu liners while other liners tested produced penetrations of about 7 to 8 C.D. Small shaped charges, 0.5 in. diam, loaded with low velocity permissible explosives did not function as well as the same charges loaded with high explosive. The depth of jet penetration in coal was proportional to the detonation velocity of the explosive. Standoff distance was critical for charges with aluminum liners. At a standoff distance of 0.25 C.D., copper lined charges formed jets with decreased penetration capabilities while aluminum lined charges did not form a cohesive jet. Physical properties of liner materials influenced liner collapse mechanisms in charges utilizing low velocity explosives. Copper liners with 100 deg apex angles collapsed uniformly about their axis while similar liners of titanium turned inside out. Jet penetration depth was observed to be approximately inversely propertional to the static tensile strength, Young's modulus, and the longitudinal wave velocity of the target.

The use of shaped explosive charges for increasing the permeability of coal for degasification purposes would require drilling horizontal holes into the virgin coal, ahead of the working face or vertical holes into the coal seam from the surface, the emplacement,

and firing of the charges. Shaped charges with a 60 deg apex angle, and a copper liner gave the greatest increase in gas flow rates when fired perpendicular to the bedding planes.

REFERENCES

1. Merritts, W.M., "Recent Research in Degasifying a Coalbed Before and During Mining," International Symposium on Mining Research, Vol. 1, Symp. Public. Div., Pergamon Press, New York,(1962), pp. 301-311.

2. Ammosov, I.I., and Eremim, I.V., Fracturing in Coal, Israel Program for Scientific Translations, Ltd., Jerusalem,(1963).

3. Clark, G.B., et al., "Investigation of the Use of Shaped Charges for Rapid Drilling and Blasting," for Du Pont Co.,(March 1970).

4. Cervik, J., "An Investigation of the Behavior and Control of Methane Gas," Mining Engineering Journal,(July 1967).

5. Palowitch, E.R., "Systems Approach to Methane Control," Methane Central Research Meeting, Bureau of Mines, Pittsburgh, Pa.,(May 1969).

6. Cervik, J., "The Methane Problem," Methane Central Research Meeting, Bureau of Mines, Pittsburgh, Pa.,(May 1969).

7. Deul, M., "Methane Central Research," Methane Central Research Meeting, Bureau of Mines, Pittsburgh, Pa.,(May 1969).

8. Cervik, J., "Behavior of Coal-Gas Reservoirs," Bureau of Mines, Methane Central Program, TP Report 10,(April 1969).

9. Perkins, J.H., and Cervik, J., "Sorption Investigation of Methane in Coal," Bureau of Mines, Methane Central Program, TP Report 14,(May 1969).

10. Hadden, J.D., and Sainato, "Gas Migration Characteristics of Coal Beds," Bureau of Mines, Methane Central Program, TP Report 12,(May 1969).

11. Recommended Practices for Determining Permeability of Porous Media, API RP 27, Amer. Pet. Inst., Div. of Prod., Dallas, Texas,(August 1956).

12. Amyx, J.W., Bass, D.M., Jr., and Whiting, R.L., Petroleum Reservoir Engineering, McGraw-Hill Co., New York (1960).

13. Scheideggen, A.E., The Physics of Flow Through Porous Media, Rev. Ed., University of Toronto Press (1960).

14. Klinkenberg, L.J., "The Permeability of Porous Media to Liquids and Gases," American Petroleum Institute, Central Committee on Drilling & Production Practices (1941).

15. Fulton, P.F., "The Effect of Gas Slippage on Relative Permeability Measurements," Producers Monthly, Vol. 15, No. 12 (1951).

16. Steward, C.R., Craig, F.F., Jr., and Morse, R.A., "Determination of Limestone Performance Characteristics by Model Flow Tests," Transactions of A.I.M.E., Vol. 198 (1953).

17. Steward, C.R., and Owens, W.W., "A Laboratory Study of Laminar and Turbulent Flow in Heterogeneous Porosity Limestone," Petroleum Transactions of A.I.M.E., Vol. 213 (1958).

18. Mangunwidjojo, A.S., "Effects of Size and Shape of Specimens and Gas Slippage Phenomena in the Measurement of Coal Permeability to Gas Flow," unpublished M.S. thesis, Virginia Polytechnic Institute, Blacksburg, Va. (1967).

19. Lin, J.P., "Fracture Effect on Coal Permeability," unpublished M.S. thesis, Virginia Polytechnic Institute, Blacksburg, Va. (1966).

20. Wang, Y.J., "Effects of Specimen Size on Permeability Measurements of Gas Flow in Coal," unpublished M.S. thesis, Virginia Polytechnic Institute, Blacksburg, Va. (1962).

21. Huang, M.S., "A Study of the Permeability of Coal to the Flow of Gas," unpublished M.S. thesis, Virginia Polytechnic Institute, Blacksburg, Va. (1961).

22. Koo, S.M., "A Study of the Factors that Affect the Permeability of Coal," unpublished M.S. thesis, Virginia Polytechnic Institute, Blacksburg, Va. (1960).

23. Sevenster, P.G., "Diffusion of Gases Through Coal," Fuel, Vol. 38, (1959).

24. Clark, G.B., "Studies of the Design of Shaped Charges and Their Effect in Breaking Concrete Blocks," American Institute of Mining Engineers, Technical Paper 2157 (1947).

25. Lowry, H.H., Chemistry of Coal Utilization, John Wiley & Sons, Suppl. Vol., New York (1963).

26. Karn, F.S., et al., "Diffusion Studies of Light Hydrocarbon Gases Through Coal," Bureau of Mines, RI 7441 (1970).

27. Nandi, S.P., and Walker, P.L., Jr., "Diffusion of Argon from Coals of Different Rank," Coal Science, ACS, Washington (1966).

28. Elder, C.H., "Use of Vertical Boreholes for Assisting Ventilation of Longwall Gob Areas," Bureau of Mines, T.P. Rept. 13 (1969).

29. Kickovic, S., et al., "Methane Emission Rate Studies in a Northern West Virginia Mine," Bureau of Mines, T.P. Rept. 28 (1970).

30. Evans, I., and Skinner, D.J., "The Permeability of Coking Coal to Water at Low Pressures," Colliery Eng., (August 1960).

31. Alpern, B., "Tectonics and Gas Deposits in Coalfields," a bibliographical study and examples of application, Int. Jl. Rock Mech. Min. Sci., Vol. 7, pp. 67-76 (January 1970).

32. Bertard, C., et al., "Determination of Desorbable Gas Concentration of Coal," Int. Jl. Rock Mech. & Min. Sci., Vol. 7, pp. 43-65 (January 1970).

33. Ettinger, I., et al., "Natural Factors Influencing the Coal Sorption Properties," I. Petrography and the Sorption Properties of Coal, Fuel, Vol. 45, No. 4 (1966).

34. Evans, I., et al., "The Compressive Strength of Coal," Colliery Eng., (March 1961).

35. Hobbs, D.W., "The Strength and Stress-Strain Characteristics of Oakdale Coal under Triaxial Compression," Geological Mag., Vol. 47, No. 5, pp. 422-435 (September 1960).

36. Parish, Bureau of Mines, "The Effect of Rank and Particle Size in the Plastic Behavior of Coal," BR Jl. of Appl. Phys., Vol. 18.

37. Allison, F.E., and Vitali, R., "A New Method of Computing Penetration Variables for Shaped Charge Jets," BRL Rept. No. 1184 (January 1963).

38. DiPersio, R., and Simon, J., "The Penetration-Standoff Relation for Idealized Shaped Charge Jets," BRL Rept. No. 1542 (February 1964).

39. DiPersio, R., et al., "Penetration of Shaped Charge Jets into Metallic Targets," BRL Rept. No. 1296 (September 1965).

40. DiPersio, R., and Simon, J., "The Effect of Jet Breakup Time on the Penetration Performance of Shaped Charges," BRL Rept. No. 1897 (January 1968).

41. Hopkins, H.G., and Kolsky, H., "Mechanics of Hypervelocity Impact of Solids," Fourth Symposium on Hypervelocity Impact, AD 244 475 (April 1960).

42. Gault, D.E., and Heitowit, E.D., "The Partition of Energy for Hypervelocity Impact Craters Formed in Rock," Sixth Symposium on Hypervelocity Impact, Vol. II, Pt. 2 (August 1963).

43. Klamer, O.A., "Shaped Charge Scaling," Tech. Mem. 1383, Picatinny Arsenal (March 1964).

44. Brimmer, R.A., "Manual for Shaped Charge Design," NAVORD Rept. 1248, NOTS 311 (August 1950).

45. DiPersio, R., et al., "Characteristics of Jets from Small Caliber Shaped Charges with Aluminum and Copper Liners," BRL Memo Rept. 1866 (September 1967).

46. Bell, W.T., et al., "The New Titanium-Lined Shaped Charge Perforator," Oil & Gas Journal (Nov. 5, 1962).

47. Pugh, E.M., et al., "Theory of Jet Formation by Charges with Lined Conical Cavities," Jl. Appl. Phys., Vol. 23, p. 532 (1952).

48. Pack, D.C., and Evans, W.M., "Penetration by High Velocity (Munroe) Jets: I," Proc. Phys. Soc. of London, Sec. B, Vol. 64, p. 299 (1951).

49. Eichelberger, R.J., "Re-examination of the Theories of Jet Formation and Penetration by Lined Cavity Charges," Ph.D. thesis, Carnegie Inst. of Tech., (May 1954).

50. Zernow, L., and Simon, J., "High Strain Plasticity of Liner Metals and Jet Behavior," Trans. of Symp. on Shaped Charges, BRL (AD 58899), Aberdeen Proving Grounds, Maryland (1953).

51. Cook, M.A., The Science of High Explosives, Reinhold Publishing Corp., New York (1958).

52. Rollins, R.R., Clark, G.B., Konya, C.J., "Investigation of the Use of Shaped Explosive Charges for Increasing the Permeability of Coal," Final Rept., Grant No. G0101590 (MIN-36), Rock Mech. & Explos. Res. Cntr., UMR, Rolla, Mo., for the Bureau of Mines, Pittsburgh, Pa. (Dec. 1971).

53. DiPersio, R., and Simon, J., "Resistance of Solid Homogeneous Targets to Shaped Charge Jet Penetration," BRL Rept. 1417 (Oct. 1968).

APPENDIX A

CALCULATIONS FOR SANDSTONE STANDARD

Oven Dried Sample

Index	P_1 (atm)	P_2 (atm)	$\frac{P_1+P_2}{2}$	P_1-P_2	Q (cc/sec)	$\frac{P_2}{\frac{P_1+P_2}{2}}$	Q_{Avg}*	$\frac{Q_{Avg}}{A}$	$\frac{P_1-P_2}{L}$
2.5	1.1774	1.0142	1.0958	0.1632	25.83	0.9255	23.096	2.238	0.0510
5.0	1.3418	1.0168	1.1793	0.3250	50.83	0.8622	43.826	4.103	0.1015
7.5	1.4866	1.0326	1.2595	0.4540	75.83	0.8197	62.158	5.820	0.1418
10.0	1.6326	1.0590	1.3458	0.5736	100.00	0.7868	78.680	7.367	0.1792
12.5	1.7668	1.0800	1.4234	0.6868	122.5	0.7587	92.94	8.702	0.2146
15.0	1.9274	1.1168	1.5221	0.8066	147.50	0.7337	108.22	10.132	0.2520

*Q_{Avg} is determined by

$$Q_{Avg} = (Q)\frac{P_2}{(P_1+P_2)/2}$$

Klinkenberg Correction

$(P_1-P_2)/L$	Q/A	K	$1/P_m$
0.1015	4.103	0.739	0.848
0.1418	5.820	0.750	0.794
0.1792	7.367	0.751	0.743
0.2146	8.702	0.742	0.703
0.2520	10.132	0.735	0.657

APPENDIX B

MATERIAL PROPERTIES

Material	Longitudinal Velocity (m/sec)	Shear Wave Velocity (m/sec)	Tensile Strength $\left[\frac{dynes}{cm^2} \times 10^8\right]$	Specific Gravity	Shore Hardness Number	μ	E $\left[\frac{dynes}{cm^2} \times 10^{11}\right]$
Air	335	--	--	0.012			
Water	1448	--	--	1.0			
Plexiglas	2683	1067	7.25	1.19	73.7	0.40	0.31
Dolomite	4451	2622	--	2.5		0.23	
Coal	833* 1388**		0.345	1.10	68		
Brass	4700	2110	33.8	8.47		0.37	10.3
Aluminum	6420	3040	25.0	2.82		0.35	7.1
Copper	5010	2270	21.3	8.96		0.37	11.2
Titanium	6070	3125	54.0	4.5	50	0.32	11.6
Steel	5941	3251	27.6	7.8	27	0.28	17.2
Lead	1960	690	1.77	11.34	12.9	0.43	1.38

*perpendicular to bedding planes
**parallel to bedding planes

APPENDIX C

PROXIMATE ANALYSIS OF COAL FROM ILLINOIS NO. 6 SEAM

Analysis on Dry Basis

Ash	15%
Sulfur	0.7%
Volatiles	37%

Fixed Carbon Content = 100% - (Ash + Volatiles)

= 48%

BTU Value 10,800

Analysis Data Furnished by Inland Steel, Sesser, Illinois